

Exploring the Application of Field-Deployed Optical Sensors for Real-Time Indication of Fecal Contamination in the Clinton River Watershed

Christine N. Brown

A master's thesis submitted in partial fulfillment of the requirements for the degree of
Master of Science in Natural Resources

School for Environment & Sustainability
The University of Michigan

May 1st, 2020

Thesis Committee:

Dr. Paul Seelbach, Committee Chair

Dr. Andrew Gronewold, Co-Chair

Dr. Branko Kerkez, Co-Chair

Christine N. Brown

cncbrown@umich.edu

© University of Michigan, 2020

Dedication

To my fellow SEAS folk, with our comradery we charged through difficult and strange times.

To my father, who from a young age inspired me to explore streams.

To Dina DiSantis, who inspired me to study streams and forever changed the course of my career.

And to Bob Muller, who poetically described the underground “Ghost Rivers” of our cities.

*“Only a few, with eyes wide open, can see the ghost of the river
and are able to look into the past.”*

Acknowledgments

This master's thesis would not have been possible without the help of the many people who are bound in the effort to restore the Clinton River Watershed. Foremost, I'd like to thank my thesis advisors, Dr. Paul Seelbach, Dr. Andrew Gronewold, and Dr. Branko Kerkez. I wholeheartedly appreciate the dedication you brought to the research mission and to my professional growth.

I gratefully acknowledge the help from the dedicated staff at OHM Advisors, Inc. for their aid in study design, field assistance, thought-provoking discussion, and moral support, including Dr. Karlin Danielsen, Nathan Zgnilec, Vicki Putala, Robert Czachorski, Valerie Novaes, Derek Klenke, Kayla McRobb, Wade Rose, Nataly Figueroa, James Jones, Mackenzie Johnson, Laura Gallagher, and Humaira Jahangiri.

Thanks to the students from the University of Michigan School for Environment and Sustainability, Department of Civil and Environmental Engineering, and the Doris Duke Conservation Scholars Program for field assistance and data support, especially Megan Houle, Alexander Vandeweghe, Lindsay Canaday, Isaac Balinski, Brandon Wong, and Abhiram Mullapudi. Thanks to Thomas Yavaraski of the University of Michigan Department of Civil and Environmental Engineering for laboratory support in fluorescence spectra analysis.

I'd like to acknowledge the support of Dr. David Szlag of Oakland University and the Huron to Erie Alliance for Research and Training (HEART), Freshwater Center Field Station at Lake St. Clair Metro Park for useful discussion on microbial indicators of fecal contamination and sample processing at all hours of the night.

Special thanks to our project partners in the Clinton River Watershed: Stacey McFarlane with the Macomb County Public Health Department; Candice Miller, Jeffery Bednar, and Amanda Oparka with Macomb County Public Works; James Wineka, Joel Kohn, and Gary Nigro with the Oakland County

Water Resources Commission; and Chris Bobryk with the Clinton River Watershed Council. I hope that this information will be useful in your quest to restore water quality in the Clinton River Watershed.

I wholeheartedly thank the staff from the United States Geological Survey Upper Midwest Water Science Center, especially Lisa Fogarty, Thomas Weaver, and Steven Corsi, for providing guidance from their research experience in fecal contamination monitoring, and for help with citing field monitoring stations.

Finally, I express immense gratitude to our funder, the Michigan Department of Great Lakes, and Energy (EGLE). This project came to fruition with the leadership of Jon Allan (former Director of the Michigan Office of the Great Lakes), and the organizational wisdom of Michelle Selzer (Lake Coordinator in the EGLE Water Resources Division).

Table of Contents

Dedication	ii
Acknowledgments	iii
Table of Contents	v
List of Tables	vii
List of Figures	viii
Abstract	xiii
Chapter 1 - Introduction	1
Fecal Contamination Impacts to Surface Waters	1
Sources of Fecal Contamination	2
Management Policies	2
Monitoring Techniques	3
Study Rationale	6
Chapter 2 - Study Locations	8
Historical Context	8
Geography	9
Geology	10
Land use	13
North Branch Subwatershed	13
Middle Branch Subwatershed	13
Red Run Drain Subwatershed	14
Hydrology	17
North Branch Clinton River	17
Middle Branch Clinton River	17
Red Run Drain	18
Chapter 3 - Methods	20
Field Study Scheme	20
Continuous Water Quality Sampling	20
Continuous Discharge and Water Depth Sampling	21
Discrete E. coli Sampling	22

Detection of Additional Optical Signatures	22
Data Analyses	23
Application of Temperature and Turbidity Correction Algorithms	23
Assessment of Continuous Water Quality Patterns	24
Characterization of Turbidity, TLF, and OB relationships with <i>E. coli</i>	24
Chapter 4 - Results.....	25
Summary of Patterns in Discharge and Water Depth Data.....	25
Summary of Patterns in Continuous Water Quality Parameters	0
Summary of <i>E. coli</i> Data.....	8
Characterization of Turbidity, TLF, and OB relationships with <i>E. coli</i>	10
Investigation of Additional Optical Signatures.....	19
Chapter 5 – Discussion and Conclusions	25
Patterns in Fecal Contamination Indicators	25
Diurnal Patterns	25
Seasonal Patterns	26
Flow-dependent Patterns.....	27
Investigation of Optical Signatures.....	29
Lessons Learned in Field Monitoring	30
Advantages and Disadvantages to Monitoring System Configuration	31
Reporting Units for TLF and OB.....	32
Logistical Constraints of Discrete <i>E. coli</i> Monitoring during Wet-Weather Events	32
Conclusions.....	33
Chapter 6 - Compensating For The Effects of Temperature and Turbidity on Tryptophan-like-Fluorescence and Optical Brighteners	35
Background.....	35
Methods	36
Temperature and Turbidity Corrections for Tryptophan-like-Fluorescence.....	36
Temperature and Turbidity Correction for Optical Brighteners	37
Results and Discussion	40
Calibration Response	40
Optical Brightener Concentration Prediction Models.....	40
Correction Model Evaluation.....	42
Chapter 7 - Bibliography	49

List of Tables

Table 4-1: Descriptive statistics for surface discharge and water depth data collected at the North Branch (NB), Middle Branch (MB), and Red Run Drain (RR) monitoring stations in the Clinton River Watershed over three baseflow seasons (S1, S2, S3). “ND” indicates “no data available”.....	27
Table 4-2: Summary of E. coli data collected at the North Branch (NB), Middle Branch (MB), and Red Run Drain (RR) monitoring stations in the Clinton River Watershed over three storm sampling events (ST1, ST2, ST3). “MPN” indicates the maximum-probable-number of viable cells per 100 mL...	10
Table 4-3: OLS regression model equations, coefficients, and metrics of model performance for correlations between E. coli and turbidity, TLF, or OB over different hydrograph phases, including data isolated to the ascending limb (AL), the descending limb (DL), and the full dataset (FD).....	18
Table 6-1: Calibration equations and measures of fit of laboratory trials based on reference standard solutions of OBs prepared with commercial laundry detergent in deionized water.....	40
Table 6-2: Form of equations for OB concentration (ppm) prediction models with temperature and turbidity correction compensation showing evaluated (E) and selected (S) parameters with coefficients, along with measures of model skill and fit.....	47

List of Figures

Figure 2-1: Valley Segments of the Clinton River. Maps are modified images from the Michigan DNR Fisheries Division, Special Report 39, Clinton River Assessment ³⁹	11
Figure 2-2: Water quality monitoring stations within the Clinton River Watershed, shown with active discharge and flow depth gages from the USGS, flow depth sensors from the University of Michigan Real-Time Water Systems Lab, and streams with active TMDL requirements.	12
Figure 2-3: Extent and classifications of landscape ecosystems (Maumee Lake Plain, Sandusky Lake Plain, Ann Arbor Moraines, and Jackson Interlobate) of the Clinton River Watershed, shown based on surficial geology (top) and topography (bottom). Maps are modified images from the Michigan DNR Fisheries Division, Special Report 39, Clinton River Assessment ³⁹	15
Figure 2-4: Surface Geology of the Clinton River Watershed. Maps are modified images from the Michigan DNR Fisheries Division, Special Report 39, Clinton River Assessment ³⁹	16
Figure 2-5: Comparison of flow duration curves for the Middle Branch and North Branch monitoring stations.....	19
Figure 3-1: Comparison of pump and flow-through cell (left) versus in-situ deployment (right) monitoring configurations. Pump and flow-through cell configuration includes a peristaltic pump, bringing surface water in series through the YSI EXO 2 and Turner Designs C3™ water quality sondes, and outflow back into the stream, as well as power and telemetry devices. The in-situ deployment includes both water quality sondes deployed directly in-stream and protective PVC housing with flow openings (power and telemetry devices are not shown).	21
Figure 4-1: Variation in the distribution of discharge (cfs) or gage height (ft) values across monitoring stations. Boxplots are organized by stormflow or baseflow conditions, and then by baseflow	

season. Baseflow season #1 (S1) represents high spring flows, baseflow season #2 (S2) represents summer low flows, and baseflow season # 3 (S3) represents intermediate fall flows. 26

Figure 4-2: Diurnal fluctuation in temperature, turbidity, TLF, and OB during selected baseflow periods in the summer low flow seasons. Representative TLF data from the summer low flow season was unavailable. 1

Figure 4-3: Variation in the distribution of observed temperature (°C) values across monitoring stations. Boxplots are organized by stormflow or baseflow conditions, and then by baseflow season. Baseflow season #1 (S1) represents high spring flows, baseflow season #2 (S2) represents summer low flows, and baseflow season # 3 (S3) represents intermediate fall flows. 3

Figure 4-4: Variation in the distribution of observed turbidity (NTU) values across monitoring stations. Boxplots are organized by stormflow or baseflow conditions, and then by baseflow season. Baseflow season #1 (S1) represents high spring flows, baseflow season #2 (S2) represents summer low flows, and baseflow season # 3 (S3) represents intermediate fall flows. 4

Figure 4-5: Variation in the distribution of specific conductance (µS/cm) values across monitoring stations. Boxplots are organized by stormflow or baseflow conditions, and then by baseflow season. Baseflow season #1 (S1) represents high spring flows, baseflow season #2 (S2) represents summer low flows, and baseflow season # 3 (S3) represents intermediate fall flows. 5

Figure 4-6: Variation in the distribution of TLF (ppm) values across monitoring stations. Boxplots are organized by stormflow or baseflow conditions, and then by baseflow season. Baseflow season #1 (S1) represents high spring flows, baseflow season #2 (S2) represents summer low flows, and baseflow season # 3 (S3) represents intermediate fall flows. 6

Figure 4-7: Variation in the distribution of OB (ppm) values across monitoring stations. Boxplots are organized by stormflow or baseflow conditions, and then by baseflow season. Baseflow season #1 (S1) represents high spring flows, baseflow season #2 (S2) represents summer low flows, and baseflow season # 3 (S3) represents intermediate fall flows. 7

Figure 4-8: Variation in the distribution of E. coli (MPN) values across monitoring stations. Boxplots are organized by sampling event. Sampling event #1 (ST1) represents sampling that occurred between 6/13 and 6/15/2019, sampling event #2 (ST2) represents sampling that occurred on 10/02/2019, and sampling event #3 (ST3) represents sampling that occurred between 10/22 and 10/24/2019. The red dashed line indicates the upper detection limit for E. coli using Colilert-18, as was pertinent during ST1 when many samples breached this limit. 9

Figure 4-9: Patterns in fecal contamination indicators, including E. coli (MPN), turbidity (NTU), TLF (ppm), and OB (ppm) in response to discharge (cfs) at the North Branch monitoring station during two separate discrete E. coli sampling events. Flow-dependent variation in fecal contamination indicators is exhibited. The numbering of events is consistent with other stations, and sampling during event # 2 was abandoned due to a lack of hydrologic response to precipitation at the North Branch monitoring station. 12

Figure 4-10: Patterns in fecal contamination indicators, including E. coli (MPN), turbidity (NTU), TLF (ppm), and OB (ppm) in response to flow at the Middle Branch monitoring station during three separate discrete E. coli sampling events. OB data was unavailable during sampling events #2 and #3 due to sensor failure. Flow-dependent variation in fecal contamination indicators is exhibited. 13

Figure 4-11: Patterns in fecal contamination indicators, including E. coli (MPN), turbidity (NTU), TLF (ppm), and OB (ppm) in response to flow (gage height (ft) serves as proxy) at the Red Run Drain monitoring station during three separate discrete E. coli sampling events. Flow-dependent variation in fecal contamination indicators is exhibited. 14

Figure 4-12: Relationships between turbidity (NTU) and E. coli (MPN) with 95% confidence intervals using the entirety of the field sampling dataset (left), data isolated to the descending limb of the hydrograph (center), and data isolated to the descending limb of the hydrograph (right). 15

Figure 4-13: Relationships between TLF (ppm) and E. coli (MPN) with 95% confidence intervals using the entirety of the field sampling dataset (left), data isolated to the ascending limb of the hydrograph (center), and data isolated to the descending limb of the hydrograph (right). 16

Figure 4-14: Relationships between OB (ppm) and E. coli (MPN) using the entirety of the field sampling dataset (left), data isolated to the ascending limb of the hydrograph (center), and data isolated to the descending limb of the hydrograph (right) with 95% confidence intervals. 17

Figure 4-15: Excitation-emission matrices recorded from surface water samples at the North Branch Monitoring Station during baseflow conditions. Letters represent peak signal names associated with excitation and emission pairs. Coloration indicates relative fluorescence intensity within the sample, increasing from cool to warm colors. High intensities on the diagonal are indicative of light scattering associated with identical excitation and emission wavelengths, and should be ignored. 20

Figure 4-16: Excitation-emission matrices recorded from surface water samples at the Middle Branch Monitoring Station during baseflow conditions. Letters represent peak signal names associated with excitation and emission pairs. Coloration indicates relative fluorescence intensity within the sample, increasing from cool to warm colors. High intensities on the diagonal are indicative of light scattering associated with identical excitation and emission wavelengths, and should be ignored. 21

Figure 4-17: Excitation-emission matrices recorded from surface water samples at the Red Run Drain Monitoring Station during baseflow conditions. Letters represent peak signal names associated with excitation and emission pairs. Coloration indicates relative fluorescence intensity, increasing from cool to warm colors. High intensities on the diagonal are indicative of light scattering associated with identical excitation and emission wavelengths, and should be ignored..... 22

Figure 4-18: Excitation-emission matrices recorded from surface water samples from the wastewater treatment plant influent during baseflow conditions. Letters represent peak signal names associated with excitation and emission pairs. Coloration indicates relative fluorescence intensity within the sample, increasing from cool to warm colors. High intensities on the diagonal are indicative of light scattering associated with identical excitation and emission wavelengths, and should be ignored. 23

Figure 4-19: Excitation-emission matrices recorded from surface water samples from the wastewater treatment plant effluent during baseflow conditions. Letters represent peak signal names associated with excitation and emission pairs. Coloration indicates relative fluorescence intensity within

the sample, increasing from cool to warm colors. High intensities on the diagonal are indicative of light scattering associated with identical excitation and emission wavelengths, and should be ignored. 24

Figure 6-1: Temperature quenching effect on OB fluorescence at six reference standard concentration (50, 25, 12.5, 6.25, 2.5, 0.25ppm). 44

Figure 6-2: Comparison of temperature compensation coefficient estimation for individual OLS regressions for a series of known reference standard solutions of OB. 45

Figure 6-3: Turbidity inference effects on OB Fluorescence for four reference standards (2.5, 6.25, 12.5, and 50 ppm). 46

Figure 6-4: Reference standard concentrations versus predicted concentrations using a generalized linear model with both log-linear and squared transformation of predictor variables, including temperature and turbidity as interaction terms. Diagonals are presented to show the idealized prediction model ($m = 1, \beta_0 = 0$) and deviations in bias with reference standard concentration. 48

Abstract

Fecal contamination is a wide-spread impairment to riverine and near-shore environments across the state of Michigan. Where fecal contamination is present, harmful human pathogens are likely to exist, potentially resulting in infectious diseases such as giardia, hepatitis, cholera, and other gastrointestinal upsets. Fecal contamination may also carry with it contaminants such as nutrients, pharmaceuticals, endocrine disruptors, and toxic compounds that cause adverse disruptions to aquatic ecosystems. Water quality indicators, such as Escherichia coli (E. coli), are used by state and local governments to characterize the extent of fecal contamination. While E. coli water quality standards have laid the groundwork for monitoring fecal contamination, they are limited by the poor timeliness between E. coli sampling and lab analysis results. Additionally, wet-weather monitoring of E. coli requires substantial personnel availability and poses safety risks for those sampling. However, emergent technologies present a potential solution to these restrictions. Particularly, optical signals such as tryptophan-like-fluorescence (TLF) and optical brighteners (OB), along with nephelometric turbidity, have been correlated with fecal contamination in previous studies. These parameters can be monitored more easily than E. coli, and in a continuous fashion to provide high volumes of data.

My research demonstrates the applicability of optical sensors for real-time indication of fecal contamination and provides specific recommendations for using this technology in the Clinton River Watershed. In this study, a team of researchers conducted a six-month pilot study to evaluate the validity and practicality of using these parameters across various hydrologic conditions at three unique monitoring locations. I tested the predictive ability of TLF, OB, and turbidity to detect the magnitude of fecal contamination by correlating these parameters with discrete E. coli samples enumerated through culture-based methods. I demonstrated that all three parameters were significant predictors of E. coli concentration across hydrograph phases, and prediction strength was strongest using data from the ascending limb of the hydrograph. Turbidity and TLF demonstrated either linear or log-linear regression relationships with E. coli in all models. The relationship between OB and E. coli was best fit for a cubic curve using data from the ascending limb of the hydrograph, yet the model for the descending limb was linear. Using TLF and turbidity as predictor variables, values for correlation strength were comparable with previous studies. Correlation strength using OB was highest among all parameters ($r = 0.77$). Model fit was relatively weak and highly dependent on sample size, demonstrating the need for additional data from multiple storms in the same season. Hydrology patterns influenced seasonal ranges for all three parameters. Additionally, strong diurnal patterns demonstrated the need for instrument-specific temperature correction algorithms.

In addition to validating the predictive ability of TLF, OB, and turbidity to detect E. coli, I provide extensive “lessons-learned” on the practicality of using optical sensors for continuously detecting fecal contamination. This study demonstrated noteworthy constraints associated with long-term deployments, compelling practitioners to optimize deployment configurations, maintenance plans, and data post-processing protocol in future applications. Despite these constraints, this study reveals how optical sensors could be used to provide a rapid indication of microbial pollution, and aide practitioners in source tracking of fecal contamination.

Chapter 1 - Introduction

Fecal Contamination Impacts to Surface Waters

Fecal contamination is a wide-spread impairment to riverine and near-shore environments across the State of Michigan. Where fecal contamination is present, harmful human pathogens are likely to exist, resulting in infectious diseases and gastrointestinal upsets. Common disease-causing pathogenic organisms include *Vibrio cholera* (bacterium causing Cholera) and *Salmonella typhimurium* (bacterium causing typhoid), which are endemic across the world and cause up to 143,000¹ and 223,000² annual deaths, respectively. In the United States, the former diseases are of historical importance, while *Giardia lamblia* (causing beaver fever) and *Cryptosporidium parvum* today pose a greater concern. Exposure to fecal contamination in surface waters comes from a variety of pathways, including ingestion via partial and total body contact in recreational waters, contamination of drinking water sources, and consumption of contaminated seafood (primarily bivalves). Antibiotic-resistant bacteria are now being found in natural waters³, an ominous prelude to the future effectiveness of antibiotics and disease prevention.

Fecal contamination from wastewater often comes alongside contaminants such as nutrients, pharmaceuticals, endocrine disruptors, microplastics, and toxic compounds that cause adverse disruptions to aquatic ecosystems. Contaminants at a specific stream or river site depend on the source of wastewater. For instance, domestic wastewater often contains detergents, fat sources, and trace pharmaceuticals. Agricultural wastewater may carry with it salts, pesticides, and fertilizers. Urban wastewater from combined sewers and storm drains often transports petrochemicals from roadways. Industrial wastewater contains a wider range of pollutants including those previously listed, and are also known to contain acids and radioactive materials.

Bacteria and other organisms living in wastewater streams consume oxygen to metabolize the sewage they accompany. For this reason, sewage is deemed an oxygen-demanding material. The

consumption of dissolved oxygen (DO) poses a threat to aquatic life forms. When DO levels drop below critical levels for various species, hypoxic “dead zones” can form and mortality ensues.

Sources of Fecal Contamination

Fecal contaminants can enter aquatic ecosystems from either point or nonpoint sources, and are typically associated with human or animal feces. Wastewater treatment plants and combined sewer overflows are the most significant point sources of human fecal contamination. Other point sources include illicit connections of sanitary lines to storm sewers, and the illegal dumping of waste material. Nonpoint sources vary depending on the predominant land-use type in a given watershed. Nonpoint sources from urban areas include leaky sewer lines, pet waste, wildlife, and urban litter. In agricultural areas, fecal contamination tends to stem from failing septic systems, confined animal feeding operations (CAFOs), and the application of manure as fertilizer⁴.

Management Policies

In an attempt to address the detrimental impacts of fecal contamination, public lawmakers developed measures to assist communities in remediating fecal contamination from surface waters in the United States (and worldwide). The Federal Clean Water Act Section 303(d)⁵ outlines the processes used to address water quality standard exceedances in surface waters. This act authorizes the Environmental Protection Agency (EPA) to assist states, territories, and authorized tribes in listing impaired waters and developing Total Maximum Daily Loads (TMDLs) for these water bodies. A TMDL establishes the maximum amount of a pollutant allowed in a waterbody and serves as the starting point or planning tool for restoring water quality.

Water quality indicators, such as *Escherichia coli* (*E. coli*), are used by state and local governments to characterize the extent of fecal contamination. In Michigan, state water quality standards (WQS) were developed for *E. Coli* to protect overall human health and recreational water use. The Lower Clinton River does not meet the current WQS for *E. coli*⁶, and thus the Michigan Department of Environment, Great Lakes, and Energy (EGLE) developed a TMDL requirement as a tool to restore water

quality in the watershed. The TMDL requirement for *E. coli* is a flow-based approach, setting load targets based on a location's flow duration curve and assigning load allocations to various point and non-point sources. Point source discharges are addressed through discharge permits (US EPA NPDES), while nonpoint sources are left to be addressed by watershed managers and local stakeholders.

Monitoring Techniques

To effectively reduce the harmful side effects of fecal contamination to waterways, watershed managers across the globe use monitoring techniques to track down resources and prioritize remediation efforts. In the United States, the principal indicators for waterborne pathogens are total coliform, fecal coliform, enterococci, and *E. coli* bacteria. Of the four, *E. coli* is the most numerous member of the coliform group found in the feces of warm-blooded animals. Historical efforts were made to develop a more sensitive way to discern fecal contaminated water (a fecal contamination index) in the late 19th century by Theodore Escherich of Germany, and a presumptive test using lactose-based fermentation tube tests in 1891 was developed by the New York Department of Health⁷. Work performed under the United States Public Health Service (USPHS) in Cincinnati demonstrated that *E. coli* measurements could be used to estimate *Salmonella typhimurium* in sewage latent waters⁸. Further research demonstrated that *E. coli* were resistant to disinfection as compared to other bacterial pathogens⁹ and therefore, this measurement technique became solidified as a method for determining fecal contamination in water resources.

Method refinement to the traditional *E. coli* test is constantly evolving as questions have surfaced concerning the suitability of *E. coli* as a bacterial indicator of sewage-contaminated waters. In tropical and subtropical climates, the suitability of *E. coli* as a sewage indicator has been questioned as some *E. coli* populations can be naturally present in the environment¹⁰⁻¹³. *Enterococcus*¹⁴ and *Clostridium perfringens*¹⁵ have been used as alternatives indicators to address these issues. Despite method refinements, the detection of these indicators via culture-based methods provides relative abundance, but little information related to the origin of the contamination (human versus non-human). For water quality

managers, this can further complicate remediation efforts. Microbial source tracking (MST) methods surfaced to detect host-associated DNA markers and identify different sources of fecal contamination, including humans, cows, gulls, and dogs¹⁶⁻²¹. MST methods are now available as quantitative polymerase chain reaction (qPCR) tests, enabling the rapid quantification of sources and providing information more quickly than traditional culture-based methods.

Even still, surface water monitoring of bacterial pathogens is limited by the poor timeliness between sampling and lab analysis, thereby hindering the availability of results and the ability to capture target conditions (e.g. peak *E. coli* levels) for use in early warning systems. Peak *E. coli* levels in riverine systems often occur during the “first-flush” when rapid changes in water quality occur in the early phases of a storm event (ascending limb of the hydrograph). Wet-weather monitoring of *E. coli* (throughout the storm and associated stream flood) requires substantial personnel availability, particularly when the aim is to characterize how multiple sites respond to the same storm. In extremely flashy runoff events with short-term peak flows, periodic discrete grab sampling of *E. coli* has a low probability of identifying microbial concentrations that indicate human health risk. Even when characterization is successful, the effort poses safety risks to those sampling through exposure to fecal contamination and the risk of drowning in floodwaters, among other hazards.

However, emergent technologies using fluorescence spectrophotometry present a potential solution to these restrictions. The use of submersible fluorometers is emerging as an alternative to traditional fecal contamination monitoring. Modern fluorometers are capable of continuously measuring sewage-associated fluorophores, and transmitting data remotely when coupled with telecommunication devices. Surface waters laden with fecal contamination exhibit optical characteristics that can be detected in specific regions of the fluorescence and absorbance spectra. That is, an Excitation-Emission-Matrix (EEM) can be created by simultaneously scanning of excitation and emission wavelengths through an aqueous sample. Each fluorophore (a fluorescent chemical compound that can re-emit light upon light excitation) in the sample is said to have an excitation-emission pair, and appears on the EEM as a peak or series of peaks associated with the excitation-emission pair. The most common fluorophores in natural

surface waters are humic-like, derived from plant material decay (peaks C and A). “Tryptophan-like-fluorescence” (TLF or peak T at 280 nm excitation/360 nm emission wavelength) has been shown to relate to the microbial activity in natural surface waters, showing strong correlations with BOD₅²² and fecal contamination associated with *E. coli*, which is typically associated with warm-blooded animals. Cumberland et al.²³ demonstrated positive correlations between enumerated total coliforms, *E. coli*, and heterotrophic bacteria; and TLF ($R^2=0.78, 0.72, \text{ and } 0.81$, respectively) from uncultured samples of diluted river water and sewage networks with a portable fluorometer. Sorenson et al.²⁴ demonstrated the use of in-situ fluorometers targeting TLF as a rapid indicator of the presence or absence of thermotolerant fecal coliforms found in groundwater-derived potable water supplies.

Another fluorophore, associated with a class of compounds called optical brighteners (OB), boasts promise as a surrogate for detecting fecal contamination. These fluorescent whitening agents are added to most laundry detergents²⁵, and emit light in the blue range (415-445 nm). Signal peaks in this range may thus indicate the presence of domestic wastewater streams. The measurement of OB with fluorometers is gaining popularity as a method for source tracking applications to indicate human-derived fecal contamination. Several studies have demonstrated that high fluorometric readings of OB are indicative of high fecal indicator bacteria counts²⁶⁻²⁸. Yet, this was not the case for pioneer studies^{29,30}, where it is thought that unidentified chemicals that absorb and emit light at similar wavelengths to that of OB (organic matter and aromatic compounds) led to false detection. In this way, the validity of OB in detecting fecal contamination from residential sewage sources seems to be dependent on the site-specific water quality conditions. Therefore, it is necessary to validate the relationship between *E. coli* and OB at specific monitoring sites before it is employed in a continuous fashion.

Additionally, turbidity is becoming increasingly popular as an indicator of microbial water quality in both riverine^{31,32} and near-shore^{33,34} environments. Watersheds impacted by development exhibit higher levels of suspended solids and associated turbidity during storm events relative to unimpacted watersheds. Fecal-associated microorganisms are often transported during surface runoff events, although this occurrence depends on land use and stormwater infrastructure³⁵. Therefore, the

association of turbidity with fecal contamination is specific to catchment conditions and local stormwater management practices.

Turbidity, OB, and TLF can be monitored continuously with in-situ water quality sondes, and in real-time using cellular telemetry, to overcome the challenges of traditional field sampling methods. Continuous data collection also generates greater quantities of data than discrete sampling, and can provide insight on how fecal contamination levels vary with flow conditions. This could greatly improve monitoring efforts and subsequent management actions with respect to TMDL regulations. Real-time data availability can help guide the timing of grab samples by providing visual confirmation of spikes in fluorescence intensity during wet-weather events. Together, these indicators can help assess inputs of fecal contamination.

Study Rationale

Despite the potential for TLF and OB to serve as effective, continuous, and real-time indicators of fecal contamination, limited studies exist that demonstrate their effectiveness at high-resolutions through the progression of stormflow events. Correlation strength between these fluorophores and fecal indicator bacteria (such as *E. coli*) has yet to be evaluated in this scenario. Understanding these relationships is paramount for managing fecal contamination in stormwater runoff. Does flow magnitude influence the strength of these correlations? Are there flow magnitude thresholds? How do these relationships vary with other water quality parameters, such as turbidity, temperature, and specific conductance? Do other fluorophores (e.g. dissolved organic matter) interfere with the signals of TLF and OB?

I sought to answer these research questions as applied to a specific study area, the Clinton River Watershed. My primary objective was to evaluate the validity of different fecal contamination monitoring indicators, including fluorescence from TLF and OB, across various hydrologic conditions. We tested the ability of these parameters to predict the magnitude of fecal contamination by correlating continuous TLF, OB, and turbidity data with discrete *E. coli* samples enumerated through culture-based methods. Monitoring data were collected over a six-month monitoring campaign at the mouths of three different

tributaries to the Clinton River, each with a distinct flow regime. Additionally, I performed a preliminary exploration of the full excitation-emission spectrum at each site to determine if other signals may be stronger indicators of fecal contamination, and if signal interference among fluorophores was present. My second objective was to explore the practicality of using in-situ optical sensors to monitor fecal contamination in the riverine environment. This pilot study will provide information to practitioners on the “lessons learned” of working with these emergent technologies. My final study objective was to characterize the water quality patterns at each monitoring location through descriptive statistics. This information will allow practitioners to understand the flow-driven behaviors of local water quality impairments, aside from fecal contamination, for improved restoration and management efforts.

Chapter 2 - Study Locations

Historical Context

The Clinton River Watershed, located north of Detroit in Southeast Michigan, is the focus of water quality restoration efforts due to contamination problems that stem from industrial pollution and rapid urbanization. The Lower Clinton River and two tributaries, the Red Run Drain, and Bear Creek do not meet the Michigan WQS for *E. coli*, and thus the Michigan Department of Environment, Great Lakes, and Energy (EGLE) developed Total Maximum Daily Load (TMDL) requirements for both tributaries as tools to restore water quality^{6,36}. The numeric targets for the TMDL are based on the Total Body Contact (TBC) and Partial Body Contact (PBC) beneficial uses for recreational waters. Exceedances are either determined by a daily maxima or 30-day geometric mean limitation. The daily maxima for TBC is 300 *E. coli* per 100 mL, and 1,000 *E. coli* per 100 mL for PBC. The 30-day geometric mean is 130 *E. coli* per 100 mL. By not meeting the WQS, these beneficial uses are determined to be “impaired”. In the Lower Clinton River TMDL assessment, the highest 30-day geometric means reached 1,778 *E. coli* per 100 mL in the Harrington Drain tributary, and the highest daily maxima for *E. coli* reached 32,166 *E. coli* per 100 mL following a minor rainfall event of 0.09 inches⁶.

The TMDL requirement for *E. coli* is a flow-based approach, setting load targets based on a site’s annual flow duration curve and assigning load allocations during lower and higher flows that relate to various point and non-point sources. Point source discharges are addressed through discharge permits (US EPA NPDES), while non-point sources are left to be addressed by watershed managers and local stakeholders. Addressing the *E. Coli* TMDL requirement is a primary concern for the watershed managers in the area, and the state has led numerous efforts to fund *E. coli* source tracking and infrastructure improvements, including a comprehensive illicit discharge elimination program³⁷. Much of the funding for remediation comes through the U.S. EPA Great Lakes Restoration Initiative (GLRI). The U.S. EPA

designated the Clinton River as one of thirty-one U.S. Areas of Concern (AOC) under the 1987 Great Lakes Water Quality Agreement. This designation allows local watershed managers to apply for project funding through the GLRI to remediate priority water quality impairments, namely heavy metals, polychlorinated biphenyls, and conventional pollutants including oil and grease, nutrients, total dissolved solids, and fecal coliform bacteria. With GLRI support, an assemblage of local watershed managers and stakeholders have undertaken a sophisticated modeling and monitoring effort. My study was to explore how TLF and OB indicators might help with this larger effort.

The most likely sources of fecal contamination in the Clinton River Watershed are of non-point source origins, including stormwater runoff from urban areas, failing septic systems, sediment resuspension related to altered hydrology, sanitary sewer overflows, wildlife, pet waste, illegal dumping of waste material, and illicit connections to the storm sewer system³⁸. However, the degree to which any source contributes to the overall load is specific to each subwatershed and related tributary. Additionally, each subwatershed presents varying streamflow regimes based on surficial geology, topography, catchment size, land use, and other human alterations. It is reasonable to hypothesize that the relationship between flow and the degree of contamination, and thus the validity of fecal contamination indicators, will vary in tune with the local flow regime. Therefore, three sites with varying source contributions and flow regimes within the Clinton River Watershed were selected for my pilot study.

Geography

The Clinton River drains approximately 763 square miles of Southeast Michigan, emptying into Lake St. Clair. The main stem of the river receives flow from 260 miles of major tributaries. The physical, chemical, and biological characteristics of the Clinton River vary considerably from the headwaters to the mouth of the river. The river can be divided into five valley segments with different flow regime drivers; the headwaters, the middle segment, the upper segment, the lower segment, and the mouth segment (Figure 2-1)³⁹.

Three monitoring stations were selected for this pilot study, all three were in the lower river segment (Figure 2-2). Monitoring stations were near the mouths of tributaries that each drained distinctive sub-watershed landscapes; these were the North Branch Clinton River, the Middle Branch Clinton River, and the Red Run Drain. Selection criteria for stations within these tributaries included access and safety, deployment feasibility, opportunities for vandalism, representation of water quality in each subwatershed, availability of surface-water discharge data, and prior fecal contamination monitoring. The North Branch monitoring station is located at the M-59 (Hall Road) crossing, approximately 3.8 miles upstream of the confluence with the Clinton River main stem. The Middle Branch monitoring station is located at the crossing with Romeo Plank Road, approximately 9.5 miles upstream of the main stem. The Red Run Drain station is located at the 14-mile road crossing, approximately 3.1 miles upstream of the main stem.

Geology

Glaciation during the Pleistocene Epoch was the major driver of Michigan's landscape and geology (Figure 2-3)³⁹. The far west end of the watershed is characterized by "kettle hole" geology (Jackson Interlobate) due to rapid glacial retreat, forming numerous lakes and wetlands. End moraines (Ann Arbor Moraines) structured the hilly landscape in the mid-section of the Clinton River, whereas the eastern side formed from flat-lying former lacustrine deposits (Maumee Lake Plain). All three of the monitoring stations rest within the Maumee Lake Plain formation. The North Branch subwatershed begins on glacial outwash sand and gravel, and crosses into medium-textured till from end moraines; however the majority drains lacustrine deposits of sand, clay, and silt.

Above the surficial geology, fine-textured lacustrine soils define much of the poor infiltration capacity of the subwatersheds. The Red Run Drain stations drains a lacustrine clay and silt subwatershed, while the Middle Branch subwatershed soils are slightly coarser lacustrine sand and gravel (Figure 2-4)³⁹. Finer soils with reduced hydraulic capacity are likely to yield more run-off than coarser soils, which we expect to be reflected in the hydrologies of the various tributaries.

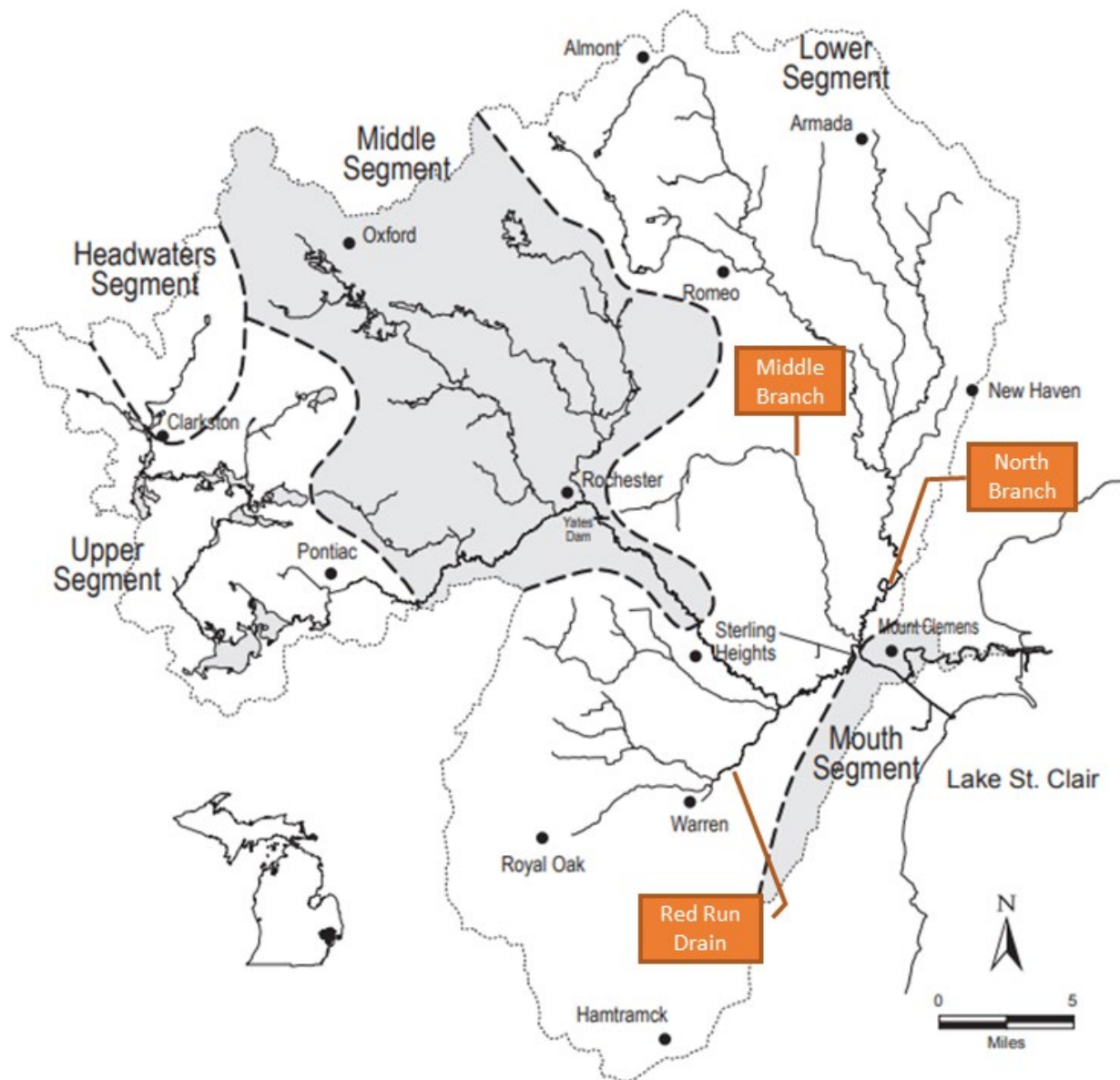
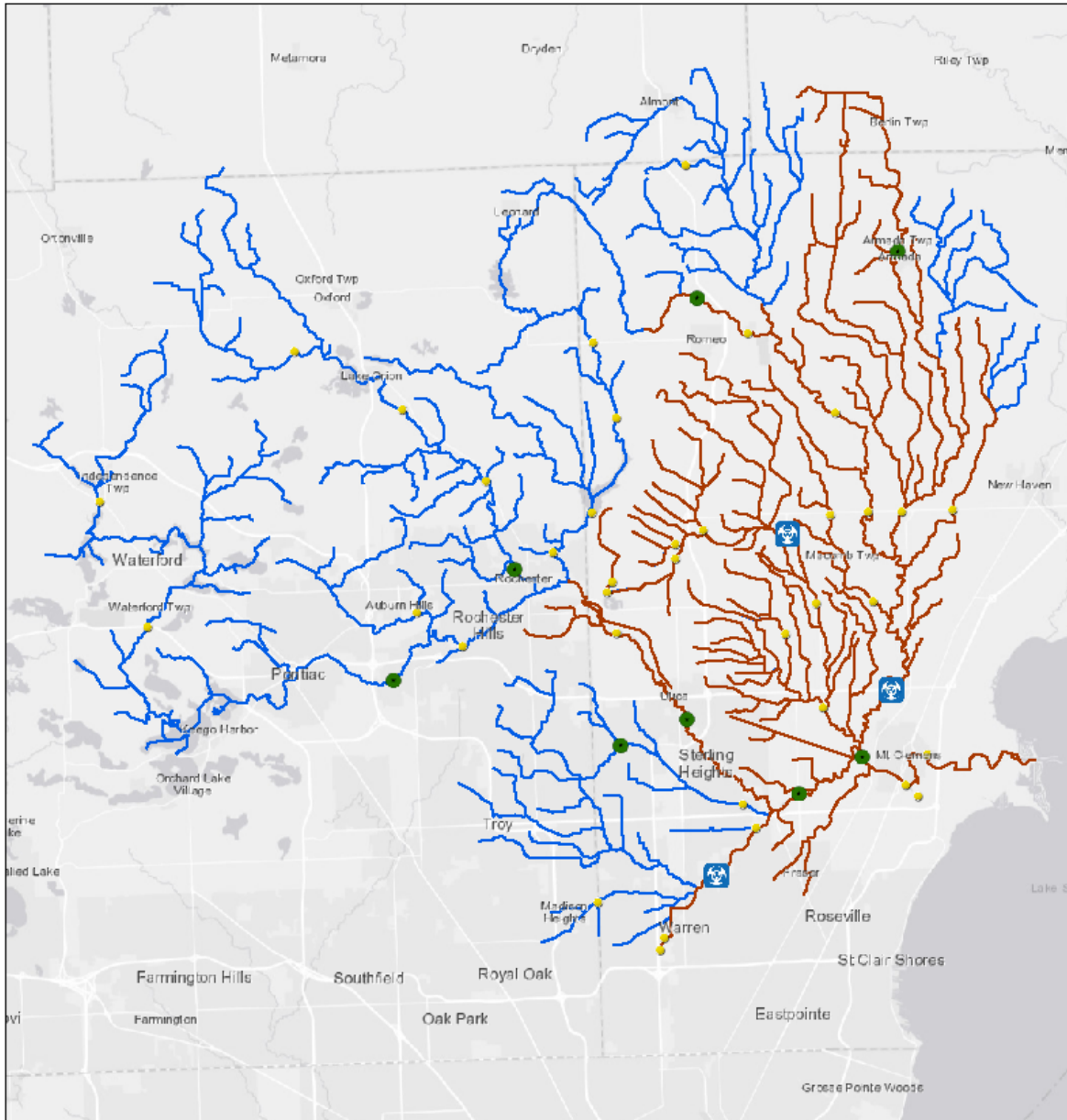







Figure 2-1: Valley Segments of the Clinton River. Maps are modified images from the Michigan DNR Fisheries Division, Special Report 39, Clinton River Assessment³⁹.



March 25, 2020

-  Water Quality Monitoring Locations
-  USGS Active Gage Station
-  U of M Water Elevation Sensors
-  Clinton River Network - TMDL Streams
-  Clinton River Network

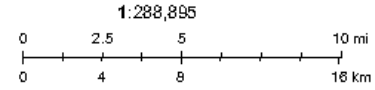


Figure 2-2: Water quality monitoring stations within the Clinton River Watershed, shown with active discharge and flow depth gages from the USGS, flow depth sensors from the University of Michigan Real-Time Water Systems Lab, and streams with active TMDL requirements.

Land use

North Branch Subwatershed

Land use type is an important factor influencing the physical conditions in the watershed, primarily in that it determines the amount of low-permeability and impervious surfaces that drive stormwater runoff. Impervious area routes fast-moving stormwater runoff into collection systems, and in many areas of the subwatershed this flow is routed directly into streams from stormwater outfalls. Of the 200 acres in the North Branch Subwatershed, nearly half (99 acres) is cultivated land (agricultural). The next major classifications include residential development (29 acres), open space (21 acres), urban development (8 acres), or woodland area (25 acres), with the remainder comprising of open water or areas without data. Together, the varying land use types yield an estimated impervious area coverage of 6.5%, as determined by the Clinton River North Branch Subwatershed Management Plan⁴⁰. Likely sources of fecal contamination associated with large areas of cultivated land are failing drainage tile systems, pastured animals with direct stream access, and groundwater contamination of surface waters where animal waste is allowed to accumulate near surface waters. Additional sources linked to residential land use in this subwatershed are failing septic systems, wildlife and pet waste, and illicit connections (either directly to surface waters or storm sewers)⁶.

Middle Branch Subwatershed

Development patterns in the Middle Branch Subwatershed fall somewhere between the other two stations in terms of impervious area coverage. Of its 41.6 acres, the primary land uses are residential development (18.36 acres) and cultivated land (15.88 acres), followed by woodland and wetlands (2.82 acres), commercial uses (1.77 acres), and the remainder is spread across, industrial, institutional, transportation, and open water uses. The combined land use types yield an estimated impervious cover of 13.5%, as determined by the Clinton River East Subwatershed Management Plan³⁸. Similar to the North Branch, illicit connections, wildlife and pet waste, and failing septic systems are sources of concern in this subwatershed, with agricultural resources to a lesser degree⁶.

Red Run Drain Subwatershed

Of the three subwatersheds, the Red Run Subwatershed is by far the most urbanized and impervious, yielding much higher runoff rates than the other two stations. Of the 91 acres of drainage area, more than half is residential development (54 acres), succeeded by industrial uses (11 acres), commercial uses (11 acres), institutional spaces (5 acres), active construction (3 acres), followed by limited areas of open space, woodland and wetlands, open water, and cultivated land⁴¹. The combined land use types yield an estimated impervious area coverage of 34.1%. Given that majority of the watershed is in a highly populated urban area, the most likely sources of *E. coli* are from human-derived sources. During dry-weather, illicit connections of wastewater to storm sewers are a primary concern. Several illicit connections, including subdivision drains, business parks, public schools, and an apartment complex, were confirmed in the 2006 TMDL. Leaking septic or sanitary sewers may also contribute to contamination during dry-weather. During wet-weather, fecal contamination is mobilized throughout the subwatershed. Surface run-off carries wildlife and pet waste. High flows can overwhelm the sewer system, with excessive infiltration into leaky sewers driving sanitary sewer overflows (SSOs). In areas with combined sewers, excessive stormwater quantity can lead to combined sewer overflows (CSOs), and discharges from the City of Warren Wastewater Treatment Plant (WWTP)³⁶.

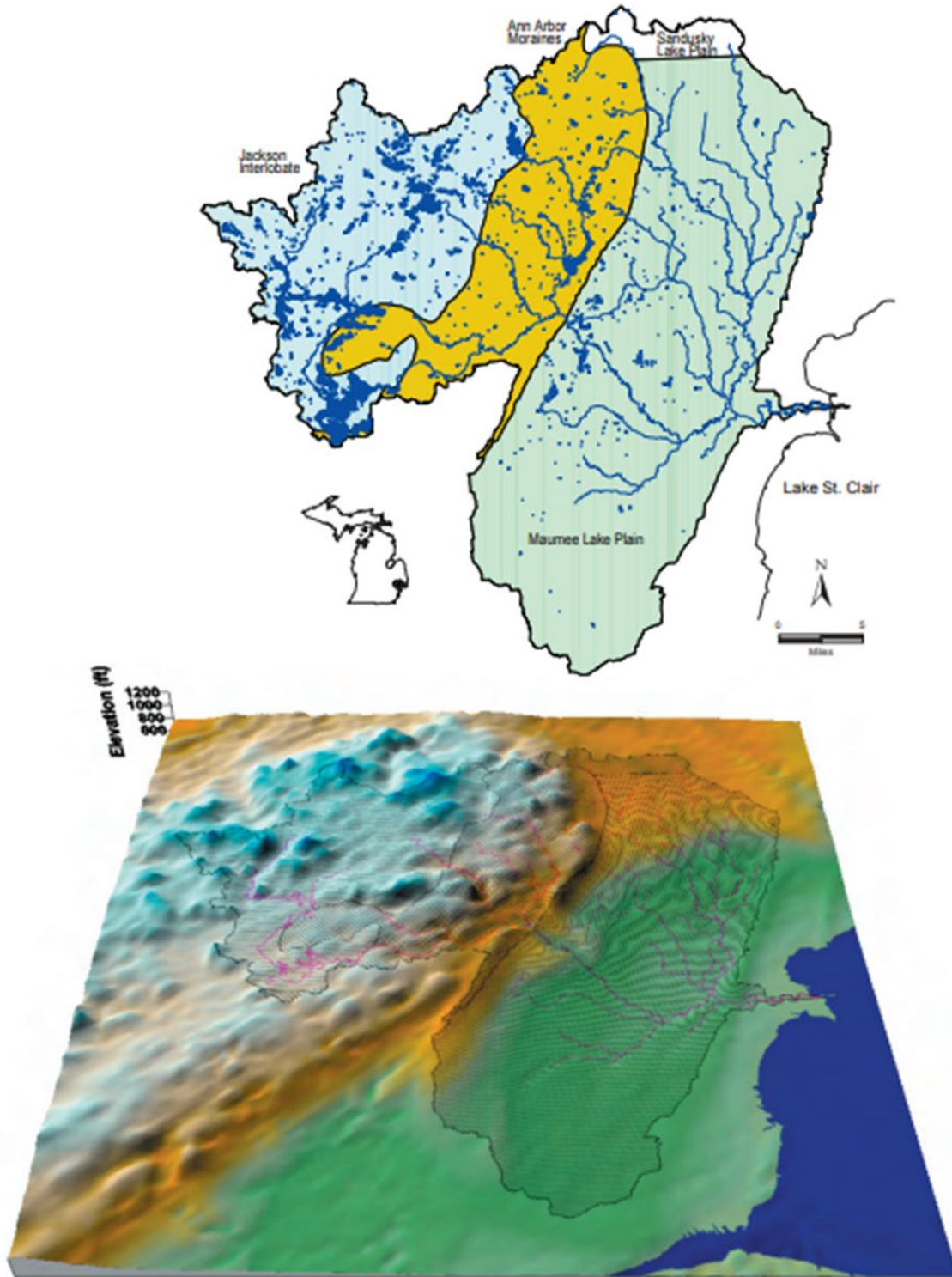


Figure 2-3: Extent and classifications of landscape ecosystems (Maumee Lake Plain, Sandusky Lake Plain, Ann Arbor Moraines, and Jackson Interlobate) of the Clinton River Watershed, shown based on surficial geology (top) and topography (bottom). Maps are modified images from the Michigan DNR Fisheries Division, Special Report 39, Clinton River Assessment³⁹.

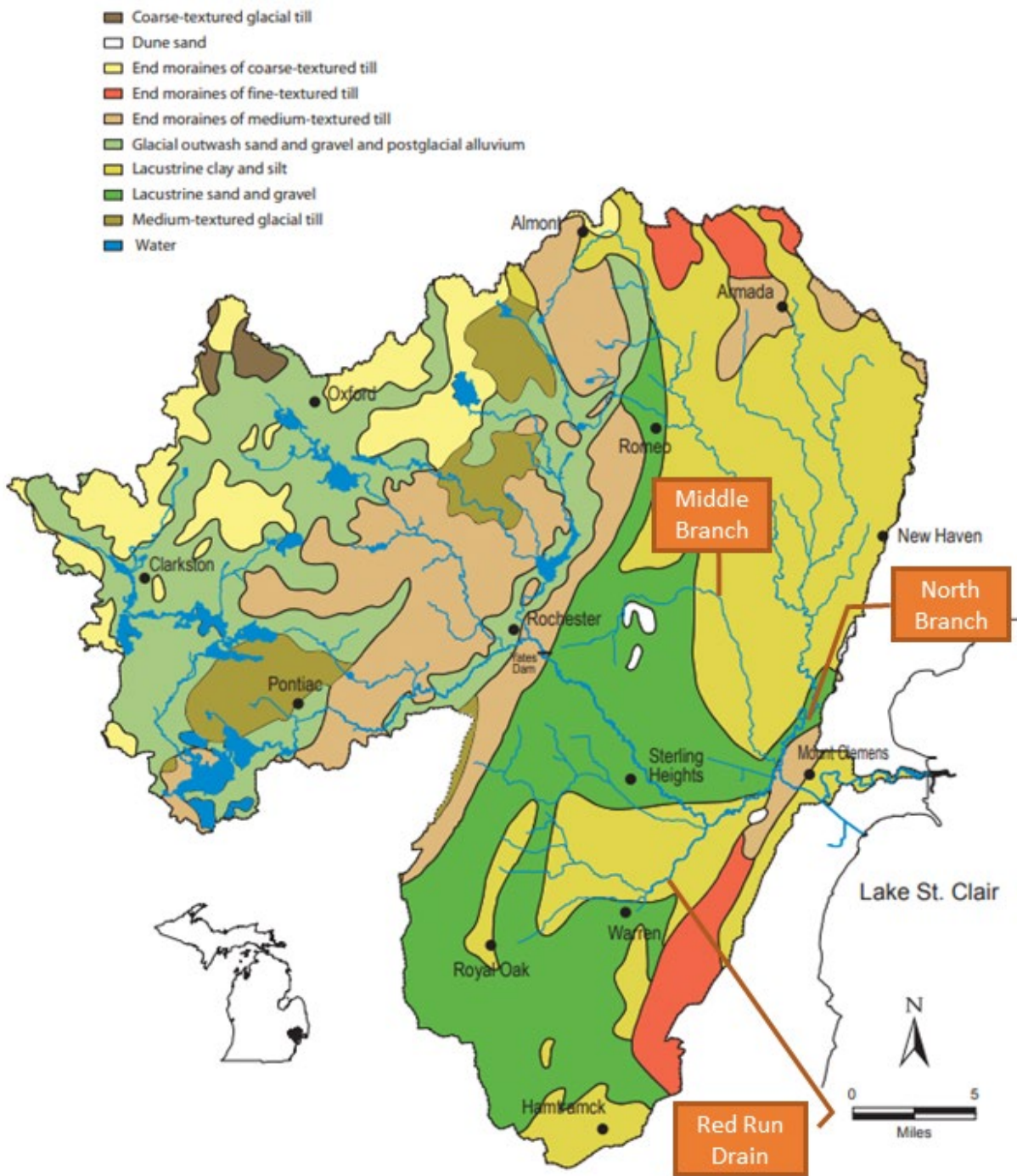


Figure 2-4: Surface Geology of the Clinton River Watershed. Maps are modified images from the Michigan DNR Fisheries Division, Special Report 39, Clinton River Assessment³⁹

Hydrology

North Branch Clinton River

The North Branch of the Clinton River drains approximately 200 square miles, running nearly forty-three miles from the headwaters in Almont and Bruce Townships to the confluence with the main stem. It has the largest of the three subwatersheds in this study. Somewhat coarse glacial materials in a small portion of the northwest region of the subwatershed allow for positive groundwater flow, and the potential for groundwater/surface water interactions. However, lacustrine deposits throughout the remainder of the subwatershed limit these interactions, causing poor infiltration throughout the majority of the watershed. Therefore, surface runoff dictates much of the flow variation in this tributary. Monthly mean flows for 2018 peaked in February at 453 cfs, in stark contrast with the minimum mean flows in September at 19.5 cfs, indicating that the flow regime is quite variable and heavily influenced by seasonality. Over the period of record at the USGS gaging station (04164500) that sits adjacent to the North Branch monitoring station, the maximum discharge reached 6,400 cfs and the minimum dropped to 0.09 cfs⁴². In comparison to undeveloped watersheds of similar surficial geology and slope, the North Branch likely provides much higher storm flows since the hydrologic response is influenced by land use changes. Increasing hydrologic response is expected with the development that has occurred across the subwatershed over the past forty years. Types of development that may contribute to the increase hydrologic response over time may include residential development, and the collection of precipitation by drainage tiles that would otherwise be evaporated, infiltrated, or absorbed⁴⁰.

Middle Branch Clinton River

The Middle Branch drains approximately 19.4 acres, beginning at the Village of Romeo and Bruce Township, then moving downstream through Washington, Ray, Shelby, and Macomb Townships and into Clinton Township where it enters into the North Branch of the Clinton River upstream of Cass Ave. The steady and cool baseflow here is fed by a valley of lacustrine sand and gravel. Despite this seemingly stable input of groundwater, this station still experiences great variability in the seasonal flows

and rapid hydrologic response to storm events. Monthly mean flows for 2018 reached their maximum in February at 89.5 cfs, and dropped to a low in July at 8.16 cfs, constituting an order of magnitude in difference⁴². Impervious area coverage falls between that of the North Branch and the Red Run Drain, yet infiltration rates are also driven by coarse-textured surficial geology (sand and gravel lacustrine deposits). In comparing the flow duration curves between the North Branch and the Middle Branch stations, it's clear that both stations exhibit steep curves, indicating flashy flow regimes (Figure 2-5). Yet, the Middle Branch station produces a higher baseflow yield due to steady seepage from groundwater storage.

Red Run Drain

Insufficient data exist to characterize the hydrology at the Red Run Drain monitoring station. Fluvial geomorphology indicators (incised stream banks, large-scale channelization, streambank erosion, etc.), flood event records, and land use patterns in the subwatershed suggest the system is extremely responsive to rainfall⁴¹. Analyzing flow trends at this station is complicated by drainage system modifications, including the George W. Kuhn combined sewer system, which drains a significant portion of the subwatershed. This flow is routed to the Detroit Water Sewer District, Wastewater Treatment Plant, unless combined sewer overflows discharge portions of it back into the Red Run Drain. The City of Warren Wastewater Treatment Plant continuously releases treated effluent discharge approximately 0.9 miles upstream of the monitoring station, providing the majority of baseflow in summer months.

Flow Duration Curves

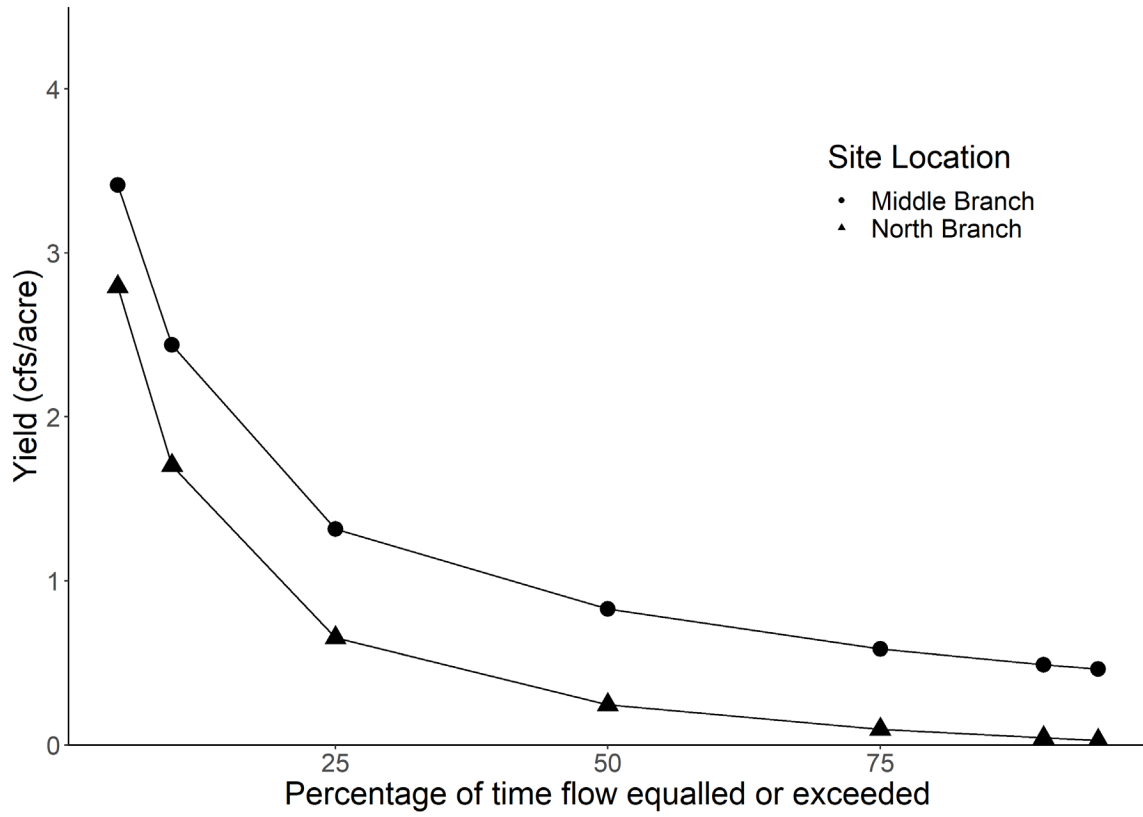


Figure 2-5: Comparison of flow duration curves for the Middle Branch and North Branch monitoring stations.

Chapter 3 - Methods

Field Study Scheme

Continuous Water Quality Sampling

A team of researchers worked together to deploy water quality monitoring stations at three stations in the Clinton River Watershed (Figure 2-2) between May, 23rd, 2019, and October 31st, 2019. Data were collected at each station using two multi-parameter instruments: the EXO2 Multi-Parameter Water Quality Sonde (YSI Inc., Yellow Springs, OH) and the C3TM Water Quality Sonde (Turner Designs, Sunnyvale, CA) (submersible fluorometer). Collected parameters from the EXO2 included pH, specific conductance, turbidity, and temperature; while the C3TM collected TLF and OB fluorescence intensity measured in raw fluorescence blank (RFUb) subtracted mode.

The research team selected station configurations based on access, deployment feasibility, power demand, and cost. Two monitoring stations, at the Red Run Drain and the Middle Branch stations, were configured as pump and flow-through cell monitoring systems with the EXO2 and C3TM connected in series and housed inside a shelter. Reinforced vinyl intake tubing was placed perpendicular to streamflow, approximately six inches off the bed of the stream to prevent dry out and avoid entraining sediments from the bed. PeriMax PM 600 peristaltic pumps (24 VDC) (Simply Pumps, Westmoreland City, PA) were run continuously to deliver surface water samples to the sondes. The North Branch monitoring station was configured as an in-situ deployment, with the EXO2 and C3TM housed in protective PVC piping. Instruments were situated perpendicular to streamflow with sensors heads approximately six inches off the bed. Photographs of both monitoring configurations are shown in Figure 3-1.

In all deployment configurations, we used communication cables to deliver monitoring data from the sondes to an X2 Environmental Data Logger (NexSens Technology, Fairborn, OH) at ten-minute intervals, and utilized cellular telemetry to send monitoring data to a viewing platform, WQ Data Live

(NexSens Technology, Fairborn, OH). The Red Run Drain and Middle Branch stations were powered through AC Power connections, while the North Branch station utilized solar power.



Figure 3-1: Comparison of pump and flow-through cell (left) versus in-situ deployment (right) monitoring configurations. Pump and flow-through cell configuration includes a peristaltic pump, bringing surface water in series through the YSI EXO 2 and Turner Designs C3™ water quality sondes, and outflow back into the stream, as well as power and telemetry devices. The in-situ deployment includes both water quality sondes deployed directly in-stream and protective PVC housing with flow openings (power and telemetry devices are not shown).

Continuous Discharge and Water Depth Sampling

We deployed water quality monitoring stations alongside USGS stream discharge gaging stations at the Middle Branch (04164800), and the North Branch (04164500), with readings collected at fifteen-minute intervals. Prior to this study, surface water discharge data was unavailable in the Red Run Drain. Therefore, water depth data were collected with an *Open Storm*⁴³ sensor node and used as a surrogate for discharge at this station, with readings collected at fifteen-minute intervals. Sensor nodes include an

ultrasonic depth sensor pointed at the stream surface, and a low-power embedded computer with wireless communication capabilities. Depth readings were calibrated with depth-to-bed measurements periodically throughout the season.

Discrete E. coli Sampling

To assess the suitability of using turbidity, TLF, and OB as effective indicators of fecal contamination, a research team of up to seven personnel collected discrete surface water quality samples for *E. coli* enumeration in conjunction with the aforementioned parameters. Three instances of wet-weather sampling occurred, where the team was deployed in shifts to take periodic grab samples during different hydrograph stages (baseflow, ascending hydrograph limb, descending hydrograph limb, post-storm) at each station. Samples from event #1 were taken between 6/13-6/15/2019, samples from event #2 were taken on 10/02/2019, and samples from event #3 were taken between 10/22-10/24/2019. Samples were collected in sterilized 100 mL polystyrene bottles with sodium thiosulfate to prevent decay from chlorine residuals in the surface water. Unfiltered samples were stored on ice and transported to the Huron to Erie Alliance for Research and Training (HEART), Freshwater Center Field Station at Lake St. Clair Metro Park within six hours of collection. Here, enumeration of *E. coli* was conducted by researchers from Oakland University using Colilert-18 (IDEXX, Westbrook, Maine) methods and reported in Most Probable Number (MPN). This reporting metric refers to the approximate number of viable cells per 100 mL volume sample. During the first storm event, dilutions were not applied and several samples with *E. coli* concentrations above the Colilert-18 threshold limit (2,500 MPN) were compromised. Methods were adapted to accommodate high *E. coli* concentrations during the second and third events, with serial dilutions (10X and 100X) applied at both Middle Branch and Red Run Drain stations.

Detection of Additional Optical Signatures

In search of additional optical signals that may either interfere with TLF and OB detection, I performed a preliminary assessment of the optical signal peaks at all stations during baseflow conditions.

Signal peaks were identified through fluorescence spectra recording using EEMs and “peak-picking” by identifying optical signatures based on maximum intensity associated with excitation and emissions pairs. EEMS represent fluorescence contours maps of relative fluorescence intensity, which comprise a series of repeated emission scans recorded in a range of excitation wavelengths.

Conditions were assessed during a single sampling event on 11/24/2019. Samples were collected at all three monitoring stations, plus the influent and effluent streams on a wastewater treatment plant within the Red Run Drain subwatershed. Separate samples were taken for *E. coli* enumeration and full spectra fluorescence scans, with *E. coli* enumeration samples handled and processed in the same way as was conducted for wet-weather sampling. Full spectra scans were stored on ice in 100 mL glass amber bottles and shielded from light degradation in coolers for no greater than four hours, then transferred to refrigerators for no more than 24-hours. Full spectra scans were performed using an Agilent 1260 Infinity II Fluorescence Detector, and visualized using isoplots of relative fluorescence intensity. Samples were excited at 10 nm intervals from 0-600 nm. Emissions were measured at the same frequency and range. The companion software application to the fluorescence detector required axes adjustment to change the color scale of the legend, and thus axes are variable between isoplots.

Data Analyses

I analyzed all monitoring data, including surface water discharge, water depth, continuous water quality, and discrete *E. coli* data, using either R version 3.6.1 or Microsoft Excel 2016 version 16.0.4966.1000.

Application of Temperature and Turbidity Correction Algorithms

Fluorophores are known to be sensitive to a wide variety of interferences, including signal amplification or signal quenching. To account for signal interference, I applied temperature and turbidity correction algorithms to both TLF and OB monitoring data. Details on the process for correction factor development, selection, and application are covered in Chapter 6- "Compensating for the effects of temperature and turbidity on tryptophan-like-fluorescence and optical brighteners". While other

interferences from solution pH and color are relatively well understood^{44,45}, accounting for these interferences was infeasible given the capacity and resource availability for this study.

Assessment of Continuous Water Quality Patterns

To assess the strength of turbidity, TLF, and OB as fecal contamination indicators across various flow conditions, I organized water quality time series data into three distinct baseflow seasons, and further baseflow and stormflow events. This process entailed reviewing the entire surface water discharge or water depth dataset, and determining ranges of stable baseflow. Baseflow seasons varied in exact date by station, but generally were distinguished by transitions between late spring high flows, summer low flows, and fall intermediate flows. Within each baseflow season, tables of timestamps for baseflow and stormflow periods were used to organize the data. Stormflow periods were distinguished by the first sign of hydrologic response to the return to baseflow values. In situations of consecutive storms when discharge levels did not return to baseflow, these time spans were considered the same stormflow period. Each distinct period of baseflow or stormflow received a unique identifier to use in data grouping. The final datasets were plotted on normalized time axes to visualize patterns in water quality. In addition to time series visualization, descriptive statistics were visualized with box plots to better understand the expected range for each parameter.

Characterization of Turbidity, TLF, and OB relationships with *E. coli*

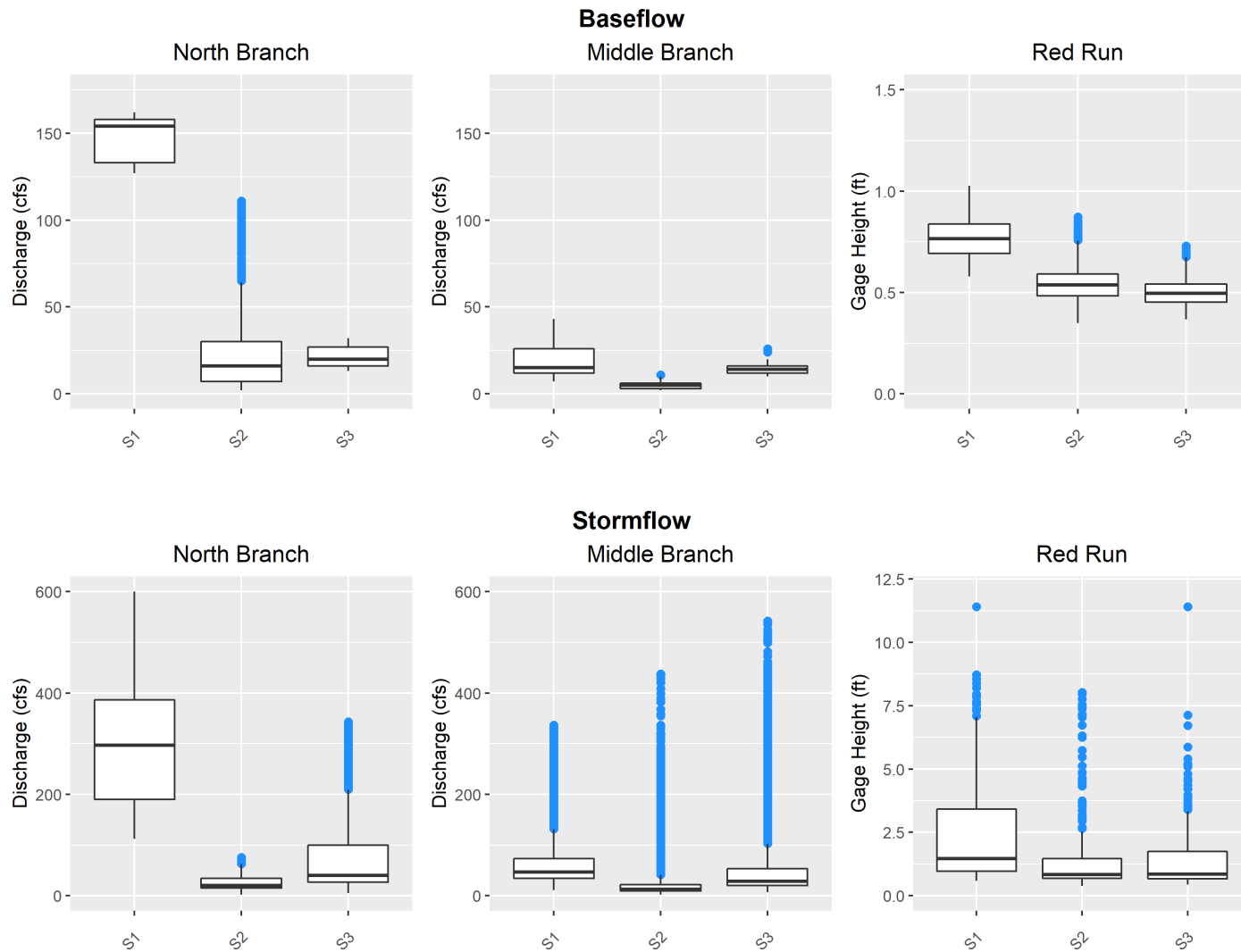
I developed box plots to visualize descriptive statistics for *E. coli* measurements across baseflow and stormflow periods, and to better understand the expected range for each station under different flow scenarios. I examined the relationships between turbidity, TLF, and OB with *E. coli* using Ordinary Least Squares (OLS) regression. Separate models were developed using (i) the entirety of the *E. coli* dataset, (ii) isolated datasets to the ascending limb of the hydrograph, and (iii) isolated data to the descending limb of the hydrograph. For all models, transformations were applied to predictor and dependent variables to meet linearity assumptions and improve model fit.

Chapter 4 - Results

Summary of Patterns in Discharge and Water Depth Data

Seasonal variations in baseflow discharge and water depth data were apparent at all three monitoring stations (Figure 4-1), typical of regional trends. For most stations, flow magnitude followed a pattern of high spring flows (expected with snowmelt and spring rains), low summer dry-season flows, and intermediate fall flows. Hydrological response at the North Branch station was much slower than the other two stations. During the spring baseflow season, flows rarely returned to baseflow conditions before the next precipitation event. This monitoring station also demonstrated the most drastic difference between high spring flows and low summer flows. The apparent transition between seasonal baseflow levels occurred in late June over approximately 230 hours of dry weather conditions. The Middle Branch and Red Run Drain stations experienced similar transitions, but to a lesser degree. Unlike the other two stations, the Red Run Drain continued to decrease mean flow values into the fall, however, the decrease in median gage height between the two seasons was marginal (0.042 FT). Noteworthy diurnal fluctuation patterns in flow at the Red Run Drain station indicate what is likely to be nightly effluent discharges from the upstream City of Warren WWTP. These discharges provide a consistent baseflow to the Red Run Drain, and explain the limited seasonal variation between summer and fall flows.

Seasonal variation in median discharge and water depth for stormflow conditions mirrored that for baseflow conditions. Maximum stormflow values peaked in the spring at the North Branch station, whereas the highest stormflow values for the Middle Branch were seen in the fall. Water depth values at the Red Run Drain station reached a maximum of 11.4 FT in both spring and fall, demonstrating the upper limit of the ultrasonic depth sensor. In these cases, the sensor was submerged underwater and therefore, true maxima are unknown. A summary of descriptive statistics for discharge and water depth data can be seen in Table 4-1.



1

2

3 *Figure 4-1: Variation in the distribution of discharge (cfs) or gage height (ft) values across monitoring stations. Boxplots are organized by*
 4 *stormflow or baseflow conditions, and then by baseflow season. Baseflow season #1 (S1) represents high spring flows, baseflow season #2 (S2)*
 5 *represents summer low flows, and baseflow season #3 (S3) represents intermediate fall flows.*

1 *Table 4-1: Descriptive statistics for surface discharge and water depth data collected at the North Branch (NB), Middle Branch (MB), and Red*
 2 *Run Drain (RR) monitoring stations in the Clinton River Watershed over three baseflow seasons (S1, S2, S3). “ND” indicates “no data*
 3 *available”.*

Monitoring Station	Season	Discharge (cfs)				Water Depth (FT)			
		Median	SD	Max	Min	Median	SD	Max	Min
Baseflow									
NB	S1	154	11.8	162	127	ND	ND	ND	ND
	S2	16	24.6	111*	2.0	ND	ND	ND	ND
	S3	20.0	5.90	32.0	13.0	ND	ND	ND	ND
MB	S1	15.0	9.68	43.0	7.00	ND	ND	ND	ND
	S2	5.00	1.94	11.0	2.00	ND	ND	ND	ND
	S3	14.0	2.90	26.0	10.0	ND	ND	ND	ND
RR	S1	ND	ND	ND	ND	0.765	0.100	1.03	0.580
	S2	ND	ND	ND	ND	0.537	0.0898	0.872	0.349
	S3	ND	ND	ND	ND	0.495	0.0787	0.731	0.367
Stormflow									
NB	S1	297	127	600	112	ND	ND	ND	ND
	S2	20.0	15.1	76.0	2.00	ND	ND	ND	ND
	S3	40.0	83.3	343	5.00	ND	ND	ND	ND
MB	S1	47.0	49.7	337	11.0	ND	ND	ND	ND
	S2	13.0	46.1	438	2.00	ND	ND	ND	ND
	S3	28.0	90.8	542	7.00	ND	ND	ND	ND
RR	S1	ND	ND	ND	ND	1.47	2.75	11.4**	0.580
	S2	ND	ND	ND	ND	0.836	1.42	8.02	0.393
	S3	ND	ND	ND	ND	0.844	1.49	11.4**	0.435

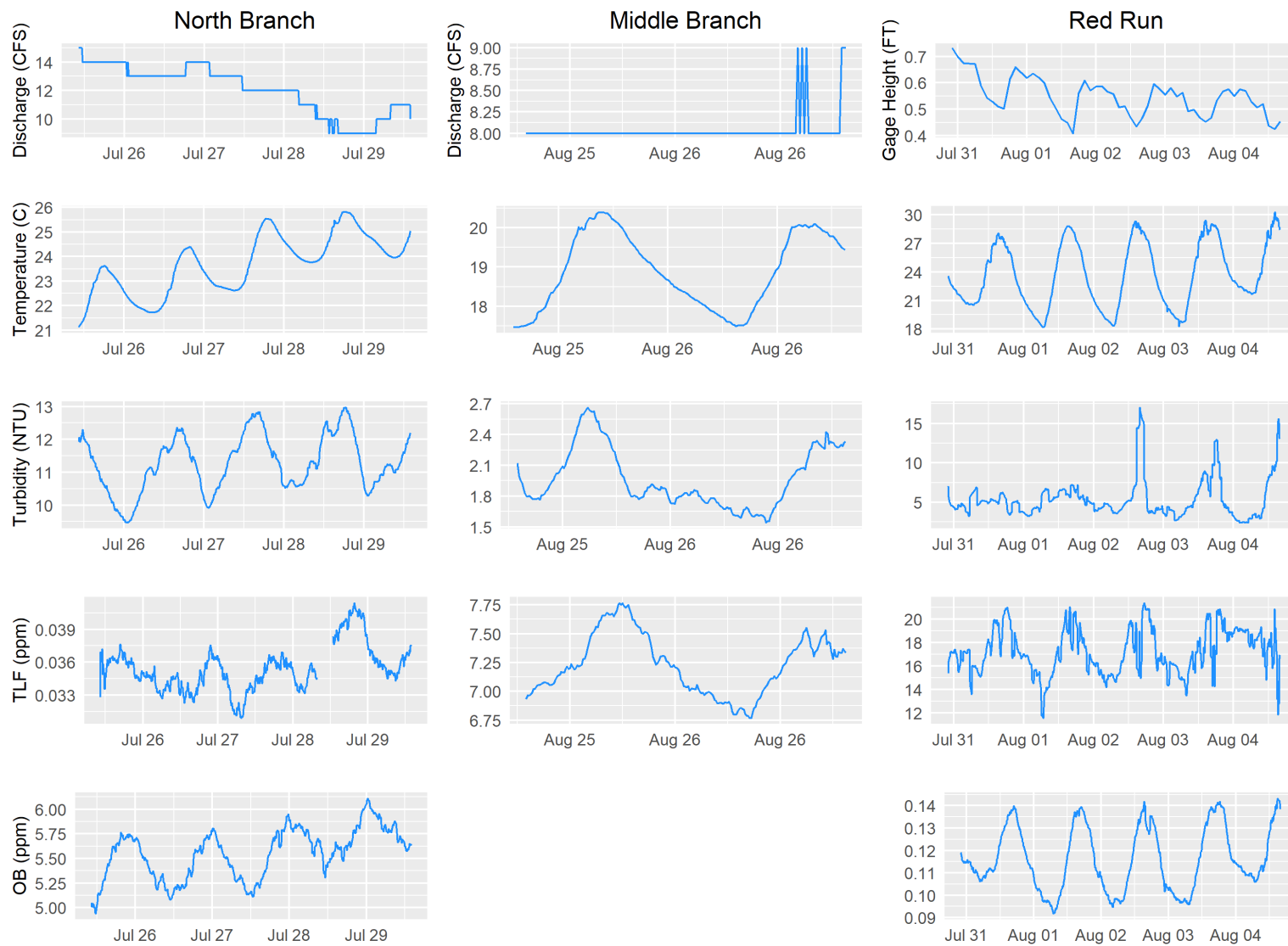
4 * Maxima representative of transitional baseflow between season 1 and season 2 ** Maxima representative of ultrasonic depth sensor limit (i.e. sensor submerged)

Summary of Patterns in Continuous Water Quality Parameters

Temperature data varied by station, and were generally warmest during low summer flows and coolest during intermediate fall flows for both baseflow and stormflow conditions. Diurnal fluxes in temperature were apparent during baseflow, and most pronounced during the lower summer flows. The Red Run Drain displayed the highest diurnal flux in temperature (approximately 10°C shift in temperature per day). Diurnal fluxes were also present in turbidity, TLF, and OB during baseflow conditions, although peaks in these parameters were variably aligned with peaks in temperature (Figure 4-2). At all stations, diurnal flux occurred during certain stormflow conditions, yet these patterns were muted once flows exceeded roughly 400 cfs.

Turbidity, specific conductance, TLF & OB data all exhibited low signal-to-noise ratios. Stations configured with pump and flow-through cell systems showed the most noise. Of these parameters, turbidity presented the highest standard deviations relative to the mean for all seasons and flow conditions. Diurnal fluxes in turbidity were apparent during baseflow conditions. The anticipated spike in turbidity that is characteristic of the “first flush” phenomena was seen during larger storms. Flow thresholds for this occurrence varied by station; North Branch spikes occurred above 70 cfs; Middle Branch spikes occurred above 50 cfs, and; Red Run Drain spikes occurred at depths above 1 FT. Overall, no one station consistently showed the highest or lowest turbidity level. However, the highest means recorded over the field season were at the Red Run Drain during fall stormflow.

Baseflow levels of specific conductance were consistently highest at the Red Run Drain station across the seasons, yet seasonal patterns for this parameter were not apparent during baseflow or stormflow conditions. At all stations, a pattern of dilution was apparent during nearly all stormflow events, with specific conductance levels showing an initial small spike, followed by levels dropping as flow increased.

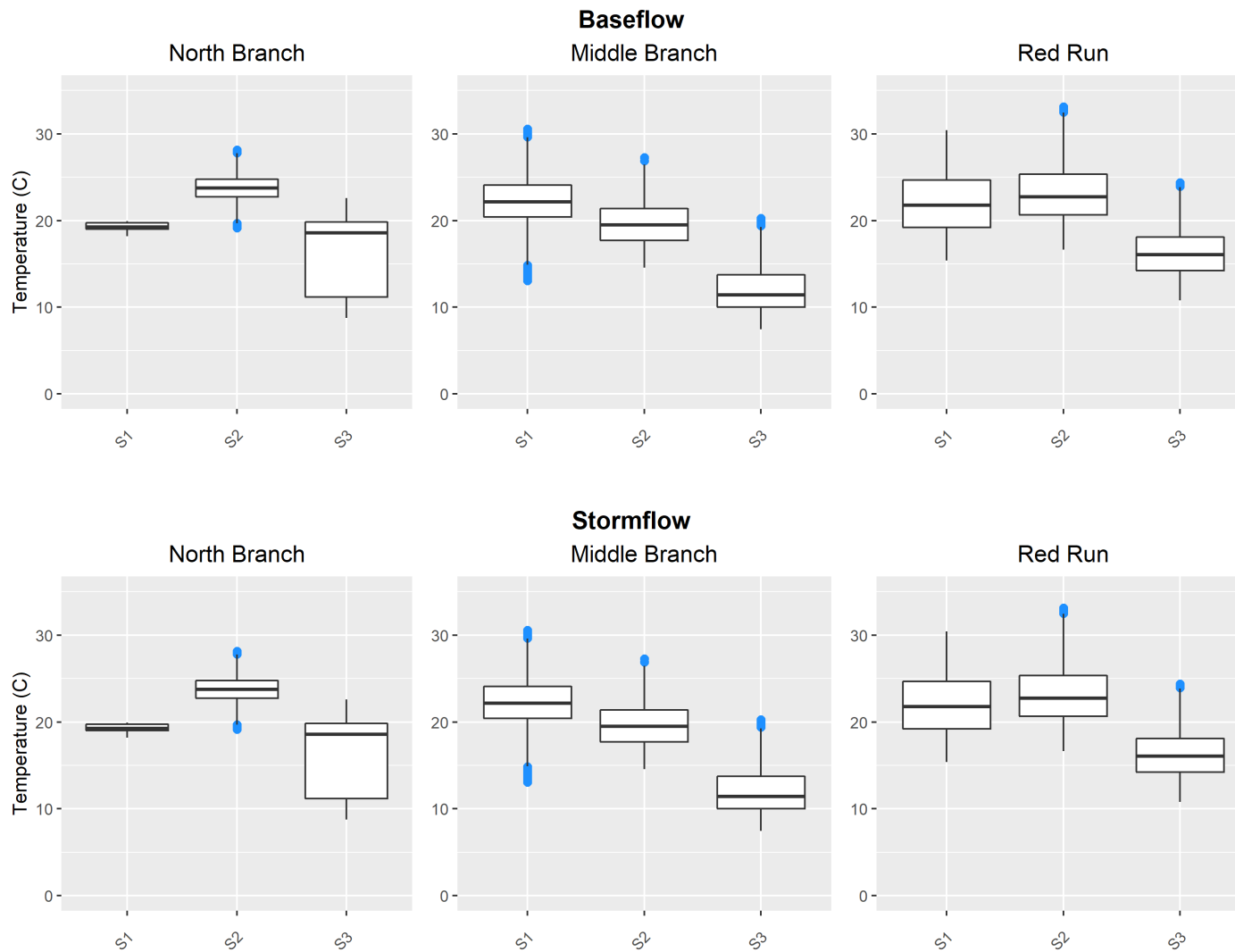


1
 2 *Figure 4-2: Diurnal fluctuation in temperature, turbidity, TLF, and OB during selected baseflow periods in the summer low flow seasons.*
 3 *Representative TLF data from the summer low flow season was unavailable.*

1 The Red Run Drain displayed the highest levels of TLF for baseflow and stormflow conditions
2 across the seasons, with the exception of stormflow conditions in season #2 (led by the Middle Branch
3 station). Diurnal patterns were also apparent during baseflow, indicating temperature compensation
4 algorithms were likely insufficient for this study. Seasonal patterns demonstrated higher levels of TLF
5 during spring and summer flows at the Red Run Drain and Middle Branch stations, as compared to fall
6 levels. TLF levels at the North Branch station demonstrated little seasonal variation. Storm response
7 patterns in TLF were dependent on flow magnitude. In instances of smaller storms, a spike in TLF
8 characteristic of the “first flush” was shown. However, during larger storms TLF levels presented
9 dilutions patterns similar to those seen with specific conductance. There were no clear flow thresholds for
10 this occurrence, and more monitoring data are needed to tease out the drivers for these two patterns.

11 Strong seasonal variation in the concentration of OB was apparent, with the highest levels in the
12 summer across baseflow and stormflow conditions. Extremely low outliers were seen during the fall
13 season at the Red Run Drain. No one station consistently demonstrated the highest values of OB. Storm
14 response patterns were similar to specific conductance and TLF, in that strong dilution patterns were seen
15 during large storms.

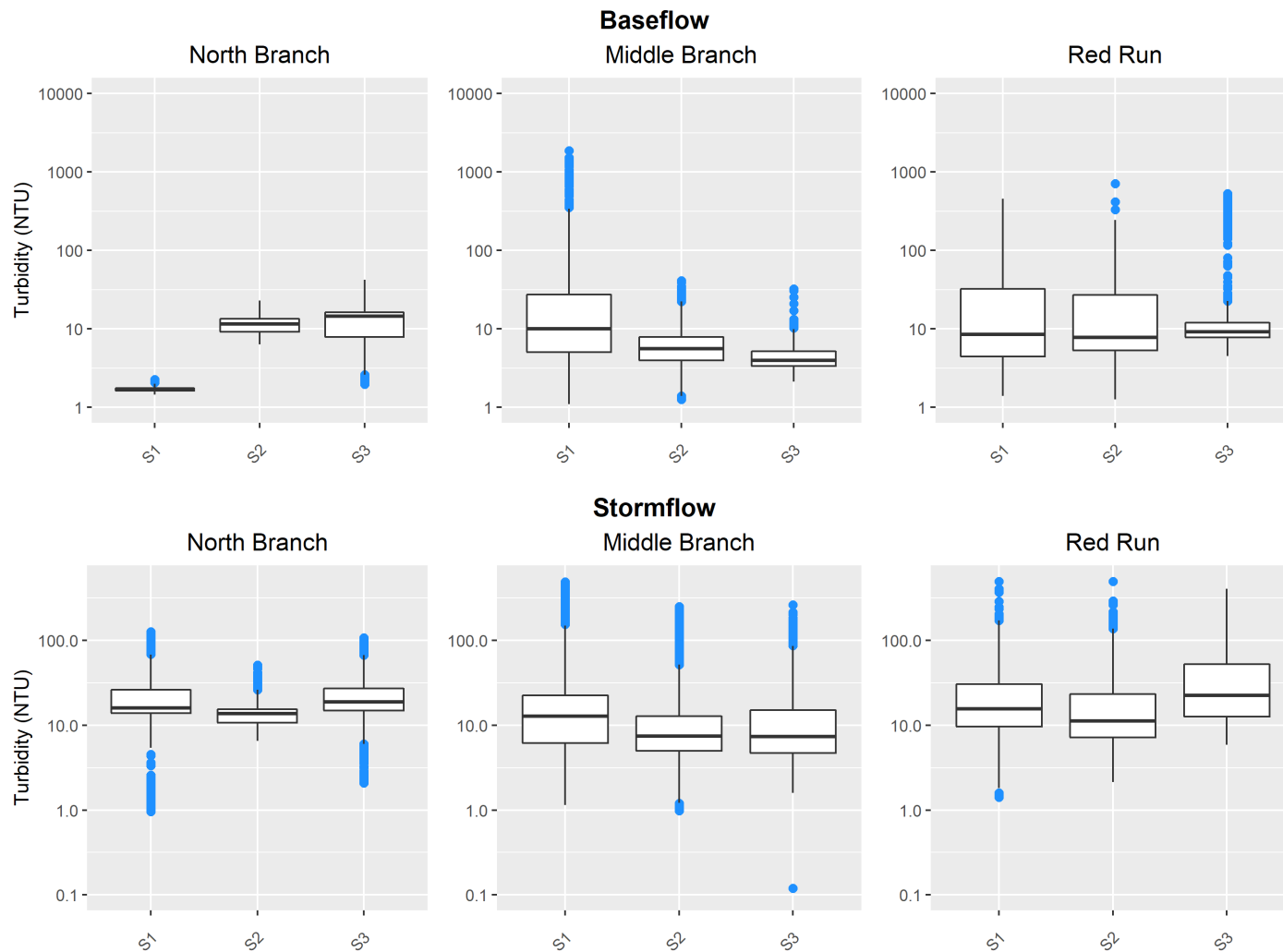
16 As previously described, the distribution of each continuous water quality parameter varied
17 seasonally, and across flow conditions (Figure 4-2 through Figure 4-7).



1

2

3 *Figure 4-3: Variation in the distribution of observed temperature (°C) values across monitoring stations. Boxplots are organized by stormflow or*
 4 *baseflow conditions, and then by baseflow season. Baseflow season #1 (S1) represents high spring flows, baseflow season #2 (S2) represents*
 5 *summer low flows, and baseflow season # 3 (S3) represents intermediate fall flows.*



1

2

3 *Figure 4-4: Variation in the distribution of observed turbidity (NTU) values across monitoring stations. Boxplots are organized by stormflow or*
 4 *baseflow conditions, and then by baseflow season. Baseflow season #1 (S1) represents high spring flows, baseflow season #2 (S2) represents*
 5 *summer low flows, and baseflow season # 3 (S3) represents intermediate fall flows.*

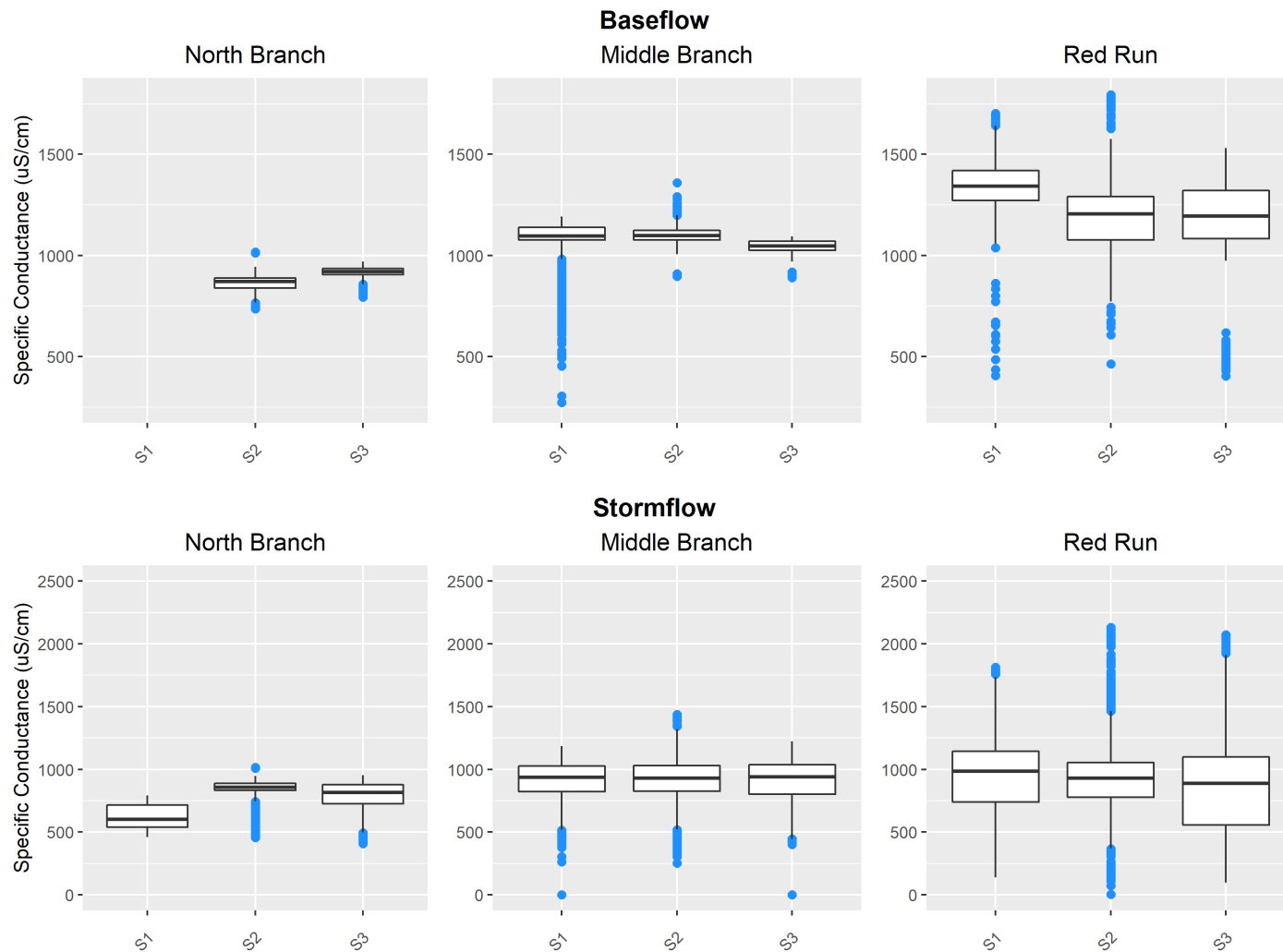


Figure 4-5: Variation in the distribution of specific conductance ($\mu\text{S}/\text{cm}$) values across monitoring stations. Boxplots are organized by stormflow or baseflow conditions, and then by baseflow season. Baseflow season #1 (S1) represents high spring flows, baseflow season #2 (S2) represents summer low flows, and baseflow season #3 (S3) represents intermediate fall flows.

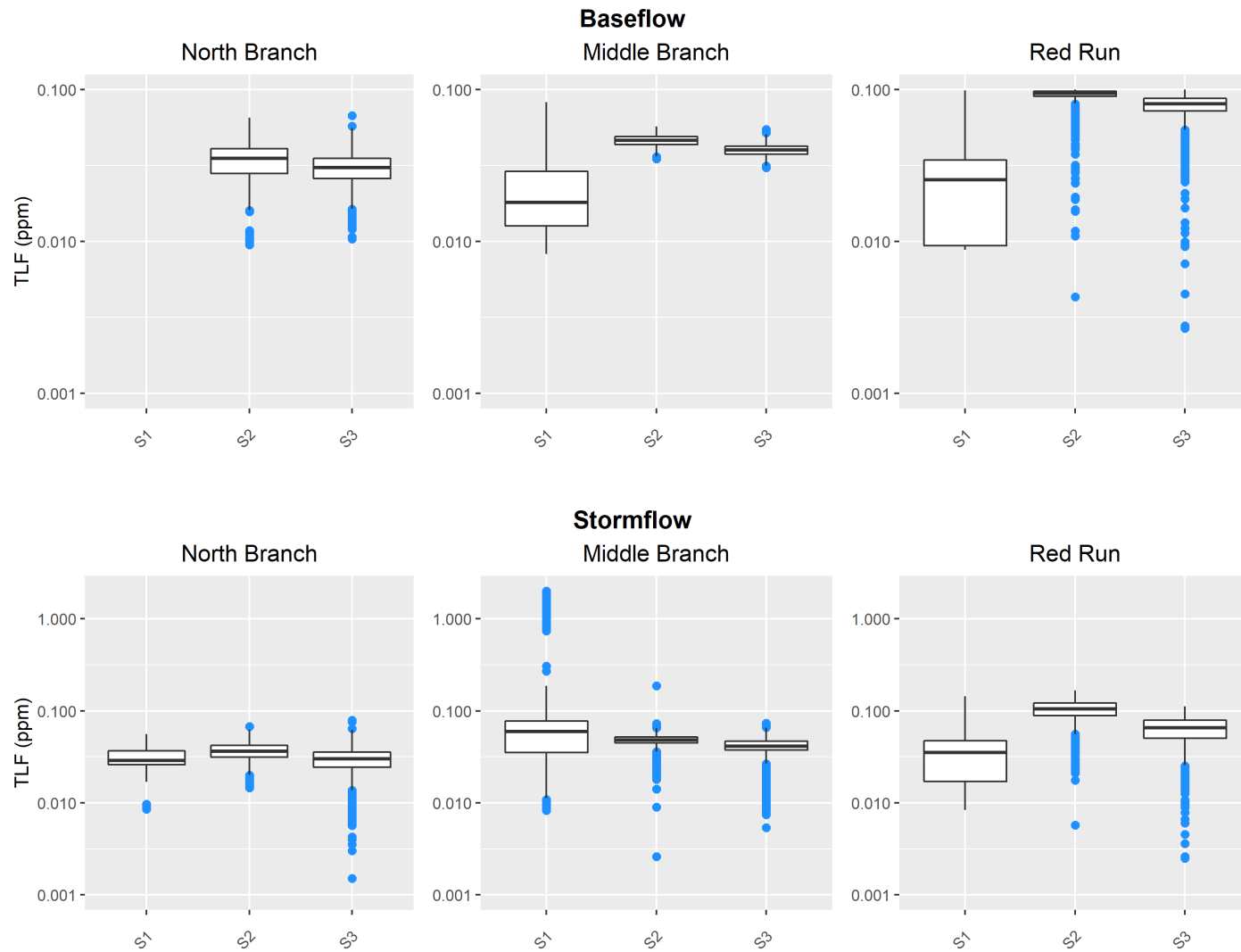
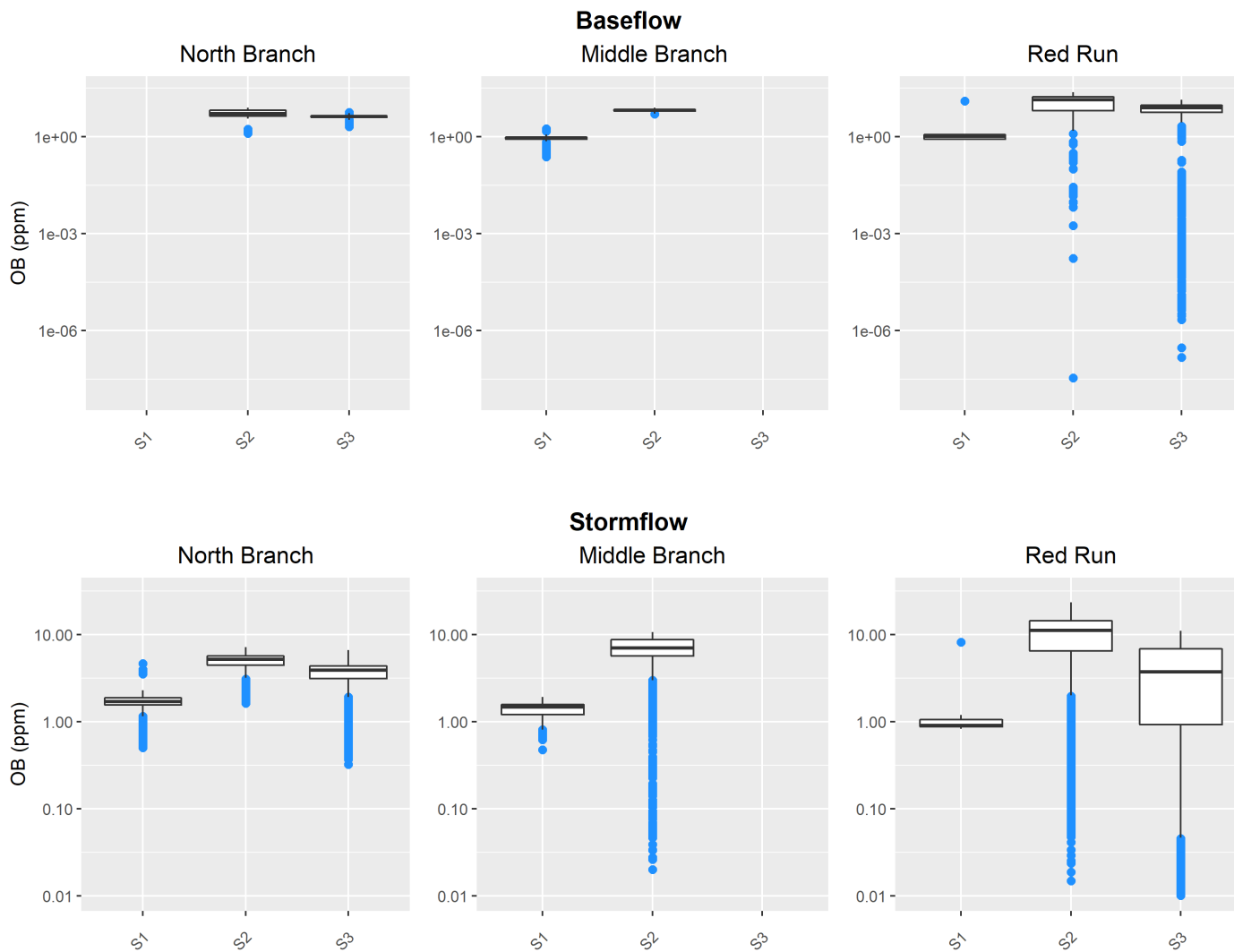


Figure 4-6: Variation in the distribution of TLF (ppm) values across monitoring stations. Boxplots are organized by stormflow or baseflow conditions, and then by baseflow season. Baseflow season #1 (S1) represents high spring flows, baseflow season #2 (S2) represents summer low flows, and baseflow season #3 (S3) represents intermediate fall flows.



1

2

3

4

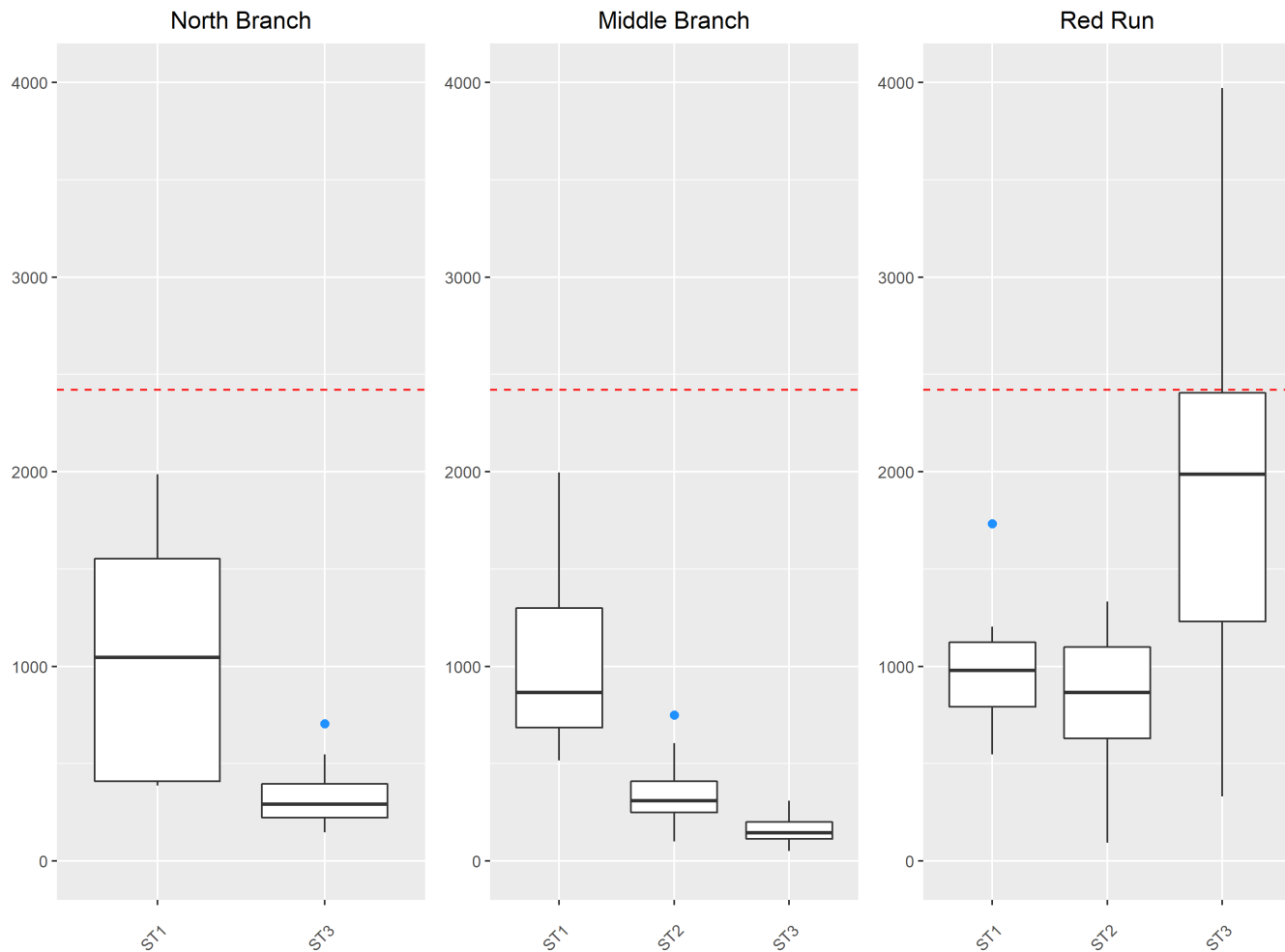
5

Figure 4-7: Variation in the distribution of OB (ppm) values across monitoring stations. Boxplots are organized by stormflow or baseflow conditions, and then by baseflow season. Baseflow season #1 (S1) represents high spring flows, baseflow season #2 (S2) represents summer low flows, and baseflow season # 3 (S3) represents intermediate fall flows.

1 **Summary of *E. coli* Data**

2 Relationships between *E. coli* and discharge varied across stations and sampling events (Figure
3 4-8). While the intent was to sample during wet-weather events, in some cases storms dissipated earlier
4 than anticipated. Hydrological response was greatest during the first event, very limited during the second
5 event, and only responsive at the Red Run Drain during the third event. With the exception of the Red
6 Run Drain, monitoring data from the second and third events were not significantly different from
7 baseflow. Sampling at the North Branch was abandoned during the second event due to a lack of
8 hydrologic response to precipitation. When hydrological response to precipitation was present, a typical
9 *E.coli*-flow hysteresis curve was apparent, with an initial pulse of *E.coli* during the ascending limb of the
10 hydrograph, followed by decreasing concentrations after towards baseline levels.

11 During the first (and largest) storm event, the North Branch demonstrated the highest median *E.*
12 *coli* concentration (although the previously mentioned dilution limits should be taken into consideration).
13 Median levels reached 1046 MPN, almost 3.5× the daily geometric mean Michigan WQS for surface
14 waters with TBC recreational usage (300 *E. coli* per 100 mL). Median levels at the Middle Branch and
15 Red Run Drain reached concentrations greater than 2.75× the Michigan WQS. Even during the second
16 event, when flow values were near baseflow, concentrations reached 750 MPN at the Middle Branch and
17 1334 MPN at the Red Run Drain. During the last storm event, with moderate levels of hydrologic
18 response at the Red Run Drain, maximum *E. coli* concentration peaked at more than an order of
19 magnitude above the Michigan WQS (4106 MPN). A noteworthy limitation to these results is the failure
20 to apply serial dilutions to samples collected during the first wet-weather monitoring event. As a result *E.*
21 *coli* concentrations reached an upper limit of 2420 MPN (the maximum possible value using the Colilert-
22 18 method) during and beyond the hydrograph peak at all three stations. Even so, it is clear from the
23 available wet-weather monitoring data that harmful levels of fecal contamination are mobilized into
24 surface waters even during events with even limited hydrological response. A summary of *E. coli* data
25 from the three monitoring events is shown in Table 4-2.



1

2

3

4

5

Figure 4-8: Variation in the distribution of E. coli (MPN) values across monitoring stations. Boxplots are organized by sampling event. Sampling event #1 (ST1) represents sampling that occurred between 6/13 and 6/15/2019, sampling event #2 (ST2) represents sampling that occurred on 10/02/2019, and sampling event #3 (ST3) represents sampling that occurred between 10/22 and 10/24/2019. The red dashed line indicates the upper detection limit for E. coli using Colilert-18, as was pertinent during ST1 when many samples breached this limit.

1 *Table 4-2: Summary of E. coli data collected at the North Branch (NB), Middle Branch (MB), and Red*
 2 *Run Drain (RR) monitoring stations in the Clinton River Watershed over three storm sampling events*
 3 *(ST1, ST2, ST3). “MPN” indicates the maximum-probable-number of viable cells per 100 mL.*

Monitoring Station	Storm Event	<i>E. coli</i> (MPN)			
		Median	SD	Max	Min
NB	ST1	1046	630	2420*	387.3
	ST2	ND	ND	ND	ND
	ST3	292	131	706	148
MB	ST1	866	459	2420*	517
	ST2	310	159	750	100
	ST3	146	61.2	52.0	310
RR	ST1	980	381	2420*	548
	ST2	865	331	1334	94.0
	ST3	2000	935	4106	332

4 * Representative of the upper detection limit of Colilert-18 test, indicating that true concentrations are higher than the reported value.

5
 6 **Characterization of Turbidity, TLF, and OB relationships with E. coli**

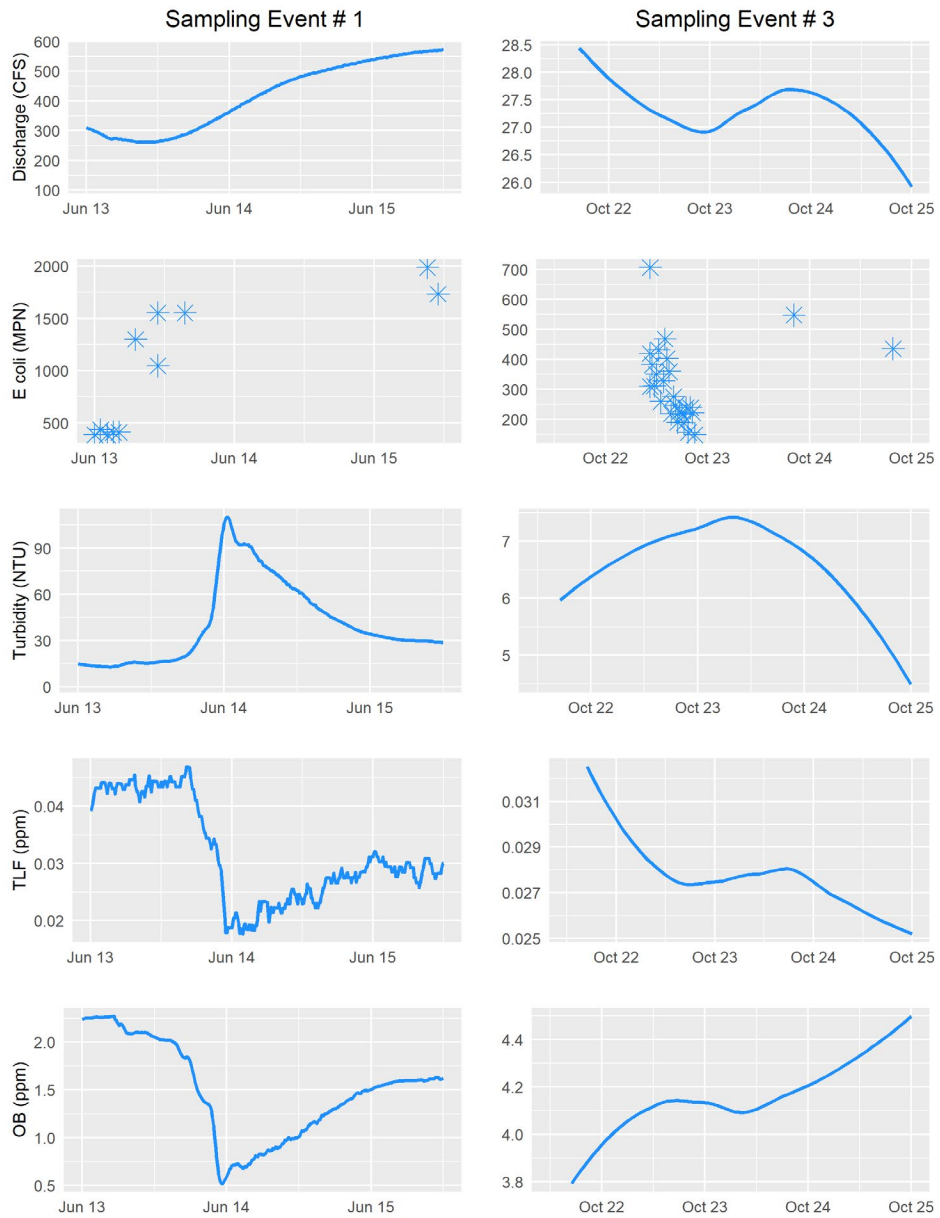
7 As previously mentioned, during sampling events with significant hydrological response, the
 8 relationship between *E. coli* and flow showed a hysteresis pattern that is typical of pollutant loading.
 9 However, the relationships between turbidity, TLF, and OB and flow varied and were dependent upon the
 10 degree of hydrological response (see *Summary of patterns in continuous water quality parameters*). In
 11 turn, the relationships between the three fecal contamination indicators and *E. coli* varied across the three
 12 sampling events, and hydrograph phases. Flow-dependent patterns in fecal contamination indicators
 13 showed varied responses across sampling events (Figure 4-9 through Figure 4-11). Flow-dependent
 14 variation in fecal contamination indicators was observed; the first event demonstrates a typical response
 15 in fecal contamination indicators during high flow events, the second demonstrates responses during near
 16 baseflow levels, while the last event shows responses during low-to-intermediate flows.

1 Turbidity and TLF demonstrated either linear or log-linear regression relationships with *E. coli* in
2 all models (full dataset, ascending limb, descending limb; Figure 4-12 and 4-13, respectively). For both
3 these parameters, the relationship with *E. coli* was positive. The relationship between OB and *E. coli* was
4 best fit for a cubic curve using the full dataset and the ascending limb, yet the model for the descending
5 limb was linear (Figure 4-14).

6 In all regressions, the significance of the predictor variables reflected sample size. With the full
7 turbidity dataset, p-value = $2.02e^{-12}$ (n = 178, 95% confidence interval); including only data from the
8 ascending limb, p-value = $3.76e^{-9}$ (n = 151); for the descending limb, p-value = 0.0288 (n = 27). Models
9 for other predictor variables followed the same pattern, except for TLF from the ascending limb data,
10 which showed similar predictor variable significance as with the full dataset.

11 Model fits were weaker than expected, and highly variable among hydrograph phases for all
12 predictor variables (Table 4-3). Models of turbidity and *E. coli* performed better for the ascending limb
13 ($R^2 = 0.21$) as compared to the descending limb ($R^2 = 0.18$). The opposite was true for TLF and OB. For
14 the ascending limb with TLF, $R^2 = 0.33$; and with OB, $R^2 = 0.40$. For the descending limb with TLF, $R^2 =$
15 0.58 ; and with OB, $R^2 = 0.60$. The latter was the best measure of fit for all models that were assessed.

16 I tested assumptions of the OLS regression for all models, and assumption failures occurred in
17 certain circumstances. I decided to move forward with the regressions, with intentions to address failures
18 in future project phases. All models displayed a positive temporal autocorrelation, as evaluated through
19 Auto Correlation Function plots and the Durbin-Watson Test. Homoscedasticity of the errors was present
20 in all models, as evaluated using a Non-Constant Error Variance (NCV) Test and plots of the residuals
21 versus fitted values, except for the OB-*E. coli* model using the full dataset. Normality of the errors was
22 present in all models, with the exception of the turbidity-*E. coli* model, as evaluated with Quantile-
23 Quantile (Q-Q) plots.



1

2

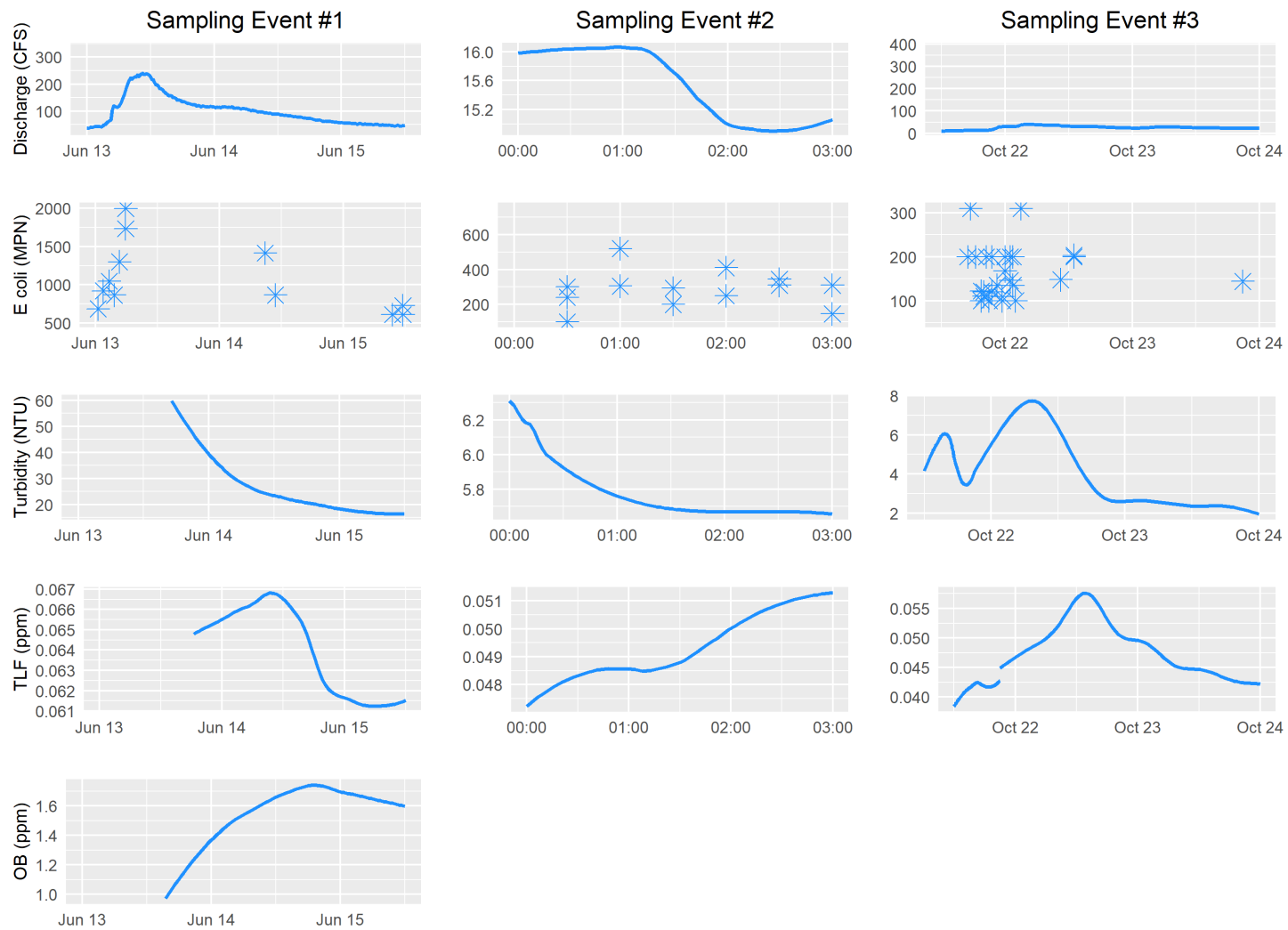
3

4

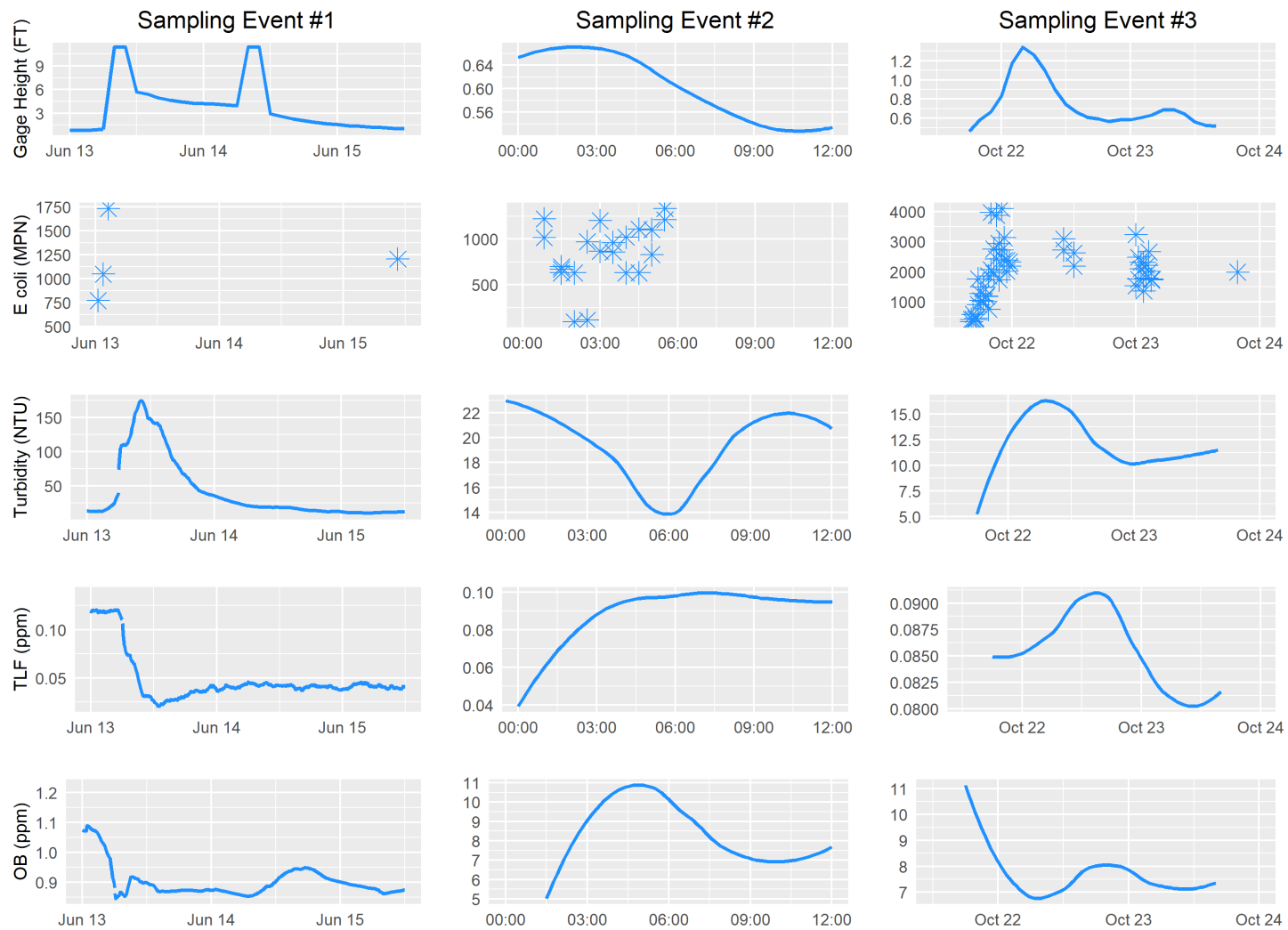
5

6

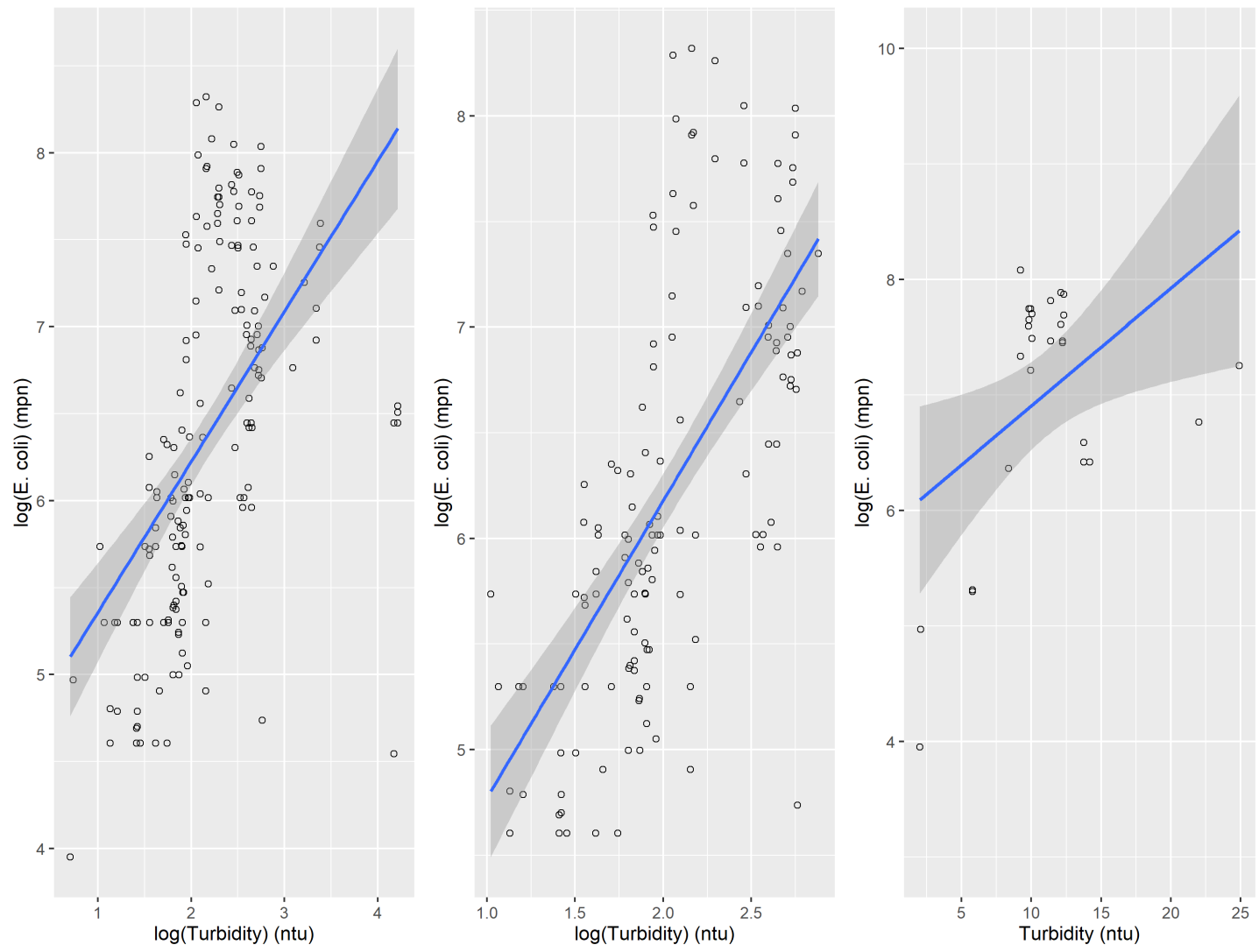
Figure 4-9: Patterns in fecal contamination indicators, including E. coli (MPN), turbidity (NTU), TLF (ppm), and OB (ppm) in response to discharge (cfs) at the North Branch monitoring station during two separate discrete E. coli sampling events. Flow-dependent variation in fecal contamination indicators is exhibited. The numbering of events is consistent with other stations, and sampling during event # 2 was abandoned due to a lack of hydrologic response to precipitation at the North Branch monitoring station.



1
2 *Figure 4-10: Patterns in fecal contamination indicators, including E. coli (MPN), turbidity (NTU), TLF (ppm), and OB (ppm) in response to flow*
3 *at the Middle Branch monitoring station during three separate discrete E. coli sampling events. OB data was unavailable during sampling events*
4 *#2 and #3 due to sensor failure. Flow-dependent variation in fecal contamination indicators is exhibited.*

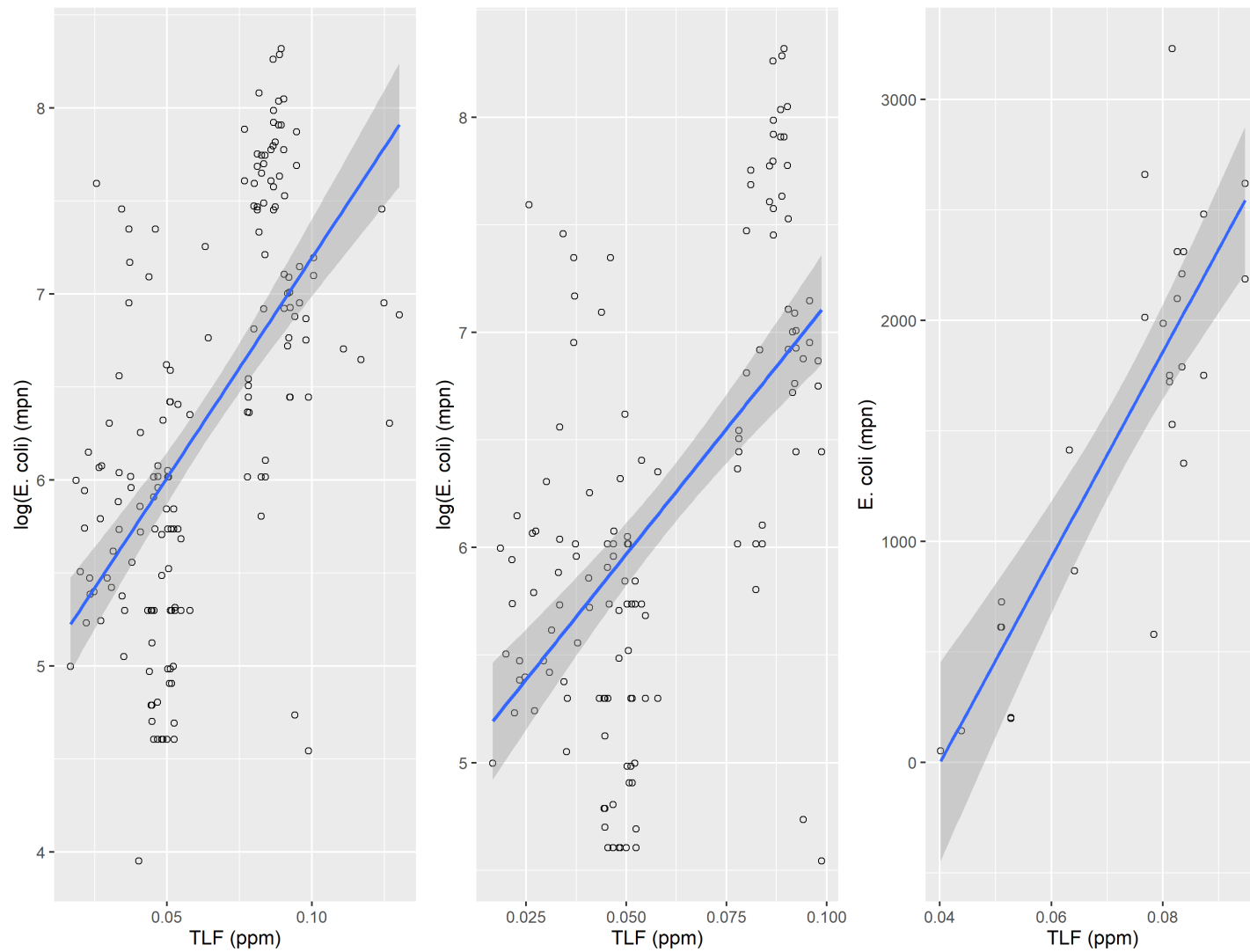


1
2 *Figure 4-11: Patterns in fecal contamination indicators, including E. coli (MPN), turbidity (NTU), TLF (ppm), and OB (ppm) in response to flow*
3 *(gage height (ft) serves as proxy) at the Red Run Drain monitoring station during three separate discrete E. coli sampling events. Flow-dependent*
4 *variation in fecal contamination indicators is exhibited.*



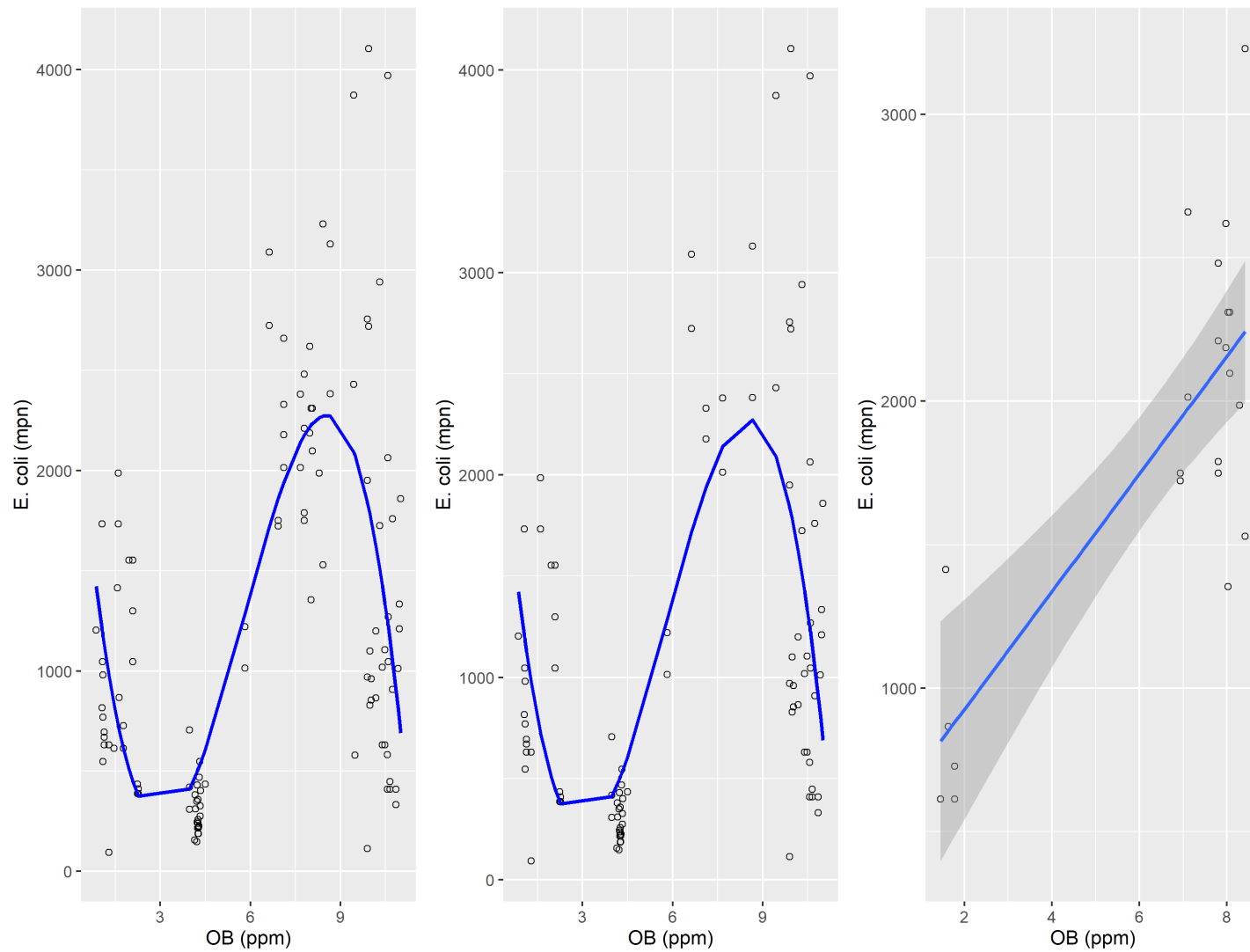
1

2 *Figure 4-12: Relationships between turbidity (NTU) and E. coli (MPN) with 95% confidence intervals using the entirety of the field sampling*
 3 *dataset (left), data isolated to the descending limb of the hydrograph (center), and data isolated to the descending limb of the hydrograph (right).*



1

2 *Figure 4-13: Relationships between TLF (ppm) and E. coli (MPN) with 95% confidence intervals using the entirety of the field sampling dataset*
 3 *(left), data isolated to the ascending limb of the hydrograph (center), and data isolated to the descending limb of the hydrograph (right).*



1

2 *Figure 4-14: Relationships between OB (ppm) and E. coli (MPN) using the entirety of the field sampling dataset (left), data isolated to the*
 3 *ascending limb of the hydrograph (center), and data isolated to the descending limb of the hydrograph (right) with 95% confidence intervals.*

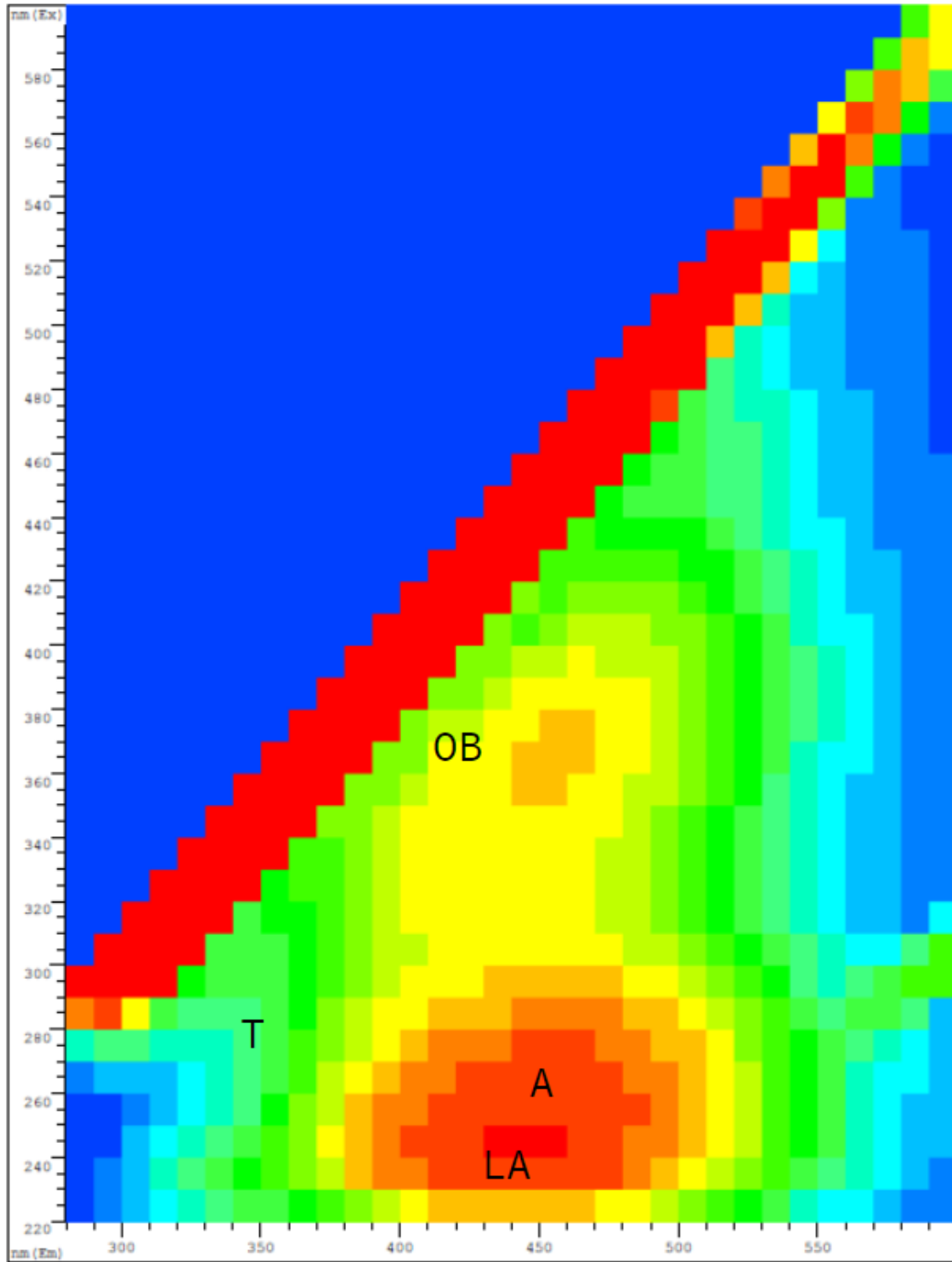
1 *Table 4-3: OLS regression model equations, coefficients, and metrics of model performance for correlations between E. coli and turbidity, TLF, or*
 2 *OB over different hydrograph phases, including data isolated to the ascending limb (AL), the descending limb (DL), and the full dataset (FD).*

<i>Parameter</i>	<i>Hydrograph Phase</i>	<i>Equation</i>	<i>Coefficient(s)</i>	<i>n</i>	<i>p-value</i>	<i>R²</i>	<i>RMSE</i>
Turbidity	FD	$\log(y) = \beta_1 \log(x) + \beta_0$	$\beta_0 = 4.57$ $\beta_1 = 0.841$	178	$2.025e^{-12}$	0.25	0.88
	AL	$\log(y) = \beta_1 \log(x) + \beta_0$	$\beta_0 = 8.12$ $\beta_1 = -0.05$	151	$3.761e^{-09}$	0.21	0.87
	DL	$\log(y) = \beta_1 x + \beta_0$	$\beta_0 = 4.70$ $\beta_1 = 0.73$	27	0.0288	0.18	0.41
TLF	FD	$\log(y) = \beta_1 x + \beta_0$	$\beta_0 = 4.81$ $\beta_1 = 24.20$	178	$2.20e^{-16}$	0.37	0.81
	AL	$\log(y) = \beta_1 x + \beta_0$	$\beta_0 = 4.930$ $\beta_1 = 21.08$	151	$8.30e^{-16}$	0.33	0.80
	DL	$y = \beta_1 x + \beta_0$	$\beta_0 = -1392$ $\beta_1 = 41603$	27	$2.27e^{-5}$	0.58	430
OB	FD	$y = \beta_1 x + \beta_2 x^2 + \beta_3 x^3 + \beta_0$	$\beta_0 = 2698$ $\beta_1 = -1820$ $\beta_2 = 406.4$ $\beta_3 = -23.32$	178	$2.20e^{-16}$	0.47	669
	AL	$y = \beta_1 x + \beta_2 x^2 + \beta_3 x^3 + \beta_0$	$\beta_0 = 2771$ $\beta_1 = -1929$ $\beta_2 = 434.5$ $\beta_3 = -25.05$	151	$2.10e^{-11}$	0.40	696
	DL	$y = \beta_1 x + \beta_0$	$\beta_0 = 515$ $\beta_1 = 205$	27	$1.34e^{-5}$	0.60	419

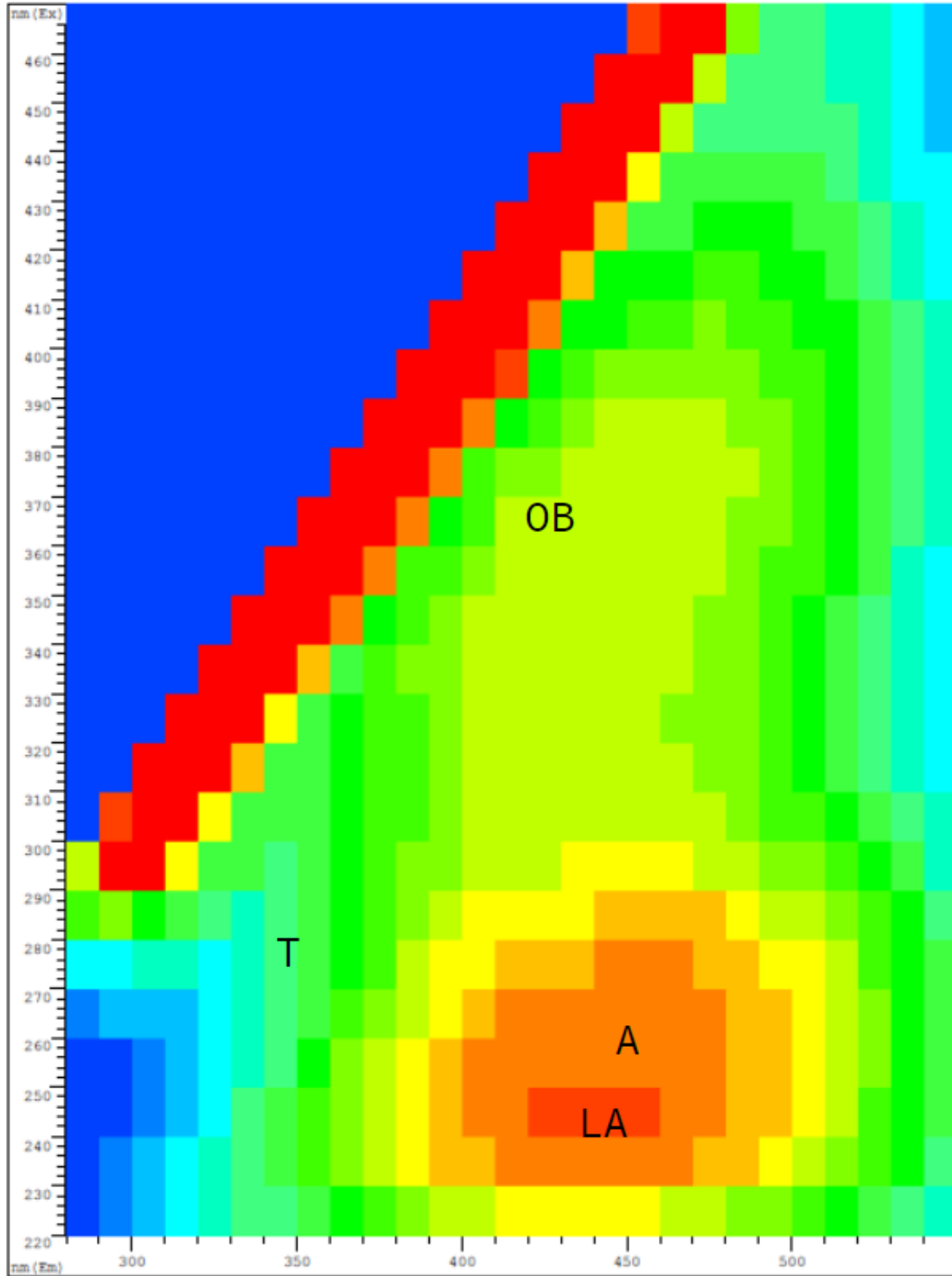
3

1 **Investigation of Additional Optical Signatures**

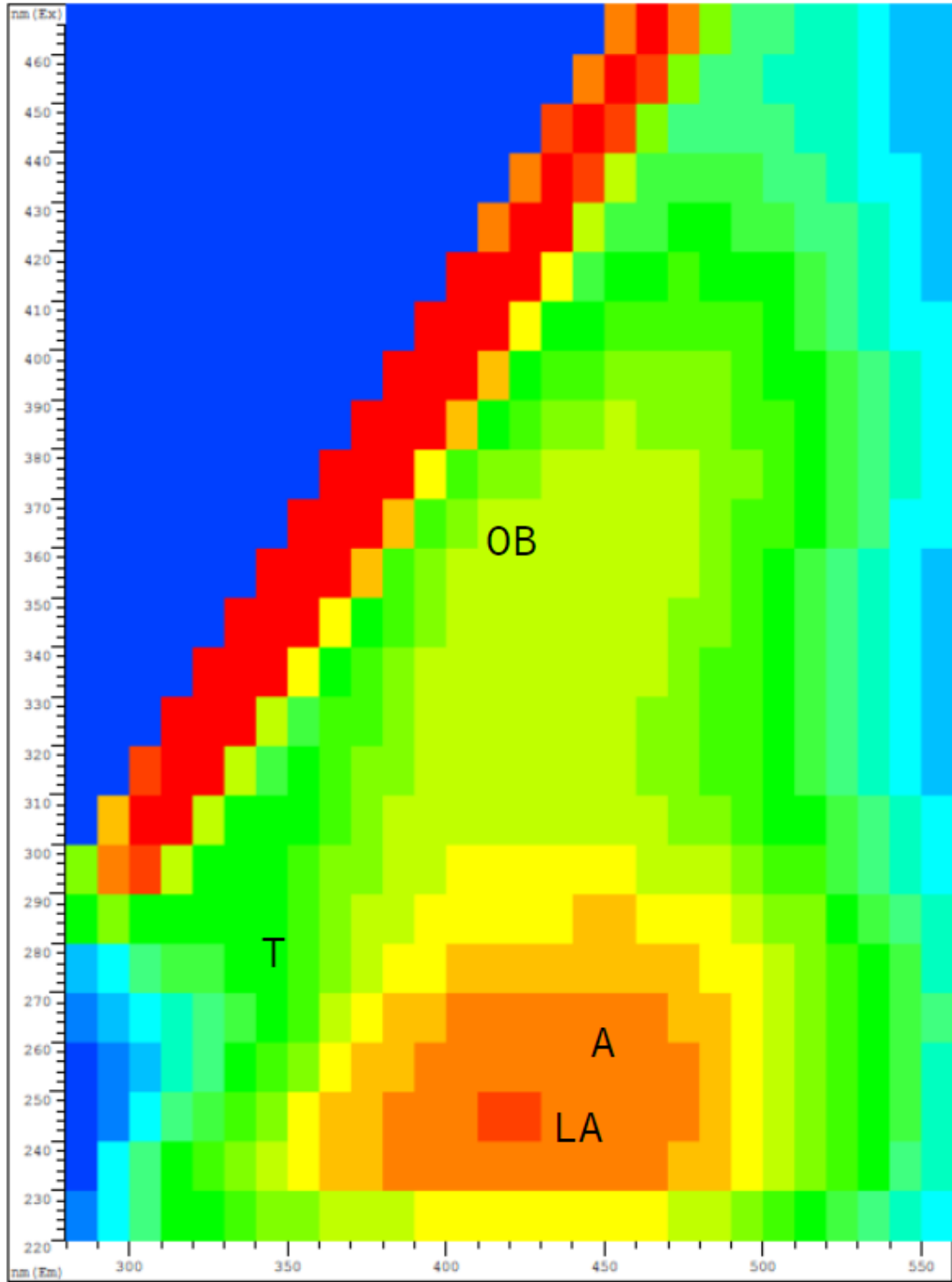
2 Full spectra analysis of baseflow conditions revealed several optical signals with higher
3 fluorescence intensity than TLF or OB (Figure 4-15 through Figure 4-19. Namely, fluorescence intensity
4 was centered around peak signal A (excitation at 260 nm, emission at 400-500 nm) and peak signal LA
5 (excitation at 240 nm, emission at 440 nm) for all samples collected at surface water monitoring stations
6 (North Branch, Middle Branch, and Red Run Drain) and wastewater treatment effluent. Peak signal A and
7 LA are associated with the fluorescence of organic matter in wastewater streams, and are also common in
8 natural and engineered water systems. Fluorescence intensity recorded from the wastewater influent
9 sample was centered on the excitation range of 220-240 nm and the emission range of 310-350 nm. To
10 my knowledge, there is no commonly accepted signal peak name associated with fluorescence in this
11 region.



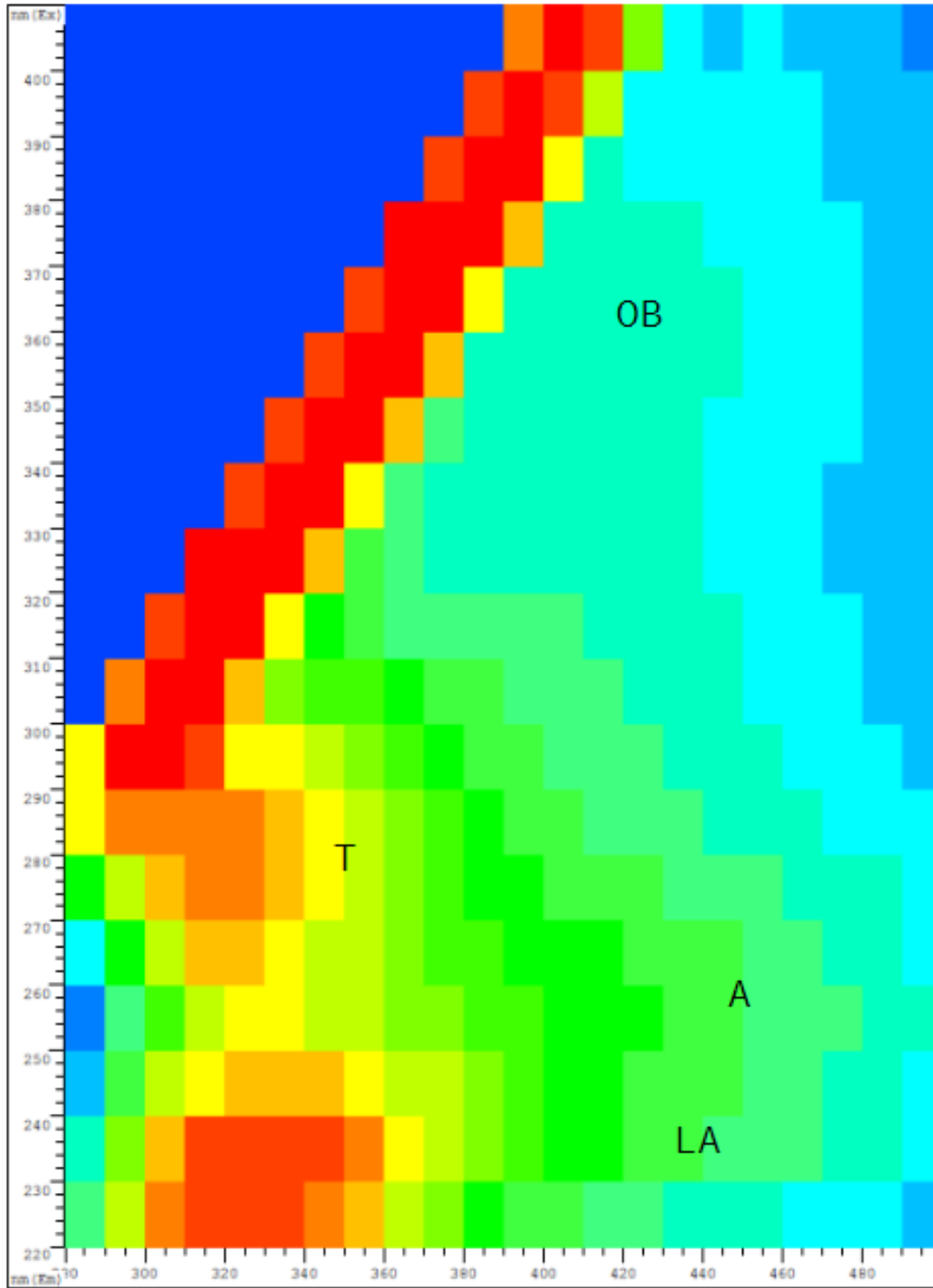
1
 2 *Figure 4-15: Excitation-emission matrices recorded from surface water samples at the North Branch*
 3 *Monitoring Station during baseflow conditions. Letters represent peak signal names associated with*
 4 *excitation and emission pairs. Coloration indicates relative fluorescence intensity within the sample,*
 5 *increasing from cool to warm colors. High intensities on the diagonal are indicative of light scattering*
 6 *associated with identical excitation and emission wavelengths, and should be ignored.*



1
 2 *Figure 4-16: Excitation-emission matrices recorded from surface water samples at the Middle Branch*
 3 *Monitoring Station during baseflow conditions. Letters represent peak signal names associated with*
 4 *excitation and emission pairs. Coloration indicates relative fluorescence intensity within the sample,*
 5 *increasing from cool to warm colors. High intensities on the diagonal are indicative of light scattering*
 6 *associated with identical excitation and emission wavelengths, and should be ignored.*



1
 2 *Figure 4-17: Excitation-emission matrices recorded from surface water samples at the Red Run Drain*
 3 *Monitoring Station during baseflow conditions. Letters represent peak signal names associated with*
 4 *excitation and emission pairs. Coloration indicates relative fluorescence intensity, increasing from cool*
 5 *to warm colors. High intensities on the diagonal are indicative of light scattering associated with*
 6 *identical excitation and emission wavelengths, and should be ignored.*



1

2

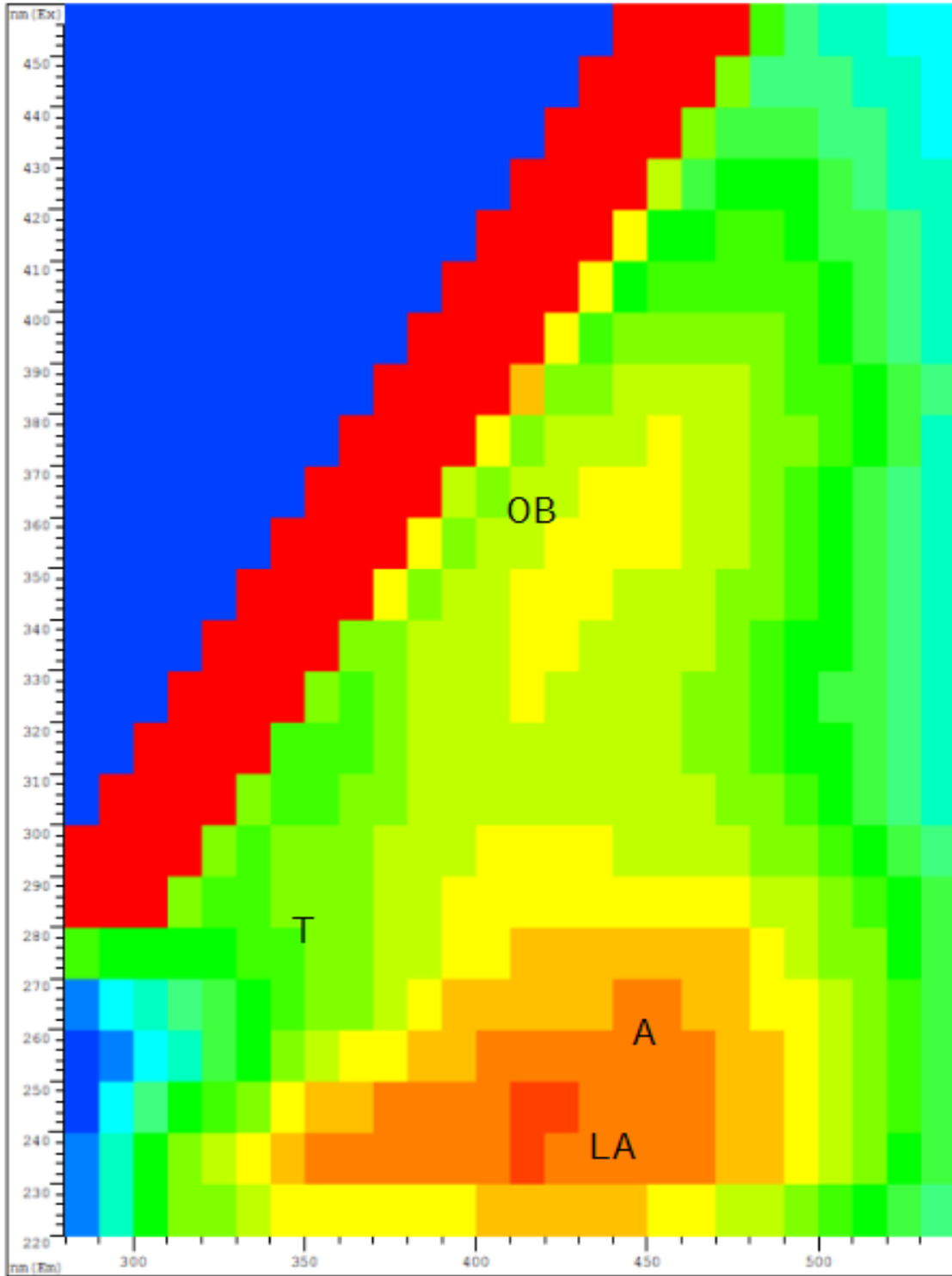
3

4

5

6

Figure 4-18: Excitation-emission matrices recorded from surface water samples from the wastewater treatment plant influent during baseflow conditions. Letters represent peak signal names associated with excitation and emission pairs. Coloration indicates relative fluorescence intensity within the sample, increasing from cool to warm colors. High intensities on the diagonal are indicative of light scattering associated with identical excitation and emission wavelengths, and should be ignored.



1
 2 *Figure 4-19: Excitation-emission matrices recorded from surface water samples from the wastewater*
 3 *treatment plant effluent during baseflow conditions. Letters represent peak signal names associated with*
 4 *excitation and emission pairs. Coloration indicates relative fluorescence intensity within the sample,*
 5 *increasing from cool to warm colors. High intensities on the diagonal are indicative of light scattering*
 6 *associated with identical excitation and emission wavelengths, and should be ignored.*

Chapter 5 – Discussion and Conclusions

In this study, I explored the use of novel, optical indicators of fecal contamination, turbidity, TLF and OB, in the Clinton River Watershed to determine the practicality of their use in water quality monitoring. I developed regression models to measure the correlation strength between these indicators and *E. coli*, a widely used fecal indicator bacteria, over various stages of the flow regime. I compared the correlation strength of these indicators with that of turbidity, another emerging indicator of fecal contamination. The results of these regressions are indicative of the potential to use turbidity, TLF, and OB as surrogate indicators of fecal contamination, and perhaps shift the needle towards using continuously collected monitoring data to gain detailed insight on water quality patterns and the sources of fecal contamination. By collecting this information in tandem with other water quality parameters, I was able to observe families of response patterns that inform guidelines for appropriate usage. In this section, I elaborate on response patterns and regression models from the study results, justify appropriate use guidelines, and provide “lessons learned” in field monitoring to aid in the development of future deployment schemes.

Patterns in Fecal Contamination Indicators

Diurnal Patterns

Temperature data demonstrated diurnal patterns during baseflow across all study stations, mirroring ambient air temperature. Increasing temperatures are known to attenuate the readings of other water quality parameters, particularly in fluorometry where temperature quenches fluorescence⁴⁶ (i.e. fluorescence readings are lower than “true” values at high temperatures). Although temperature compensation was either applied directly by internal correction with water quality sondes (in the case of turbidity) or in post-processing (as applied to TLF and OB data), diurnal fluxes in these parameters during

1 baseflow conditions were apparent at all stations. This condition was most obvious during baseflow
2 season #2 (summer low flows). However, diurnal fluxes were not always timed as would be expected if a
3 lack of temperature compensation caused this issue. With temperature quenching, I would expect to see a
4 decline in observed values of fluorescent parameters with increasing temperature. At all three stations,
5 diurnal turbidity peaks were aligned with temperature peaks at baseflow (Figure 4-1). At the Red Run
6 Drain, the same was true for TLF and OB, and the peaks of all three parameters aligned with the negative-
7 peaks of flow (daily minima) At other stations, the temporal alignment of diurnal peaks for TLF & OB
8 were less apparent.

9 I've considered two theories to explain these observations; either the algorithms used to correct
10 for temperature overcompensate at higher temperatures, or diurnal peaks in TLF, OB, and turbidity are
11 more dependent on diurnal flow patterns than diurnal temperature patterns. The latter seems to be true of
12 the Red Run Drain, where baseflow discharge levels peaked between 02:00-04:00 AM EST from what I
13 hypothesize to be a treated wastewater effluent pulse from the City of Warren WWTP. This daily pulse of
14 relatively clean baseflow may temporarily dilute pollutants, and when flows return to negative-peak flow
15 levels, concentrations rise again. However, the timing of diurnal fluxes at other stations is likely
16 indicative of insufficient temperature compensation algorithms, and thus the need to generate instrument-
17 specific models. Khamis et al.²⁴ made the case for instrument-specific models, and for the aforementioned
18 reasons I recommend generating such models for all instruments measuring fluorescent parameters in
19 future studies. Although, diurnal fluxes in fluorescent parameters were strongest during low baseflows at
20 relatively high seasonal temperatures, and are unlikely to impact the usage of fecal contamination
21 monitoring during wet-weather events.

22 ***Seasonal Patterns***

23 Seasonal variation in hydrology informed the seasonal patterns observed in both TLF and OB. At
24 the Red Run Drain and the Middle Branch stations, both TLF and OB reached maximum levels during the
25 summer low flow seasons. Several theories may explain the seasonal spike in fecal contamination

1 indicators. The increase could be indicative of an ideal temperature range for fecal indicator bacteria
2 during the summer. Perhaps concentrations of fecal matter are greater in lower baseflows, or loading is
3 higher during summer flows with land application of manure (application of manure in spring and
4 summer is not recommended, yet not outlawed in the state of Michigan⁴⁷). Alternatively, monitoring
5 station configurations may have affected TLF concentrations at the Red Run Drain and Middle Branch
6 stations. That is, the intake tubing for the pump-and-flow through cell configurations at these stations was
7 replaced in September due to biofilm accumulation inside the tubing. Samples collected at the intake and
8 effluent of the tubing confirmed *E. coli* growth inside the tubing, which led to a biased high readings of *E.*
9 *coli*. While the tubing was replaced and routinely cleaned for the remainder of the field season (see
10 “Lessons learned in field monitoring”), it is possible that microbial activity inside the tubing led to
11 increased TLF concentrations before the establishment of this maintenance protocol. The North Branch
12 station showed limited seasonal variation in TLF, and this monitoring station was configured as an in-situ
13 (without intake tubing). Despite these considerations, I predict the seasonal variation in TLF is
14 representative of stream conditions and a product of the low flow conditions, given that OB also exhibited
15 the same seasonal increase during summer months. Future field monitoring campaigns over multiple
16 years will aid in validating the seasonal patterns in these parameters, particularly if improved maintenance
17 activities are implemented at stations configured with pump-and-flow through cells.

18 ***Flow-dependent Patterns***

19 As hypothesized, the predictive power of the analyzed fecal contamination indicators is flow-
20 dependent under wet-weather conditions. In characterizing the relationships between our predictor
21 variables (turbidity, TLF, and OB) and *E. coli* under different flow conditions, I was able to provide a
22 preliminary understanding of when their use is most promising. Predictor variables were significant in all
23 cases, and this significance was greater in models when data was isolated to the ascending limb of the
24 hydrograph as compared with data isolated to the descending limb. The significance of the correlation (as
25 measured by the p-value) between turbidity and *E. coli* was comparable with previous studies by

1 Lawrence et al in the Chattahoochee River between 2000 and 2008³¹, and by Huey et al. in 2010 the
2 Upper Pecos River Basin ³². For TLF, correlation strength by comparison of the R² values was
3 comparable with studies by Baker et al. in the Kwazulu-Natal, South Africa in 2015⁴⁸, but much weaker
4 than previous studies by Cumberland et al. in West Midlands, United Kingdom in 2012²³. Prior studies by
5 McDonald et al in 2006²⁷ and Dickerson et al in 2007²⁸ used OB to detect human-sourced fecal
6 contamination with microbial source tracking to determine the presence or absence of human-associated
7 *Enterococci*. To my knowledge, no comparable studies exist that use simple regression analyses to
8 determine the predictive ability of OB for *E. coli*.

9 Model fit was relatively weak across all regressions, and highly variable with each hydrograph
10 phase. I anticipated poor model fit given the relatively small number of storms sampled, and that data
11 were collected across only three different storms, at three different stations, and during two different
12 baseflow seasons (late spring high flows and fall intermediate flows). Ideally, the analysis would be
13 performed with considerably more data from multiple storms in the same season to make confident
14 predictions about the predictive strength of these indicators. It is clear from the regression plots that data
15 are clustered, and data availability is limited in the descending limb of the hydrograph.

16 There is also great variability in the response behavior of TLF to flow across the sampling events.
17 In instances of smaller storms, a pulse in TLF is seen with increasing flow and increasing *E. coli* levels. In
18 contrast, larger storms seem to dilute TLF after an initial small spike, in which case TLF levels decreased
19 as *E. coli* levels increased. OB exhibited a strong dilution response during large and small storms, where
20 OB levels dropped with increasing flow and then rebounded back to baseflow levels. This response
21 behavior typically occurred while *E. coli* levels were still increasing. The combination of these two
22 response behaviors help explain the cubic shape of the relationship between OB and *E. coli* in models
23 using the full dataset and data isolated to the ascending limb. For the models in this study, data were not
24 separated based on their response behavior to flow, and instead were organized by hydrograph phase. I
25 expect improvements in model can be achieved by sampling a wider range of storm events, and by
26 separating data from fecal contamination indicators into response patterns.

1 Additional limitations include the significant temporal autocorrelation of the errors across all
2 models. This is expected with times series data, where a regression model fails to effectively capture
3 time-series trends. In such a case, the random errors in the model are often positively correlated over time,
4 and therefore any given error is more likely to be correlated to the previous error than random errors
5 independent of each other. Time-series forecasting models such as ARIMA can be used to predictive
6 seasonality in the data and account for temporal autocorrelation. However, the limited amount of data
7 collected in this study are unsuitable for ARIMA models. To understand seasonal variation in the
8 predictive ability of the fecal contamination indicators, continued studies of this nature at consistent
9 monitoring stations and over longer time spans are needed.

10 *Investigation of Optical Signatures*

11 From the preliminary exploration of fluorescence spectra at baseflow conditions, I discovered
12 additional optical signatures that are present are higher fluorescence intensities than those exhibited by
13 TLF or OB. In the case of wastewater influent samples (associated with high levels of human feces and
14 microbial abundance), EEMs were centered on the excitation range of 220-240 nm and the emission range
15 of 310-350 nm. While there is no associated peak signal name with this region, several studies have
16 indicated potential fluorophores of industrial and domestic wastewater origins in this region. Determann
17 et al.⁴⁹ identified indole as a fluorophore associated with peaks from excitation at 230 nm and emissions
18 between 330-350 nm. This substance is a metabolite of tryptophan. It occurs in coal tar and human feces,
19 yet it's also a synthetic constitute of many flower-scented perfumes. A study from del Olmo et al⁵⁰
20 demonstrated that fluorescence from cresol is associated with peaks from excitation ranges of 210-285 nm
21 and excitation ranges of 290-310 nm. Cresol is a type of phenol, and its origin in wastewater streams can
22 be from pharmaceutical, fossil fuel, or pesticide manufacturing industry effluents.

23 For all samples collected from surface water monitoring stations, EEMS were centered on peak
24 signal A (excitation at 260 nm, emission from 400-500 nm) and peak signal LA (excitation at 240 nm,
25 emission at 440 nm). A 2016 review of fluorescent spectroscopy applications for wastewater monitoring

1 indicated that peak signal A is often associated with naturally occurring microbial activity and the decay
2 of organic matter derived from terrestrial and aquatic ecosystems⁵¹. Domestic wastewater streams with
3 high microbial abundance are often characterized by intense peaks from signals with emission < 380 nm,
4 especially peak signal T (i.e. TLF), and significantly lower intensities from peak signal A and peak signal
5 C (excitation at 300-350 nm and 400-500 nm, respectively)^{44,52,53}. However, other studies showed higher
6 intensities with peak signal A and peak signal C, as compared to peak signal T in wastewater effluent
7 streams^{54,55}. Similarly, the fluorescence of animal wastewater streams is known to be generally dominated
8 by peak signal T⁵⁶⁻⁵⁸.

9 It's possible that the high fluorescence intensities around peak signal A from the samples I
10 collected indicate the presence of domestic wastewater. From this anecdotal investigation, I could
11 postulate that peak signal T (i.e. TLF) and OB are inappropriate signatures at these stations for
12 wastewater monitoring at baseflow. I believe it is more likely these samples are showing signatures of
13 organic matter decomposition associated with natural ecosystem processes, based on evidence in the
14 literature. One sampling event is not enough to characterize the fluorescence spectra of these stations. I
15 recommend future studies compare EEMs across multiple seasons and flow conditions in conjunction
16 with microbial indicators of fecal contamination, before determining if other optical signatures should be
17 used.

18 **Lessons Learned in Field Monitoring**

19 Upon undertaking the challenge of applying a novel technology, I anticipated setbacks from
20 unforeseen circumstances. This study exceeded my expectations for obstacles and tested my ability to
21 maintain optimism. In this section, I will draw on my experiences to provide lessons learned in the field
22 monitoring of optical parameters in hopes that future researchers may avoid such difficulties and add to
23 the findings of this study.

Advantages and Disadvantages to Monitoring System Configuration

The team of researchers designing the field monitoring study selected monitoring system configurations based on site-specific constraints to station configuration. At the time of study design, we researched the benefits of both in-situ and flow-through cell monitoring configurations. While the general advantages and disadvantages of monitoring system configuration are well documented⁵⁹, in the case study the primary considerations were protection from vandalism, access to power sources, and shelter from the elements during station visits for calibration and sampling. These considerations led to the prioritization of flow-through cell configurations. However, in my experience there are considerable disadvantages associated with flow-through cell configurations that should direct future researchers to deploy in-situ configuration whenever possible.

Two primary disadvantages include the heightened maintenance costs and low signal-to-noise ratios associated with flow-through cell configurations. In both stations operating under flow-through cell configurations, failures in pump operation led to substantial losses in data. Certain failures were attributed to the continuous operation of the pump, leading to the premature degradation of peristaltic tubing, loss of suction, and ultimately system overheat. To reduce strain on the peristaltic tubing, I recommend using a programmable pump and employing intermittent pumping at sampling intervals. Through discussion with other researchers in the field of continuous water quality monitoring, a programmable pump can easily be employed to overcome these frustrations⁶⁰.

In addition, intake tubing often became clogged with coarse debris or coated with biofilm, necessitating the weekly flushing of the intake tubing to ensure influent wasn't compromised. An investigation of *E. coli* levels directly adjacent to the intake tubing and downstream of the water quality sondes showed that biofilm may have concentrated *E. coli*. Without accounting for this issue, there is potential for biased interpretations of the degree of fecal contamination.

None of these issues were of concern in in-situ deployments, as pumps were not utilized and biofouling was limited using a wiper blade. With this deployment, turbidity, specific conductance, TLF & OB data all exhibited low signal-to-noise ratios. In contrast, stations configured with pump and flow-

1 through-cell intakes showed considerable noise. Being that turbidity readings yielded the highest standard
2 deviations relative to the mean for all seasons and flow conditions, I postulate that stations with flow-
3 through cell intermittently pumped in “slugs” of sediment with attached pollutants (i.e. samples were less
4 homogenized). High noise levels led to additional post-processing to reveal signals, adding time to the
5 overall analysis.

6 ***Reporting Units for TLF and OB***

7 Monitoring stations were configured to allow for water quality sondes to transmit data through
8 communication cables to a data logger, then to a web-based data viewing platform with a cellular
9 network. The optical parameters were monitored using a Turner Designs C3™ Submersible Fluorometer
10 with converts fluorescence intensity measured in raw fluorescence blank (RFUb) to parts-per-million
11 (ppm) of tryptophan-like-fluorescence and optical brighteners using an internal calibration curve.
12 Initially, data were transmitted from the C3™ to four significant digits, yet the web-based platform only
13 recorded to two significant digits, leading to a loss in the resolution of data. Because data were not
14 preserved outside of the data viewing platform, this resolution was lost. Later in the field season, the
15 research team discovered that additional resolution could be provided by reporting directly in units of
16 RFUb, and using calibration curves to convert data to units of ppm in post-processing. With these
17 findings, I recommended that future researchers ensure congruency in units across sondes, data loggers,
18 and data-viewing or storage platforms and report in RFUb to achieve the highest data resolution available.
19 However, it is noteworthy that calibration curves are highly variable between different sensors, and over
20 time within the same sensor, thus frequent and sensor-specific calibration is necessary.

21 ***Logistical Constraints of Discrete E. coli Monitoring during Wet-Weather Events***

22 To fully characterize patterns of *E. coli* during wet-weather events, it was paramount to collect
23 samples at high frequencies so critical hydrograph phases were not missed. With this came substantial
24 logistical considerations in the configuration of the monitoring team. A minimum of six personnel (two
25 per station for safety considerations) were necessary, and team deployments were timed with site-specific

1 time-to-peaks to ensure sampling occurred during the first flush. Teams were on-call for storm events at
2 all hours of the night, often with capricious weather forecasts that drew limited hydrological response. To
3 ensure full staff availability when the ideal storm arrives, it is recommended that a large group of back-up
4 personnel are available. This can lead to uncertainties in the budget of the project, due to variations in
5 staffing rates, etc. All these considerations reinforce the need to improve continuous and remote water
6 quality monitoring techniques for fecal contamination, as is the primary objective of this study.

7 **Conclusions**

8 This study sought to investigate the validity and practicality of using fluorescence
9 spectrophotometry to measure fecal contamination across various hydrological conditions. Validity was
10 measured by the ability of the fluorescent parameters to predict *E. coli* at different hydrograph phases.
11 Results from the regressions models indicate that turbidity, TLF, and OB are significant in their predictive
12 ability at all hydrograph phases, yet model fits were poor due to data clustering. The response of each
13 indicator varied considerably with flow conditions, yet clear flow thresholds are not yet discernible. This
14 indicates a need to build site-specific regressions with storms of varying magnitude across longer time
15 spans to gain confidence in the predictive ability of these parameters. Rather than isolating data strictly by
16 hydrograph phases, future studies should explore the organization of regression models by patterns in
17 indicator responses (for example, pulse spikes, dilution effects, and stable baseflow).

18 To practically use fluorometry for the continuous detection of fecal contamination, practitioners
19 will need to optimize deployment configurations, maintenance plans, and post-processing protocol. The
20 use of fluorometry for the detection of fecal contamination is often praised as being a low-cost option for
21 watershed managers, particularly in reference to the use of hand-held fluorometers for spot testing. This
22 study demonstrated noteworthy constraints associated with long-term deployments, which added
23 unforeseen labor costs to the initial deployment plan. In-situ deployment of water quality sondes can
24 reduce these costs, and managers should elect to deploy in this configuration where station conditions are
25 appropriate.

1 Despite these constraints, the application of fluorometry to measure fecal contamination has the
2 potential to provide rapid indications of microbial pollution, without the need to wait for results from
3 culture-based approaches. Additionally, continuous data collection can provide watershed managers with
4 high-density datasets over longer time frames and greater spatial scales than is possible with discrete
5 sampling. In turn, they may discern detailed relationships between discharge and fecal contamination at
6 sites targeted for water quality restoration efforts, and the effects of restoration efforts can be more easily
7 monitored. This is particularly applicable to the development of TMDL regulations where high volumes
8 of fecal contamination data are needed in conjunction with flow data. While current U.S. EPA guidelines
9 suggest the use of *E. coli* or *Enterococcus* for the development of TMDLs, studies are limited by discrete
10 samples over relatively short periods (1-2 years) to estimate pollutant loads.

11 With continued research and improvements to prediction ability, this technology can aid
12 practitioners in improving source tracking of pollution. The use of OBs allows managers to detect fecal
13 contamination associated with residential sewage. Microbial source tracking can also be used to detect
14 human-specific enteric microorganisms, yet the expense of microbial source tracking techniques is often
15 prohibitive for use at watershed scales. Using submersible fluorometers to detect OBs in combination
16 with TLFs is more cost-effective than microbial source tracking techniques, and can provide similar
17 results.

18 Water quality impairment from fecal contamination is a widespread problem throughout the
19 world, and especially in the State of Michigan. The recent publication of Michigan's Statewide *E. coli*
20 TMDL indicated that 9,000 miles of streams with the TBC designated use are currently impaired due to
21 fecal contamination, and that number is expected to grow to about half of Michigan's stream miles
22 (37,000) as more monitoring is conducted⁶¹. To achieve the goal of being delisted from TMDL regulation,
23 communities must employ innovative strategies for the source tracking and management of fecal
24 contamination. It is my hope that the use of continuous fecal contamination indicators will continue to
25 improve and become a practical tool to aid water resources managers in achieving water quality goals.

Chapter 6 - Compensating For The Effects of Temperature and Turbidity on Tryptophan-like-Fluorescence and Optical Brighteners

Background

The use of TLF and OB could provide water resources managers with advanced utility in monitoring fecal contamination. However, the environmental conditions of riverine systems are highly dynamic, thus monitoring fluorescence may be subject to instrument interference. Fluorescent compounds (fluorophores) are known to be sensitive to a wide variety of interferences, known as signal amplifiers or quenchers⁶²⁻⁶⁴. Before fluorescence measurements are interpreted, compensation techniques for fluorescence quenching and signal amplification should be considered. Fluorescent compounds are known to be influenced by higher temperature⁴⁶, as higher temperatures increase collisional quenching and dampen the fluorescent signal with increasing temperature. Diurnal temperature fluctuations in riverine systems are a key driver of uncorrected fluorescent observations, particularly in streams with low summer baseflows that are greatly influenced by diurnal swings in ambient air temperature. Suspended particles create an additional challenge, as they can cause increased light scattering leading to signal amplification or attenuation depending on the degree of interference⁶⁵. Without correction, deriving the fluorescent signals of surface water pollution can be extremely challenging and misleading. To account for environmental interferences while monitoring TLF and OB as indicators of fecal pollution contamination, compensation techniques were either collected from the available literature or derived in laboratory experiments. In this chapter, I provide an overview of the development and application of temperature and turbidity compensation techniques used in this study.

1 **Methods**

2 ***Temperature and Turbidity Corrections for Tryptophan-like-Fluorescence***

3 The interference of environmental factors on fluorophore detection has long been studied. As this
4 phenomenon pertains to TLF, Khamis *et al*²⁴ quantified the effects of temperature quenching and
5 turbidity interference specific to the Cyclops 7™ (Turner Designs, Sunnyvale, CA) sonde and other
6 fluorometers containing the same sensors used in this study under different housing configurations.
7 Following the technique for temperature compensation in carbon dissolved organic material (CDOM)
8 used by Watras *et al*⁶⁶, they developed compensation algorithms for temperatures ranging from 5-35 °C.
9 Results indicated that a linear model provided the best fit for the Cyclopes 7™ TLF sensor leading to the
10 compensation technique provided in equation 6.1.

$$11 \quad TLF_{ref} = \frac{TLF_{mes}}{1 + \rho(T_{mes} - T_{ref})} \quad (6.1)$$

12 Where *TLF* is the concentration of TLF (ppb), *T* is temperature (°C) and the subscripts *mes* and
13 *ref* refer to the measured and reference values, respectively. Given that the calibration of the fluorometer
14 was performed at 20°C, I used this temperature for *T_{ref}* and calculated *TLF_{ref}* as the true value of TLF at
15 20°C. The temperature compensation coefficient, ρ , is the ratio of the slope : intercept of the OLS
16 regression modeling the relationship between temperature and the measured TLF concentration, which
17 was shown to be relatively constant regardless of fluorophore reference standard concentration. This
18 temperature compensation algorithm was applied to the TLF signal data for in-situ measurements
19 collected in this study.

20 For suspended particles, Khamis *et al*.²⁴ evaluated both clay- and silt-dominated matrices and
21 found varying effects depending on the sediment type and degree of turbidity. Both silt- and clay-
22 dominated matrices were evaluated and signal amplification of TLF was apparent in <150 NTU for clay
23 particles and <650 NTU for silt particles. Of the two matrices evaluated, silt-dominated particle size
24 distributions are most similar to the conditions observed at the monitoring stations of this study. While

1 determining the exact particle size distribution would be most ideal, conducting these types of analyses
2 was outside the scope of this study. Thus, I applied the compensation algorithm derived for silt-dominated
3 matrices to the TLF signal data from in-situ measurements collected in this study (equation 6.2).

$$4 \quad cf = a + ab + a^2 + a^2b^2 + b^3 + a^3b^2 \quad (6.2)$$

5 ***Temperature and Turbidity Correction for Optical Brighteners***

6 In contrast to the studies of environmental interference with TLF²⁴, relatively little is known
7 about similar interferences with OB in laboratory or field settings. I found only one study evaluating the
8 effects of OB readings at stable temperatures⁶⁷. However, as it is known that fluorescent compounds
9 display high sensitivity to environmental conditions, the need to evaluate the effects of temperature and
10 turbidity on OB signals became paramount. Therefore, I conducted a study to quantify the effects of
11 temperature and turbidity interference on OB fluorescence for the Cyclops 7TM.

12 ***Reference Standard Solution Preparation and Instrument Calibration***

13 I prepared reference standard solutions for calibrations with a commercial laundry detergent, Tide
14 2X Original Scent Powdered Detergent (Tide, Procter & Gamble, Cincinnati, OH) and deionized water.
15 Then, I used stock solutions of 100 ppm OB to create serial dilutions ranging from 0.25-50 ppm. Standard
16 solutions were prepared in a dark room inside acid-washed (HCl 5%) Erlenmeyer flasks wrapped in a foil
17 to prevent photo decay. Standard solutions were prepared at room temperature and refrigerated for a
18 maximum of 48 hours reaching a stable temperature of 5 °C confirmed with a thermistor. Temperature
19 measurements were stabilized over thirty seconds for all measurement runs. To convert observed
20 fluorescence measurements to concentration values at a given reference temperature, I calibrated the
21 fluorometer prior to the temperature and turbidity effects assessment. The calibration curves of two
22 reference temperatures (10 and 20 °C) were evaluated to represent the relationship between reference
23 standard concentration and observed fluorescence for both the temperature effects and turbidity effects
24 analyses.

Assessment of Temperature Effects on Optical Brighteners

To evaluate the instrument-specific effect of temperature on OB readings, I measured fluorescence over a warming cycle from 5-35°C for seven standard solutions (0.25, 2.5, 6.25, 12.5, 25, and 50 ppm). Standard solutions were cooled to 5°C overnight and transferred directly to a heated mixing plate (Corning PC-351, Corning, New York) and constantly stirred. Stirring speeds were maintained at a threshold low enough to prevent foaming of the detergent to ensure a homogenized solution. Thermistors were submerged centrally inside the flask at the mid-point of the height of the solution and taped to the flask to maintain their placement. For each standard solution, temperatures were gradually increased to 35°C over 30 minutes. Temperatures were monitored and readings with fluorescence readings taken at 5°C ($\pm 1^\circ\text{C}$) intervals. Once the desired temperature was achieved, readings were recorded with the fluorometer submerged centrally inside the flask at the mid-point of the height of the solution.

Assessment of Turbidity Effects on Optical Brighteners

To evaluate the instrument-specific effect of turbidity on OB readings, I added incremental portions of a silt standard (Ward's Science, Rochester, NY) to standard solutions to create a turbid media. Silt (versus clay) was selected based on visual observation of the dominant particle sizes at the selected monitoring stations. Standard solutions were cooled to 10°C overnight and transferred into volumetric flasks placed directly onto a mixing plate (Corning PC-351, Corning, NY). Stirring speeds were maintained at a threshold low enough to prevent foaming of the detergent, yet fast enough to maintain sediment suspension to ensure a homogenized solution. Fluorescence was measured over a series of sediment additions to give a range of turbidity (0-1000 FNU) for four standard solutions (2.5, 6.25, 12.5, and 50 ppm). For every incremental addition of silt, turbidity was measured with a YSI EXO optical turbidity sensor (599101-01, YSI Incorporated, Yellow Spring, OH) housed in the YSI EXO 2 Multi-parameter Water Quality Sonde. Fluorescence readings were recorded after a stabilization of ± 1 FNU was achieved with the fluorometer submerged centrally inside the flask at the mid-point of the height of the

1 solution. Temperature was measured periodically to ensure temperatures did not vary throughout
2 experimental runs.

3 ***Development of Optical Brightener Concentration Prediction Models***

4 I took several approaches to derive prediction models for the OB concentration given observed
5 fluorescence, temperature, and turbidity. Initially, I attempted using OLS regression (equation 36) for
6 temperature compensation as performed by Khamis *et al.*²⁴ and Watras *et al.*⁶⁶ for TLF and CDOM,
7 respectively. A key assumption of this technique is the consistency of the ratio between the slope :
8 intercept (ρ) for each reference standard in order to use the average ρ value for the model including all
9 trial runs. To evaluate this assumption, I performed individual regressions and determined $\rho \pm$ the
10 standard error. The temperature of the instrument during calibration was used as the reference
11 temperature, in this case 20°C.

12 I attempted additional approaches to model the prediction of the OB concentration given the
13 observed fluorescence, temperature, and turbidity while considering the interaction effects of these
14 parameters. First, a Generalized Linear Model (GLM) (Gaussian distribution) including all predictor and
15 modifier variables was applied, including the interaction of the observed fluorescence with turbidity and
16 temperature (equation 6.3). Then, two separate GLMs were performed were developed to include
17 observed fluorescence and either temperature or turbidity as a predictor variable and the interaction of
18 observed fluorescence with either temperature or turbidity as the respective modifier variables (equations
19 6.4 and 6.5, respectively).

20 I performed two additional stepwise GLMs to account for the non-linear relationship between the
21 reference standard concentration and the observed fluorescence. Initially, a natural logarithmic
22 transformation of both the reference standard concentration and the observed fluorescence was
23 performed, and included with temperature and turbidity as both predictor and interaction terms. Then, I
24 created additional stepwise GLM to include the square of the observed fluorescence as a predictor
25 variable, including temperature and turbidity as both predictor and interaction terms. I evaluated multiple

different equations forms for prediction models for temperature or turbidity compensations, and compared metrics of model performance (AIC and RMSE) and fit (R^2).

Results and Discussion

Calibration Response

Calibration results displayed highly significant and positive linear relationships ($R^2 > 0.95$, $P < 0.0005$) between the log-transformed reference standard concentrations and the log-transformed observed fluorescence for both calibrations performed at 10 and 20 °C (Table 6-1). The need for log transformation to derive a linear relationship raises important concerns about the accuracy of calibration at higher concentrations (>25 ppm). Although concentrations at higher ranges are easier to detect, they are less likely to be encountered in field settings.

Table 6-1: Calibration equations and measures of fit of laboratory trials based on reference standard solutions of OBs prepared with commercial laundry detergent in deionized water

<i>Calibration Temperature</i>	<i>Calibrated Relationship</i>	<i>Adjusted R^2</i>	<i>P-value</i>	<i>RMSE</i>
10 °C	$y = 10^{1.1 \log(x) - 1.22}$	0.97	0.0002	1.13
20 °C	$y = 10^{1.1 \log(x) - 0.91}$	0.97	0.0003	0.83

Optical Brightener Concentration Prediction Models

Temperature Response

For all reference standard concentrations, observed fluorescence values were negatively related to temperature, with mean OLS slopes ranging from -0.0155 ± 0.0026 (0.25 ppm) to -1.28 ± 0.29 (50 ppm) (Figure 6-1). Slope values increased with higher reference standard concentrations, indicating that perhaps the quenching effect of temperature is more apparent at higher concentrations. Temperature

1 correction coefficients varied negligibly between reference standard concentrations ($\rho = -0.023$, $\alpha =$
2 0.046) (Figure 6-2). Changes in observed fluorescence with increasing temperature observed in this study
3 are less than those reported by Khamis et al²⁴ with TLF using the same instrument model ($\rho = -0.039$, $\alpha =$
4 0.036), yet they fall within the range of values from those studying the fluorescence quenching from
5 temperature on DOM composition ($\rho = -0.009$ to -0.025)^{45,66,68}. The similarity in ranges highlight the need
6 to consider CDOM interference from OB signals when correcting field data.

7 ***Turbidity Response***

8 The relationship between turbidity and the observed fluorescence values was non-linear and
9 exhibited high spread. Yet, some consistencies in the shape of the signal were apparent across the range
10 of reference standards concentrations (Figure 6-3). For the highest three standards (50, 12.5, 6.25 ppm),
11 the observed fluorescence rapidly increased to a maximum and then gradually decreased at turbidity
12 levels near 1000 FNU. The lowest reference standard (2.5 ppm) did not exhibit the same gradual
13 decrease, rather the fluorescence signal exhibited a change in slope direction around 500 FNU and
14 increased as turbidity values approached 1000 FNU.

15 The range of turbidity values where the rapid increase in fluorescence was apparent was different
16 across reference standards, with maximum fluorescence values ranging between 10-100 FNU. The
17 increase in the observed fluorescence at low turbidity somewhat conforms with the experimental findings
18 of Khamis *et al.*²⁴ who reported similar results on the maxima of TLF signals at low to moderate (100-300
19 FNU) turbidity. However, Downing *et al.*⁴⁵ and Saraceno *et al.*⁶⁵ both reported attenuation of CDOM at
20 low and high turbidity ranges from clay-loam sediments, in line with the pattern seen for the same three
21 reference standards.

22 It is possible that an organic coating on the silt particles used in this study could have caused the
23 increased fluorescence intensity signal at lower turbidities, as the silt had not undergone standard
24 disinfection procedures (typically performed with hydrogen peroxide). Further studies with additional
25 trial runs on lower reference standard concentrations are necessary to show repeatable results and

1 distinguish between trends across reference standard concentrations. However, the ability to perform
2 repeat experiments was not available in this study and therefore compensation algorithms were derived
3 using the available data.

4 ***Correction Model Evaluation***

5 Prediction models varied in measures of model skill and fit, and models incorporating logarithmic
6 and squared transformations of predictor variables outperformed linear models (Table 6-2). Temperature
7 correction using equation 6.3 as applied by Khamis *et al*²⁴ and Watras *et al*⁶⁶ yielded negative bias for
8 higher concentrations (12.5, 25, 50 ppm) and negative bias for low concentrations (0.25 and 2.5 ppm).
9 The technique yielded fair model fit ($R^2 = 0.81$, RMSE = 5.12), leading to the desire to explore additional
10 techniques in developing interaction models considering both the effects of turbidity and temperature as
11 moderator variables.

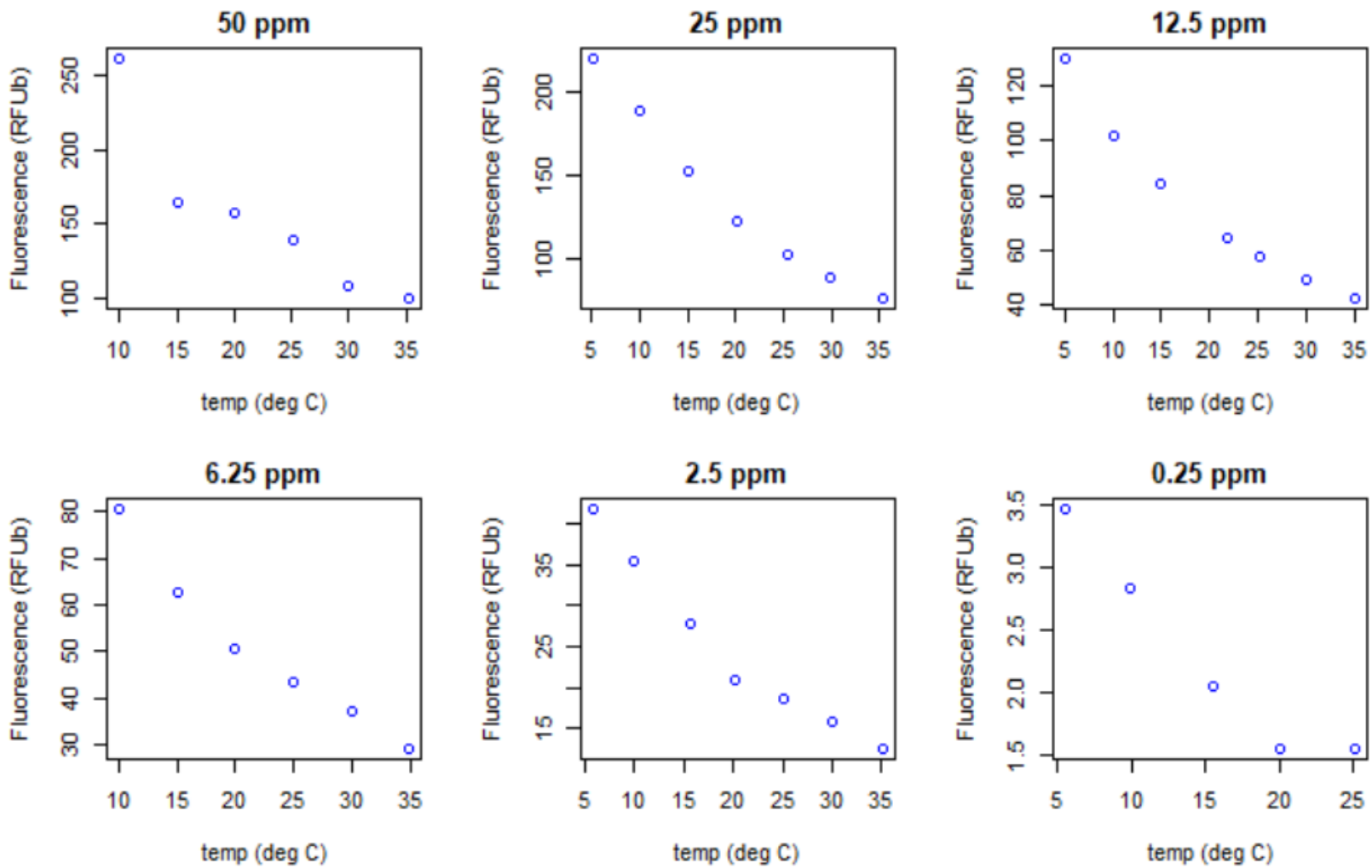
12 The model including all predictor and modifier variables without parameter transformations
13 (Equation 6.4) provided even lower measurements of model fit ($R^2 = 0.63$, RMSE = 10.47). Attempts to
14 create models excluding either temperature (equation 6.5) or turbidity (equation 6.6) as predictor and
15 moderator variables fared moderately better ($R^2 = 0.65$, RMSE = 10.30 and $R^2 = 0.82$, RMSE = 7.02,
16 respectively). Yet, with these models came high RMSE values relative to the reference concentrations.

17 In reviewing raw data trends, it was clear that the non-linear relationship between the reference
18 standard concentration and the observed fluorescence required data transformations. Models using log-
19 linear (equation 6.7) and squared (equation 6.8) transformations of these parameters outperformed the
20 prior models significantly ($R^2 = 0.87$, RMSE = 0.49 and $R^2 = 0.90$, RMSE = 0.42, respectively).

21 Based on the comparison of skill and fit metrics, the model described by equation 6.8 was
22 selected for application to field study data. Despite the measurements of model fit, the bias in the
23 prediction using this technique varies with reference standard concentration. That is, the model tends to
24 underpredict with lower concentration reference standards and over predict with higher concentration

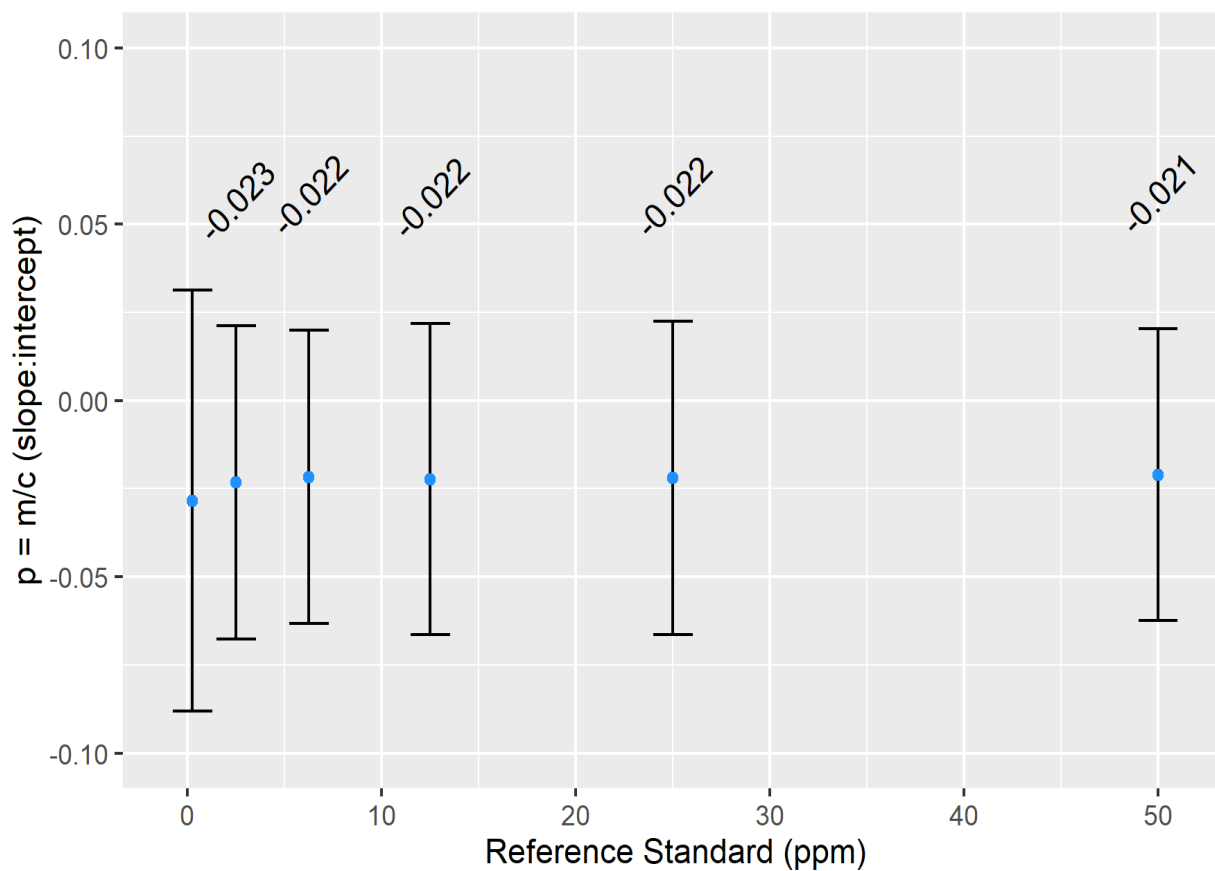
1 reference standards (Figure 6-4). In earlier chapters of this work, interpretations of OB field study data
2 were made with consideration of this model bias.

3



1
2 *Figure 6-1: Temperature quenching effect on OB fluorescence at six reference standard concentration (50, 25, 12.5, 6.25, 2.5, 0.25ppm).*

1



2

3 *Figure 6-2: Comparison of temperature compensation coefficient estimation for individual OLS*
4 *regressions for a series of known reference standard solutions of OB.*

5

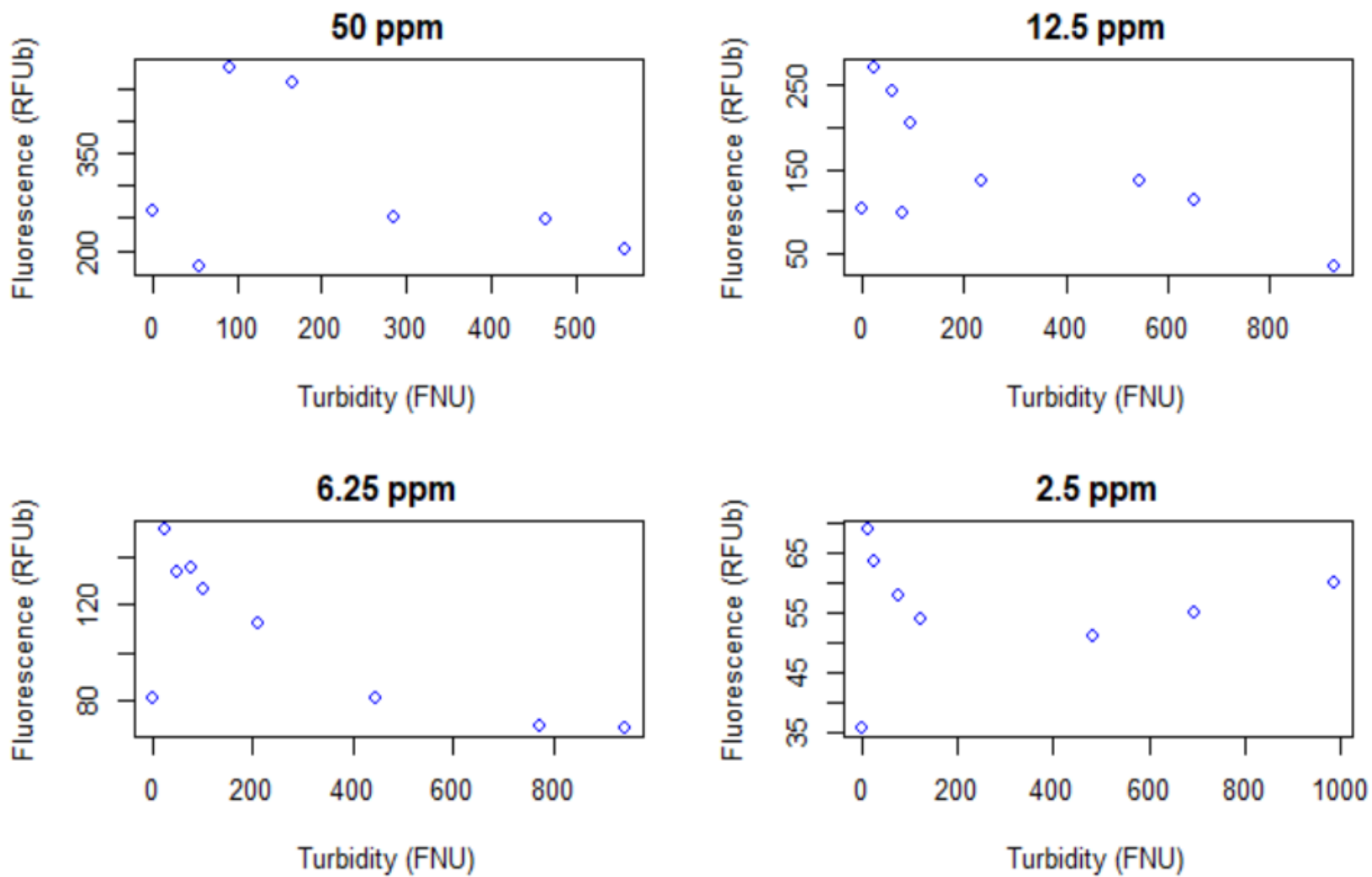


Figure 6-3: Turbidity inference effects on OB Fluorescence for four reference standards (2.5, 6.25, 12.5, and 50 ppm).

Table 6-2: Form of equations for OB concentration (ppm) prediction models with temperature and turbidity correction compensation showing evaluated (E) and selected (S) parameters with coefficients, along with measures of model skill and fit.

		AIC	R ²	RMSE
E	$OB_{True} = \frac{OB_{mes}}{1 + \rho(T_{mes} - T_{ref})} \quad (8.3)$	250	0.81	5.12
S	$OB_{True} = \frac{OB_{mes}}{1 + -0.019(T_{mes} - 20^{\circ}\text{C})}$			
E	$OB_{True} = \beta_0 + \beta_1 F_{mes} + \beta_2 TB_{mes} + \beta_3 T_{mes} + \beta_{12} F_{mes} TB_{mes} + \beta_{13} F_{mes} T_{mes} \quad (8.4)$	545	0.63	10.47
S	$OB_{True} = -2.84 + 3.44 F_{mes} + 4.45 \times 10^{-5} F_{mes} TB_{mes} + 1.08 \times 10^{-2} F_{mes} T_{mes}$			
E	$OB_{True} = \beta_0 + \beta_1 F_{mes} + \beta_2 TB_{mes} + \beta_{12} F_{mes} TB_{mes} \quad (8.5)$	256	0.65	10.30
S	$OB_{True} = -5.05 + 0.13 F_{mes} + 1.57 \times 10^{-4} F_{mes} TB_{mes}$			
E	$OB_{True} = \beta_0 + \beta_1 F_{mes} + \beta_3 T_{mes} + \beta_{13} F_{mes} T_{mes} \quad (8.6)$	264	0.82	7.02
S	$OB_{True} = -5.51 + 0.13 F_{mes} + 0.0093 F_{mes} T_{mes}$			
E	$\ln(OB_{True}) = \beta_0 + \beta_1 \ln(F_{mes}) + \beta_2 TB_{mes} + \beta_3 T_{mes} + \beta_{12} \ln(F_{mes}) TB_{mes} + \beta_{13} \ln(F_{mes}) T_{mes} \quad (8.7)$ $+ \beta_{23} TB_{mes} T_{mes}$	104	0.87	0.49
S	$\ln(OB_{True}) = -3.36 + 1.07 \ln(F_{mes}) + 0.0077 TB_{mes} + 0.058 T_{mes} - 7.0 \times 10^{-4} TB_{mes} T_{mes}$			
E	$\ln(OB_{True}) = \beta_0 + \beta_1 \ln(F_{mes}) + \beta_2 TB_{mes} + \beta_3 T_{mes} + \beta_4 \ln(F_{mes})^2 + \beta_{12} \ln(F_{mes}) TB_{mes} + \beta_{13} \ln(F_{mes}) T_{mes} \quad (8.8)$ $+ \beta_{23} TB_{mes} T_{mes} + \beta_{42} \ln(F_{mes})^2 TB_{mes} + \beta_{43} \ln(F_{mes})^2 T_{mes}$			
S	$\ln(OB_{True}) = -2.25 + 0.52 \ln(F_{mes}) + 0.034 TB_{mes} + 0.024 T_{mes} + 0.053 \ln(F_{mes}^2)$ $- 0.012 \ln(F_{mes}) TB_{mes} - 6.57 \times 10^{-4} TB_{mes} T_{mes} + 0.0012 \ln(F_{mes}^2) TB_{mes}$ $+ 0.0025 \ln(F_{mes}^2) T_{mes}$	93	0.90	0.42

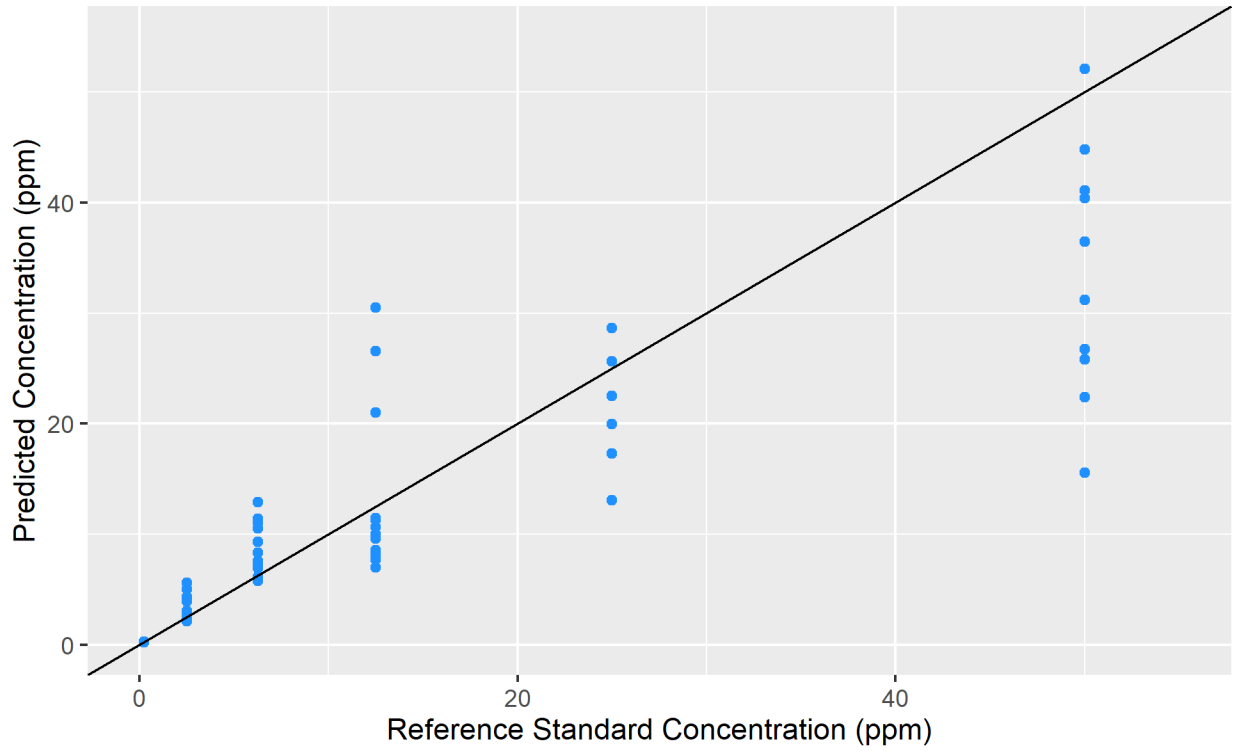


Figure 6-4: Reference standard concentrations versus predicted concentrations using a generalized linear model with both log-linear and squared transformation of predictor variables, including temperature and turbidity as interaction terms. Diagonals are presented to show the idealized prediction model ($m = 1, \beta_0 = 0$) and deviations in bias with reference standard concentration.

Chapter 7 - Bibliography

- (1) Ali, M.; Nelson, A. R.; Lopez, A. L.; Sack, D. A. Updated Global Burden of Cholera in Endemic Countries. *PLoS Negl. Trop. Dis.* **2015**, *9* (6), 1–13. <https://doi.org/10.1371/journal.pntd.0003832>.
- (2) Stanaway, J. D.; Reiner, R. C.; Blacker, B. F.; Goldberg, E. M.; Khalil, I. A.; Troeger, C. E.; Andrews, J. R.; Bhutta, Z. A.; Crump, J. A.; Im, J.; et al. The Global Burden of Typhoid and Paratyphoid Fevers: A Systematic Analysis for the Global Burden of Disease Study 2017. *Lancet Infect. Dis.* **2019**, *19* (4), 369–381. [https://doi.org/10.1016/S1473-3099\(18\)30685-6](https://doi.org/10.1016/S1473-3099(18)30685-6).
- (3) Ash, R. J.; Mauck, B.; Morgan, M. Antibiotic Resistance of Gram-Negative Bacteria in Rivers, United States. *Emerg. Infect. Dis.* **2002**. <https://doi.org/10.3201/eid0807.010264>.
- (4) United States Environmental Protection Agency. *Protocol for Developing Pathogen TDMLs*. EPA 841-R-00-002.; Washington, DC, 2001.
- (5) *Federal Water Pollution Control Act*; 33 U.S.C. 1251, 2002; p P.L. 107-303. <https://doi.org/10.2307/4591430>.
- (6) Michigan Department of Natural Resources. *Total Maximum Daily Load for E. Coli in the Lower Clinton River*; Lansing, MI, 2010.
- (7) New York State Board of Health. *A New Method for Determining Quantitatively the Pollution of Water by Fecal Bacteria*; Albany, New York, 1891.
- (8) United States Public Health Service. *Notes on the Relation between Coliforms and Enteric Pathogens*; 1943; Vol. 58.
- (9) United States Public Health Service. *Relative Resistance of Escherichia Coli and Eberthella Typhosa to Chlorine and Chloramines*; 1944; Vol. 59.
- (10) Bermudez, M.; Hazen, T. C. Phenotypic and Genotypic Comparison of Escherichia Coli from Pristine Tropical Waters. *Appl. Environ. Microbiol.* **1988**. <https://doi.org/10.1128/aem.54.4.979->

- 983.1988.
- (11) Fujioka, R. S. Monitoring Coastal Marine Waters for Spore-Forming Bacteria of Faecal and Soil Origin to Determine Point from Non-Point Source Pollution. In *Water Science and Technology*; 2001. <https://doi.org/10.2166/wst.2001.0419>.
 - (12) Fujioka, R.; Sian-Denton, C.; Borja, M.; Castro, J.; Morphey, K. Soil: The Environmental Source of Escherichia Coli and Enterococci in Guam's Streams. In *Journal of Applied Microbiology Symposium Supplement*; 1999. <https://doi.org/10.1111/j.1365-2672.1998.tb05286.x>.
 - (13) Rivera, S. C.; Hazen, T. C.; Toranzos, G. A. Isolation of Fecal Coliforms from Pristine Sites in a Tropical Rain Forest. *Appl. Environ. Microbiol.* **1988**. <https://doi.org/10.1128/aem.54.2.513-517.1988>.
 - (14) Slanetz, L. W.; Bent, D. F.; Bartley, C. H. Use of the Membrane Filter Technique to Enumerate Enterococci in Water. *Public Health Rep.* **1955**. <https://doi.org/10.2307/4589009>.
 - (15) Fujioka, R. S.; Shizumura, L. K. Clostridium Perfringens, a Reliable Indicator of Stream Water Quality. *J. Water Pollut. Control Fed.* **1985**.
 - (16) Staley, Z. R.; Edge, T. A. Comparative Microbial Source Tracking Methods for Identification of Fecal Contamination Sources at Sunnyside Beach in the Toronto Region Area of Concern. *J. Water Health* **2016**. <https://doi.org/10.2166/wh.2016.296>.
 - (17) *Microbial Source Tracking: Methods, Applications, and Case Studies*; Hagedorn, C., Harwood, V. J., Blanch, A. R., Eds.; Springer Science+Business Media, LLC: New York, 2011. <https://doi.org/https://doi-org.proxy.lib.umich.edu/10.1007/978-1-4419-9386-1>.
 - (18) Korajkic, A.; Badgley, B. D.; Brownell, M. J.; Harwood, V. J. Application of Microbial Source Tracking Methods in a Gulf of Mexico Field Setting. *J. Appl. Microbiol.* **2009**. <https://doi.org/10.1111/j.1365-2672.2009.04351.x>.
 - (19) Stoeckel, D. M.; Harwood, V. J. Performance, Design, and Analysis in Microbial Source Tracking Studies. *Appl. Environ. Microbiol.* **2007**, 73 (8), 2405–2415. <https://doi.org/10.1128/AEM.02473-06>.

- (20) Stapleton, C. M.; Wyer, M. D.; Kay, D.; Crowther, J.; McDonald, A. T.; Walters, M.; Gawler, A.; Hindle, T. Microbial Source Tracking: A Forensic Technique for Microbial Source Identification? *J. Environ. Monit.* **2007**, *9* (5), 427–439. <https://doi.org/10.1039/b617059e>.
- (21) United States Environmental Protection Agency. *Microbial Source Tracking Guide Document*; Washington, DC, 2004.
- (22) Hudson, N.; Baker, A.; Ward, D.; Reynolds, D. M.; Brunson, C.; Carliell-Marquet, C.; Browning, S. Can Fluorescence Spectrometry Be Used as a Surrogate for the Biochemical Oxygen Demand (BOD) Test in Water Quality Assessment? An Example from South West England. *Sci. Total Environ.* **2008**, *391* (1), 149–158. <https://doi.org/10.1016/j.scitotenv.2007.10.054>.
- (23) Cumberland, S.; Bridgeman, J.; Baker, A.; Sterling, M.; Ward, D. Fluorescence Spectroscopy as a Tool for Determining Microbial Quality in Potable Water Applications. *Environ. Technol.* **2012**, *33* (6), 687–693. <https://doi.org/10.1080/09593330.2011.588401>.
- (24) Khamis, K.; Sorensen, J. P. R.; Bradley, C.; Hannah, D. M.; Lapworth, D. J.; Stevens, R. In Situ Tryptophan-like Fluorometers: Assessing Turbidity and Temperature Effects for Freshwater Applications. *Environ. Sci. Process. Impacts* **2015**, *17* (4), 740–752. <https://doi.org/10.1039/c5em00030k>.
- (25) Hagedorn, C.; Weisberg, S. B. Chemical-Based Fecal Source Tracking Methods: Current Status and Guidelines for Evaluation. *Rev. Environ. Sci. Biotechnol.* **2009**, *8* (3), 275–287. <https://doi.org/10.1007/s11157-009-9162-2>.
- (26) Hagedorn, C.; Saluta, M.; Hassall, A.; Dickerson, J. Fluorometric Detection of Optical Brighteners as an Indicator of Human Sources of Water Pollution. Part II: Development as a Source Tracking Methodology in Open Waters. *Crop Soil Environ. News* **2005**, *2005–11*, 11.
- (27) McDonald, J. L.; Hartel, P. G.; Gentit, L. C.; Belcher, C. N.; Gates, K. W.; Rodgers, K.; Fisher, J. A.; Smith, K. A.; Payne, K. A. Identifying Sources of Fecal Contamination Inexpensively with Targeted Sampling and Bacterial Source Tracking. *J. Environ. Qual.* **2006**, *35* (3), 889–897. <https://doi.org/10.2134/jeq2005.0328>.

- (28) Dickerson, J. W.; Hagedorn, C.; Hassall, A. Detection and Remediation of Human-Origin Pollution at Two Public Beaches in Virginia Using Multiple Source Tracking Methods. *Water Res.* **2007**, *41* (16), 3758–3770. <https://doi.org/10.1016/j.watres.2007.02.055>.
- (29) Close, M. E.; Hodgson, L. R.; Tod, G. Field Evaluation of Fluorescent Whitening Agents and Sodium Tripolyphosphate as Indicators of Septic Tank Contamination in Domestic Wells. *New Zeal. J. Mar. Freshw. Res.* **1989**, *23* (4), 563–568. <https://doi.org/10.1080/00288330.1989.9516392>.
- (30) Wolfe, T. M. A Comparison of Fecal Coliform Densities and Fluorescent Intensities in Murrells Inlet a Highly Urbanized Estuary and in North Inlet, a Pristine Forested Estuary., University of South Carolina, 1995.
- (31) United States Geological Survey. *Escherichia Coli Bacteria Density in Relation to Turbidity, Streamflow Characteristics, and Season in the Chattahoochee River near Atlanta, Georgia, October 2000 through September 2008 — Description, Statistical Analysis, and Predictive Modeling*; Reston, VA, 2012.
- (32) Huey, G. M.; Meyer, M. L. Turbidity as an Indicator of Water Quality in Diverse Watersheds of the Upper Pecos River Basin. *Water (Switzerland)* **2010**, *2* (2), 273–284. <https://doi.org/10.3390/w2020273>.
- (33) King, A. M. Relationships Between Environmental Factors and Fecal Indicator Bacteria Contamination at Campbell Cove Beach. **2016**, 753226.
- (34) United States Geological Survey. *Factors Affecting Escherichia Coli Concentrations at Lake Erie Public Bathing Beaches*; Columbus, Ohio, 1998.
- (35) Sadowsky, M. J.; Whitman, R. L. *The Fecal Bacteria*; ASM Press: Washington, DC, 2011.
- (36) Michigan Department of Environmental Quality. *Total Maximum Daily Load for E. Coli for Red Run Drain and Bear Creek*; Lansing, MI, 2006.
- (37) Michigan Department of Environmental Quality. *Efforts and Framework for Future Protection in the Lake St. Clair Basin*; Lansing, MI, 2017.

- (38) Subwatershed Advisory Council for the Clinton River East Subwatershed. *A Clinton River Watershed Management Plan - The Clinton River East Subwatershed*; 2006.
<https://doi.org/10.1017/CBO9781107415324.004>.
- (39) Francis, J. T.; Haas, R. C. *Clinton River Assessment: Special Report 39*; 2006.
- (40) Tetra Tech. *The Clinton River Watershed Management Plan for Improving Water Quality in the North Branch Clinton River, Lake St. Clair, and the Great Lakes*; 2010.
- (41) Subwatershed Advisory Group for the Clinton River East Subwatershed. *A Clinton River Watershed Management : The Red Run Subwatershed of Macomb and Oakland Counties*; 2006; Vol. 1.
- (42) United States Geological Survey. USGS: Water-Year Summary for USA
https://waterdata.usgs.gov/nwis/wys_rpt? (accessed Mar 25, 2020).
- (43) Bartos, M.; Wong, B.; Kerkez, B. Open Storm: A Complete Framework for Sensing and Control of Urban Watersheds. *Environmental Science: Water Research and Technology*. 2018.
<https://doi.org/10.1039/c7ew00374a>.
- (44) Hudson, N.; Baker, A.; Reynolds, D. Fluorescence Analysis of Dissolved Organic Matter in Natural, Waste and Polluted Waters - A Review. *River Res. Appl.* **2007**.
<https://doi.org/10.1002/rra.1005>.
- (45) Downing, B. D.; Pellerin, B. A.; Bergamaschi, B. A.; Saraceno, J. F.; Kraus, T. E. C. Seeing the Light: The Effects of Particles, Dissolved Materials, and Temperature on in Situ Measurements of DOM Fluorescence in Rivers and Streams. *Limnol. Oceanogr. Methods* **2012**, *10* (OCTOBER), 767–775. <https://doi.org/10.4319/lom.2012.10.767>.
- (46) Stoughton, R. W.; Rollefson, G. K. The Quenching of Fluorescence in Solution. II. Temperature and Solvent Effects. *J. Am. Chem. Soc.* **1940**. <https://doi.org/10.1021/ja01866a003>.
- (47) Michigan Department of Agriculture & Rural Development. *Generally Accepted Agricultural and Management Practices for Manure Management and Utilization*; 2018.
- (48) Baker, A.; Cumberland, S. A.; Bradley, C.; Buckley, C.; Bridgeman, J. To What Extent Can

- Portable Fluorescence Spectroscopy Be Used in the Real-Time Assessment of Microbial Water Quality? *Sci. Total Environ.* **2015**, 532, 14–19. <https://doi.org/10.1016/j.scitotenv.2015.05.114>.
- (49) Determann, S.; Lobbes, J. örg M.; Reuter, R.; Rullkötter, J. ürger. Ultraviolet Fluorescence Excitation and Emission Spectroscopy of Marine Algae and Bacteria. *Mar. Chem.* **1998**. [https://doi.org/10.1016/S0304-4203\(98\)00026-7](https://doi.org/10.1016/S0304-4203(98)00026-7).
- (50) Del Olmo, M.; Díez, C.; Molina, A.; De Orbe, I.; Vílchez, J. L. Resolution of Phenol, o-Cresol, m-Cresol and p-Cresol Mixtures by Excitation Fluorescence Using Partial Least-Squares (PLS) Multivariate Calibration. *Anal. Chim. Acta* **1996**, 335 (1–2), 23–33. [https://doi.org/10.1016/S0003-2670\(96\)00350-9](https://doi.org/10.1016/S0003-2670(96)00350-9).
- (51) Carstea, E. M.; Bridgeman, J.; Baker, A.; Reynolds, D. M. Fluorescence Spectroscopy for Wastewater Monitoring: A Review. *Water Res.* **2016**. <https://doi.org/10.1016/j.watres.2016.03.021>.
- (52) Baker, A. Fluorescence Excitation - Emission Matrix Characterization of Some Sewage-Impacted Rivers. *Environ. Sci. Technol.* **2001**, 35 (5), 948–953. <https://doi.org/10.1021/es000177t>.
- (53) Hur, J.; Cho, J. Prediction of BOD, COD, and Total Nitrogen Concentrations in a Typical Urban River Using a Fluorescence Excitation-Emission Matrix with PARAFAC and UV Absorption Indices. *Sensors* **2012**. <https://doi.org/10.3390/s120100972>.
- (54) Ghervase, L.; Cârstea, E. M.; Pavelescu, G.; Borisova, E.; Daskalova, A. Fluorescence Evaluation of Anthropogenic Influence on Rivers Crossing Sofia. *Rom. Reports Phys.* **2010**.
- (55) Riopel, R.; Caron, F.; Siemann, S. Fluorescence Characterization of Natural Organic Matter at a Northern Ontario Wastewater Treatment Plant. *Water. Air. Soil Pollut.* **2014**. <https://doi.org/10.1007/s11270-014-2126-3>.
- (56) Old, G. H.; Naden, P. S.; Granger, S. J.; Bilotta, G. S.; Brazier, R. E.; Macleod, C. J. A.; Krueger, T.; Bol, R.; Hawkins, J. M. B.; Haygarth, P.; et al. A Novel Application of Natural Fluorescence to Understand the Sources and Transport Pathways of Pollutants from Livestock Farming in Small Headwater Catchments. *Sci. Total Environ.* **2012**. <https://doi.org/10.1016/j.scitotenv.2011.12.013>.

- (57) Louvet, J. N.; Homeky, B.; Casellas, M.; Pons, M. N.; Dagot, C. Monitoring of Slaughterhouse Wastewater Biodegradation in a SBR Using Fluorescence and UV-Visible Absorbance. *Chemosphere* **2013**. <https://doi.org/10.1016/j.chemosphere.2013.01.011>.
- (58) Ghervase, L.; Carstea, E. M.; Pavelescu, G.; Savastru, D. Laser Induced Fluorescence Efficiency in Water Quality Assessment. *Rom. Reports Phys.* **2010**.
- (59) United States Geological Survey. *Guidelines and Standard Procedures for Continuous Water-Quality Monitors : Station Operation , Record Computation , and Data Reporting*; Reston, VA, 2006.
- (60) Corsi, S. R. Personal Communication. 2019.
- (61) Michigan Department of Environmental Quality. *Michigan's Statewide E. Coli Total Maximum Daily Load*; Lansing, MI, 2017.
- (62) Korak, J. A.; Dotson, A. D.; Summers, R. S.; Rosario-Ortiz, F. L. Critical Analysis of Commonly Used Fluorescence Metrics to Characterize Dissolved Organic Matter. *Water Res.* **2014**, *49*, 327–338. <https://doi.org/10.1016/j.watres.2013.11.025>.
- (63) Wang, Z.; Cao, J.; Meng, F. Interactions between Protein-like and Humic-like Components in Dissolved Organic Matter Revealed by Fluorescence Quenching. *Water Res.* **2015**, *68*, 404–413. <https://doi.org/10.1016/j.watres.2014.10.024>.
- (64) Lakowicz, J. R. *Principles of Fluorescence Spectroscopy*; 2006. <https://doi.org/10.1007/978-0-387-46312-4>.
- (65) Saraceno, J. F.; Pellerin, B. A.; Downing, B. D.; Boss, E.; Bachand, P. A. M.; Bergamaschi, B. A. High-Frequency in Situ Optical Measurements during a Storm Event: Assessing Relationships between Dissolved Organic Matter, Sediment Concentrations, and Hydrologic Processes. *J. Geophys. Res. Biogeosciences* **2009**, *114* (4), 1–11. <https://doi.org/10.1029/2009JG000989>.
- (66) Watras, C. J.; Hanson, P. C.; Stacy, T. L.; Morrison, K. M.; Mather, J.; Hu, Y. H.; Milewski, P. A. Temperature Compensation Method for CDOM Fluorescence Sensors in Freshwater. *Limnol. Oceanogr. Methods* **2011**, *9* (JULY), 296–301. <https://doi.org/10.4319/lom.2011.9.296>.

- (67) Cao, Y.; Griffith, J. F.; Weisberg, S. B. Evaluation of Optical Brightener Photodecay Characteristics for Detection of Human Fecal Contamination. *Water Res.* **2009**.
<https://doi.org/10.1016/j.watres.2009.02.020>.
- (68) Ryder, E.; Jennings, E.; De Eyto, E.; Dillane, M.; NicAonghusa, C.; Pierson, D. C.; Moore, K.; Rouen, M.; Poole, R. Temperature Quenching of CDOM Fluorescence Sensors: Temporal and Spatial Variability in the Temperature Response and a Recommended Temperature Correction Equation. *Limnol. Oceanogr. Methods* **2012**, *10* (DECEMBER), 1004–1010.
<https://doi.org/10.4319/lom.2012.10.1004>.